CHARACTERIZATION AND MODELING OF ORIENTED STRAND COMPOSITES

By

Vikram Yadama

A dissertation submitted in partial fulfillment of
the requirements for the degree of

DOCTOR OF PHILOSOPHY

WASHINGTON STATE UNIVERSITY
Department of Civil and Environmental Engineering

December 2002

To the Faculty of Washington State University:

The members of the Committee appointed to examine the dissertation of VIKRAM YADAMA find it satisfactory and recommend that it be accepted.

_____
Co-Chair

_____
Co-Chair

_____

_____

Acknowledgement

I would like to express my sincere gratitude and appreciation to Dr. Michael P. Wolcott and Dr. David Pollock, my co-advisors, for their guidance and support throughout my research. I am grateful for their enthusiasm and eagerness in my work, and making my experience as a Ph.D. student memorable. The author would also like to thank Dr. Lloyd V. Smith and Dr. William Cofer for serving on my committee and always providing advice when needed. Thank you Dr. Smith for having long, but invaluable, "five minute" discussions and helping me to sort through my numerous doubts and questions; and, of course, for those hard and relaxing racquetball games.

Many thanks to Bob Duncan, Scott Lewis, Marty Lentz, and Dave Dostal for all their assistance at several stages of my research. I also want to acknowledge my friends, fellow graduate students and research associates, who helped me immensely through moral support and technical discussions: Karl Englund, Deepak Shresta, John Hermanson, Suzane Pyer, Anke Schirp, Jeff Linville, Pete Cates, Bill Parsons, David Harper, and Andrew Slaughter. Thank you Balazs for helping me with the drawing of 3-D figure of a strand. Had a blast doing it! Thanks to my research partner, Kristin Meyers, for her assistance with raw material preparation, panel manufacturing and panel testing. "Gracias" to my office mate and friend, Alejandro Bozo, for all his support and friendship. Also, my sincere thanks to Pat Smith, Janet Duncan, Judy Edmister, and Linda Miklosko for their assistance and support.

The author is extremely grateful to Audie Mitcham for providing yellow-poplar material for a major part of this research. Without his help, my research would have been delayed. I would also like to thank Louisiana Pacific Corporation's Advanced

Technology Center in Portland, Oregon, for assisting with preparation of strands. This research was supported by USDA CSREES Inland-Northwest Forest Products Research Consortium Wood Utilization Special Grants Program. My sincere thanks to Louisiana-Pacific Endowment Fund, Plywood Pioneer scholarship, and the Wood Materials and Engineering Laboratory for additional financial support. Thank you Dr. Don Bender.

The author would like to thank his brother (Gautam Yadama), aunts and uncles, in-laws, and many other friends and relatives for their continuous support and encouragement. My heart felt gratitude to Saramma and Abraham Nainan (mother- and father-in-law) for their prayers and support. Finally, I would like to dedicate this dissertation to Sudhakara Rao and UmaDevi Yadama (parents), Minie (wife), Roshan (son), and Alexa (daughter) for their relentless love, endless support, and countless sacrifices. I could not have done it without them. This work is not just a result of my hard work, but theirs too.

In closing I would like to end with a quote by Chakravarti Rajagopalachari, an Indian statesman and a philosopher, who puts learning and practice into perspective.

> "…. *When intelligence matures and lodges securely in the mind, it becomes wisdom. When wisdom is integrated with life and issues out in action, it becomes bhakthi (devotion). Knowledge, when it becomes fully mature is bhakthi. If it does not get transformed into bhakthi, such knowledge is useless tinsel. To believe that gnyana and bhakthi, knowledge and devotion are different from each other is ignorance. ...*"

CHARACTERIZATION AND MODELING OF ORIENTED STRAND COMPOSITES
Abstract

by Vikram Yadama, Ph.D.
Washington State University
December 2002

Co-Chairs: Michael P. Wolcott and David Pollock

A strong relationship exists between the spatial structure of a wood-strand composite and its compaction characteristics, density, mechanical properties, dimensional stability, and fastener performance. The following research proposes a physical model to represent an oriented strand composite panel and applies a mechanics based approach to estimate its elastic properties. The objectives of this research were to 1) review literature on recent progress in characterizing the structure and modeling of wood-strand composites, 2) understand the effects of undulating strands on the elastic behavior of a wood-strand composite and develop a general constitutive model to predict the elastic properties as a function of strand waviness, 3) characterize the elastic properties of strands and develop a response model to account for the effects of hot pressing, 4) quantify key random variables for characterizing the three dimensional structure of an oriented strand composite, and 5) validate the fiber undulation model to predict the elastic properties of an oriented strand composite.

The fiber undulation model (FUM) was shown to predict the elastic properties of wood-strand laminates with predetermined strand undulations reasonably well. Strand undulation degrades Young's modulus in both tension and compression as the undulation angle increases. Model estimates of E_x agreed very well with compression E_x (2 to 4

percent error), but were on the average 12% lower than tensile E_x. Difference between tension and compression Young's moduli is attributed to phenomenological differences in behavior of undulating strands when subjected to tension versus compression and deformation of wood at microstructure level. Response models based on mixture design, considering the hot pressing effects, were developed to predict E_1 and ν_{12} of aspen strands. This study indicates a direct relationship between densification during hot pressing and E_1. The results of the simplex analysis suggest the addition of resin tends to increase stiffness by restraining springback of strands.

The structure of a wood-strand panel was characterized with the out-of-plane undulation of strands in both the longitudinal and transverse directions, and the void volume between strands. Strand undulations were represented quite accurately with discrete Fourier expansions. A series rule of mixtures with probability density functions of undulation angle distributions was utilized to account for the effects of out-of-plane strand waviness and in-plane strand deviations on the elastic constants of a wood-strand composite. The FUM was validated for unidirectional wood-strand panels. Model predictions consistently over-predicted elastic properties from compression tests and under-predicted elastic properties from tensile tests. Average reduction in E_x due to strand undulations was approximately 6.9%. The results of this study show that random and incidental strand undulations in the longitudinal and transverse directions, which are inherent attributes of oriented strand composites, are significant and could potentially influence the physical and mechanical behavior of composite panels.

Table of Contents

List of Tables

List of Figures

CHAPTER 1

PROJECT INTRODUCTION

Introduction

Wood-based composites are engineered with wood from trees of lower quality, faster growth, and smaller diameter thus being more environmentally appealing. Wood composites, unlike solid wood, can be highly engineered to meet the needs of a particular end use. This attribute along with the fact that lower quality wood can be utilized to produce a higher quality product is one of the greatest advantages of wood composites, especially when the supply of large diameter timber is dwindling. However, to efficiently engineer wood composite products, it is important to understand the material and manufacturing variables that affect their elastic and strength behavior.

Wood is an anisotropic material, but is generally regarded to be orthotropic with three orthogonal planes of symmetry: axial or longitudinal, radial, and tangential. Thus, nine independent elastic constants are required to characterize its behavior. Wood composites such as oriented strand board (OSB) or oriented strand lumber (OSL) also exhibit orthotropic symmetry. The degree of anisotropy in composites, however, can be controlled through product engineering. The differences between the directional properties of a composite can be altered through controlling the size and orientation of elements and to a certain extent through fiber orientation in an element. Herein lies one of the biggest advantages of composite materials: their directional properties can be controlled and engineered to a much higher degree than for solid wood material. For instance, a wood composite can be manufactured such that the material exhibits similar

directional properties in the plane of its cross section. These materials are generally referred to as plane isotropic or transversely isotropic. Such materials are characterized by an infinite number of symmetry planes, all oriented in a direction normal to the plane of the cross section. The properties in the longitudinal direction differ substantially the transverse direction properties. Transversely isotropic materials can be characterized by four elastic constants.

Another advantage of wood composites is relatively small variability in their mechanical properties. It is common to obtain coefficients of variation of the order of 20 percent or higher when evaluating mechanical properties of solid wood due to inherent growth characteristics. Naturally occurring inhomogeneities, such as knots and cross grain, tend to create discontinuities in the orthotropic character of wood. But greater homogeneity can be achieved by cutting up the wood and reassembling it as is done with wood composites. The mechanical properties of wood composites, therefore, exhibit lower coefficient of variation than solid woods (Knudson 1992).

Several types of wood elements are utilized industry-wide to make a variety of wood-based products. Some of the primary wood elements are lumber, veneer, strands, flakes or chips, particles, and fibers which are used to manufacture products such as glulam, plywood, oriented strandboard, oriented strand lumber, particleboard, and medium density board. Marra (1992) identified these commonly used wood elements and classified them according to their size (Figure 1.1). A range for dimensions of these wood elements and commonly manufactured products using these elements is given in Table 1.1 (Marra 1992).

According to Marra (1992), in general, the strength of a composite diminishes as the size of the element reduces assuming that the density remains the same. However, as the element size becomes smaller it becomes more formable, quality of raw material becomes less decisive in controlling properties, and surface area per pound of wood increases dramatically. Approximate boundaries between these element sizes are indicated in Table 1.1. Size is an important factor to consider in developing analytical models because the stress distribution within the material varies as the element size varies. However, Marra (1992) points out that as the element size decreases, the strength lost can be recovered by increasing the density of the material, increasing the adhesive content, aligning the elements, and reducing the variation in the product properties.

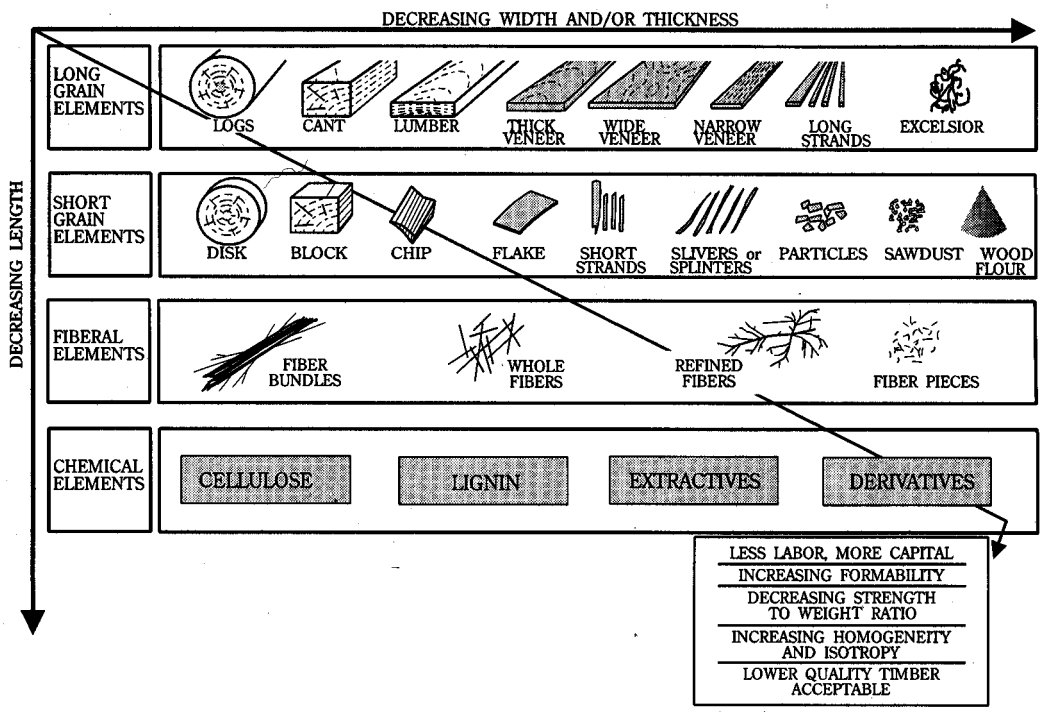

Figure 1. 1. Classification of wood elements (Marra 1992).

Table 1. 1. Dimensions of wood elements (Marra 1992).

ELEMENT	LENGTH (INCHES)	WIDTH (INCHES)	THICKNESS (INCHES)	GLUED PRODUCTS
Lumber	4–20 (ft)	4–12	.5–2	Beams and arches
Veneer	4–8 (ft)	4–48	.02–.5	Plywood and LVL
Wafers	1–3	1–3	.025–.05	Waferboard
Flakes	.5–3	.5–3	.010–.025	Flakeboard
Strands	.5–3	.25–1	.010–.025	Oriented strand board
Splinters (slivers)	.25–3	.005–.025	.005–.025	Splinterboard
Particles	.05–.5	.005–.050	.005–.050	Particleboard
Fiberbundles	.05–1	.005–.020	.005–.020	Fiberboard
Fibers	.04–.25	.001–.003	.001–.003	Paper
Cellulose/Lignin		Molecular dimensions		Plastics, films, filaments

OSL is a reconstituted, engineered lumber that can be substituted for high-quality structural lumber. It could be considered as a laminated composite structural lumber that is a combination of laminated veneer lumber (LVL) and OSB. A key feature of OSL is the use of longer strands, up to 12 inches, as its elements yielding a highly oriented product. It is available in cross section sizes similar to that of lumber and in much greater lengths than lumber. According to McNatt and Moody (1990), the strength properties of structural composite lumber products, such as OSL, are comparable to those of high-grade sawn lumber, and stiffness is comparable to that of a lower grade of structural lumber. The importance of OSL is expected to grow as demand for highly engineered wood-products increases and the wood industry shifts to a greater use of small-diameter trees, especially from thinnings and fast-growing forest resources.

For effective use of OSL as a construction material, it will be helpful to be able to predict its behavior under typical loading conditions that exist in a structure. This analysis requires information regarding material physical and mechanical properties. These properties are not only influenced by the geometry of wood elements and their arrangement, but also by the alterations the element properties undergo during the

manufacturing process of a composite. Performing experimental studies to characterize the behavior of different composites, while accounting for strand geometry and manufacturing process effects, is a time consuming and expensive process. A viable alternative is to model the composites by replacing the experimental studies with realistic and simple physical models.

The modeling process begins with identification of a system and the relevant parameters necessary for its description. Therefore, the structure of a network of particles should be understood along with the variables that influence this structure. Once the structure of the network is determined, with the aid of micro- or macro-mechanic theories the physical and mechanical properties of a system can be predicted knowing the properties of the elements of a system and their arrangement. Modules to consider the effects of manufacturing processes, such as hot pressing, on element properties can also be included in these models. The characteristics that are modeled will be different depending on the property to be predicted. The real value of modeling lies in its capacity to simplify description of properties and to identify the common characteristics of different composites (Bodig and Jayne 1982). The following research proposes a physical model to represent a wood-strand composite, such as OSL, and applies a mechanics-based approach to estimate the elastic constants of the composite.

Objectives

The primary goal of this research project is to develop a mechanics-based analytical approach to estimate the elastic properties of oriented strand composites. The specific objectives within this project are to:

1. Present a review of literature on recent progress in characterizing the structure of wood-strand composites, factors affecting the structure, and advances in modeling of elastic properties of wood composites.
2. Understand the effects of undulating strands on the elastic behavior of a wood-strand composite and develop a general constitutive model (fiber undulation model) to predict the elastic properties as a function of strand waviness.
3. Characterize the elastic properties of strands and develop a response model to account for the effects of hot pressing on strand elastic properties.
4. Quantify key random variables to contribute to characterizing the three dimensional structure of a hot pressed oriented strand composite panel.
5. Validate fiber undulation model to predict the elastic constants of a wood-strand composite.

Rationale and Significance

With the advent of finite element analysis and its crucial role in designing structures and structural members, it is critical that accurate constitutive models are developed to simulate structural behavior under typical loading conditions. With structural composite lumber replacing sawn lumber and timber for structural members

such as girders, beams, headers, joists, studs, and columns, accurate representation of their elastic behavior and strength is imperative. A strong relationship exists between spatial structure of a wood composite panel and its compaction characteristics, density, mechanical properties, dimensional stability, and fastener performance. It is important to understand the structure of the network of particles that make up a wood composite to determine its mechanical and physical behavior accurately and efficiently engineer it.

In the past, researchers (Dai and Steiner 1994a & 1994b, Lang and Wolcott 1996, Lenth and Kamke 1996, and Suchsland and Xu 1991) developed wood strand composite models that incorporated key parameters that characterize the structure of a wood-strand mat. Based on statistical and probabilistic models, they developed methods of describing the horizontal density distribution. Analyses of spatial structure of mats have been used to model stress-strain behavior of wood-strand mats in transverse compression during hot pressing. However, the structure of finished panels has not been studied in detail. If certain key parameters characterizing the finished panels are determined, then with the aid of micro- or macro-mechanic theories their properties could be predicted knowing the properties and arrangement of the particles. Previous studies (Geimer et al. 1975, Geimer 1976, Geimer 1979, Harris and Johnson 1982, Shaler and Blakenhorn 1990, Shaler 1991, Barnes 2000, Meyers 2001) generally concentrated on examining in-plane orientation of particles and how it affected composite properties. When long flakes are used in composite lumber such as OSL, the waviness along the length of the flake through the thickness of the composite could also reduce its mechanical properties. Under compressive loading the effect of fiber waviness becomes an important issue because of their tendency to buckle more readily. No studies have been conducted to study the

effects of strand waviness through the thickness of a wood-strand composite on the elastic properties of the composite.

This research is intended to contribute to an understanding of wood-strand panel structure and its effects on elastic behavior of the panel. The research focused on characterizing the spatial structure of a finished wood-strand panel with three key parameters: in-plane orientation of particles, out-of-plane or through thickness undulation of particles, and between strands void volume distribution. A novel method to describe random strand undulation in a panel is presented. Effects of hot pressing of wood-strand mats on the elastic properties of strands are investigated. Then, using the information regarding the structure of a panel and modifications to panel elements during the manufacturing process, an approach utilizing the fiber undulation model to predict the effective elastic constants of a panel is presented.

Structure of the Dissertation

Dissertation is divided into seven chapters, including this introductory chapter. Chapters two through six are written as stand-alone papers addressing each of the objectives presented in this chapter. Chapter two is a review of published research regarding structural characterization of wood composites and modeling of their elastic behavior. Chapter three introduces the fiber undulation model, commonly used to model woven synthetic composite fabrics, and verifies the model for wood-strand composites. Chapter four examines the elastic properties of strands used to manufacture panels in this study and investigates the effects of hot pressing on their elastic behavior. Chapter five discusses and quantifies parameters that could be used to characterize a wood-strand

panel structure. Chapter six utilizes the information presented in Chapters three, four, and five to validate the fiber undulation model for estimating the elastic constants of a wood-strand composite. Finally, Chapter seven summarizes the conclusions of this project based on Chapters three through six.

References

Barnes, D. 2000. An integrated model of the effect of processing parameters on the strength properties of oriented strand wood products. Forest Products Journal. 50(11/12):33-42.

Bodig, J. and B. A. Jayne. 1982. Mechanics of wood and wood composites. Van Nostrand Reinhold Company, New York, NY.

Dai, C. and P. R. Steiner. 1994a. Spatial structure of wood composites in relation to processing and performance characteristics: Part II. Modelling and simulation of a randomly-formed flake layer network. Wood Sci. Technol. 28:135-146.

_____ and _____. 1994b. Spatial structure of wood composites in relation to processing and performance characteristics: Part III. Modelling the formation of multi-layered random flake mats. Wood Sci. Technol. 28(3):229-239.

Geimer, R. L., H. M. Montrey, and W. F. Lehmann. 1975. Effects of layer characteristics on the properties of three-layer particlboards. Forest Products Journal. 25(3):19-29.

Geimer, R. L. 1976. Flake alinement in particleboard as affected by machine variables and particle geometry. USDA Forest Service Research Paper FPL 275. 16 pp.

_____. 1979. Data basic to the engineering design of reconstituted flakeboard. In Proceedings of the 13t^{h} Washington State University International Symposium on Particleboard. pp. 105-125.

Harris, R. A. and Johnson, J. A. 1982. Characterization of flake orientation in flakeboard by the von Mises probability distribution function. Wood and Fiber 14(4):254-266.

Knudson, R. M. 1992. PSL 300^{TM} LSL: The challenge of a new product. Proceedings of the 26th International Particleboard Symposium, Washington State Universtiy, Pullman, WA.

Lang, E. M. and M. P. Wolcott. 1996. A model for viscoelastic consolidation of wood-strand mats. Part I. Structural characterization of the mat via Monte Carlo simulation. Wood and Fiber Science. 28(1):100-109.

Lenth, C. A. and F. A. Kamke. 1996. Investigations of flakeboard mat consolidation. Part I. Characterizing the cellular structure. Wood and Fiber Science. 28(2):153-167.

Marra, A. A. 1992. Technology of wood bonding: Principles in practice. Van Nostrand Reinhold, New York, NY.

McNatt, J. D. and R. C. Moody. Structural Composite Lumber. Progressive Architecture 12.90:34-36.

Meyers, K. L. 2001. Impact of strand geometry and orientation on mechanical properties of strand composites. Master's Thesis. Dept. of Civil and Environmental Engineering, Washington State University. 115pp.

Shaler, M. S. and P. R. Blankenhorn. 1990. Composite model prediction of elastic moduli for flakeboard. Wood and Fiber Science. 22(3):246-261.

_____. 1991. Comparing two measures of flake alignment. Wood Sci. Technol. 26:53-61.

Suchsland, O. and H. Xu. 1991. Model analysis of flakeboard variables. Forest Products Journal. 41(11/12):55-60.

Chapter 2

Characterization of Wood Composites and Modeling of Their Elastic Properties: A Review

Introduction

Wood is an anisotropic material, but generally regarded to be orthotropic. Wood composites, such as oriented strand board (OSB), oriented strand lumber (OSL), laminated veneer lumber (LVL), or Parallam® also exhibit anisotropic behavior. The degree of anisotropy in composites, however, can be controlled through product engineering. Efficient engineering of a wood composite product requires an understanding of its structure and the changes that the constituents undergo during the manufacturing process. Once the structure of the network is determined, with the aid of basic mechanics, the properties of a system can be predicted. The real value of a model representing a wood based composite lies in its capacity to identify and capture composite's critical characteristics that influence its behavior under investigation, and yet be general enough to be applied to a class of similar composites with minor modifications to the input parameters.

Spatial structure of wood composites is extremely complicated and time consuming to characterize. It is further complicated by the mere fact that wood is a highly variable material. This complicated network of particles can be handled only by meticulous characterization of its structure and understanding how variations in this structure effect the material behavior. It is critical that a database of wood composite

structure, factors that influence this structure and the effects of structure on composite stiffness and strength be generated and consolidated.

The following paper is a review of literature on factors affecting the spatial structure of wood composites, recent progress in characterizing the spatial structure of wood composites and advances in modeling of elastic properties of wood composites.

Why is it Important to Understand Spatial Structure of Wood Composites?

Particle geometry, arrangement, and processing parameters play an important role in influencing the physical and mechanical properties of wood composites. A strong relationship exists between spatial structure of a wood composite panel and its compaction characteristics, density, mechanical properties, dimensional stability, and fastener performance. As Steiner and Dai (1993) point out, the spatial relationship between the constituents of a composite will determine the ultimate density distribution in a composite panel and it is a known fact that density effects a composite's elastic and strength behavior. Besides density, stress transfer between particles depends on the quality of contact between particles within a panel, which in turn is affected by particle geometry and arrangement. Therefore, establishing relationships between properties, geometry, and arrangement of particles and composite behavior would be beneficial for evaluation of raw materials for a desired composite, as well as product design.

Variables Influencing Spatial Structure of Wood Composites

Spatial structure of a wood composite panel could be characterized with several variables, such as particle orientation, void distribution, void size, and horizontal and

vertical density variations. Incorporation of these factors is important in developing models that predict structure-property relationships. However, these panel variables are effected by particle geometry, particle properties, and mat formation parameters; research conducted regarding these variables will be discussed first followed by studies done on mat and panel structure characterization.

Particle Geometry

Dinwoodie (1997) describes a wood-based composite as particles of variable length and thickness bonded together with a matrix to provide an artifact that possesses a measure of cohesive strength. A wood particle, besides possessing some inherent strength and stiffness, should also be sufficiently long to allow adequate overlap for transfer of applied stress from one particle to the next (Simpson 1977, Laufenberg 1984, Barnes 2001). The resin must have tensile and shear properties at least as good as those of the wood particle in order to transfer the applied stress.

Several studies (Brumbaugh 1960, Jorgensen and Murphey 1961, Post 1958, Post 1961, Suchsland 1968, Kelly 1977, Geimer 1979, Barnes 2001) dealt with the effects of particle geometry on the resultant composite mechanical properties. Suchsland (1968) boiled it down to the fact that tensile strength of a particleboard is determined either by the tensile strength of the individual lamina or by the shear strength of the adhesive joints. Increase in particle length will result in an increase in overlap length of particles causing larger forces to be transferred through adhesive joints. Thus, the tensile strength of a composite will be improved as the overlap length is increased until the ultimate tensile strength of the particle is reached. However, there exists a critical overlap length

below which the chances of glue failure due to shear forces are higher and above which the wood will generally fail in tension.

Slenderness ratio, a ratio of strand length-to-thickness, has been found to have an effect on board properties, thus it has been used to develop empirical equations specific to a study. Nelson (1997) cites strand geometry as crucial in obtaining optimum board properties. Post (1958,1961) investigated the effects of changing flake length and thickness on bending strength and stiffness of oak flake board. He varied the flake lengths from 0.5 to 4 inches and flake thickness from 0.006 to 0.050 inch. The study concluded that more than either of the two flake dimensions, flake slenderness ratio was a better measure of the influence of flake's geometry on the board properties. The average length of overlap increased as the flake length-to-thickness ratio is increased. Longer flakes at a given thickness did give higher strength, and Post (1958, 1961) states that changing flake length is probably more economical. His study also found that increased flake thickness decreased strength, which was attributed to fewer resin bonds with thicker flakes.

Wang and Lam (1999) developed empirical relationships for modulus of rupture (MOR) and modulus of elasticity (MOE) using three-dimensional surface maps to generate quadratic regression models based on flake slenderness ratio, orientation, and board density. For flake lengths from 50 to 100 mm (approximately 2 to 4 inches) the optimum slenderness ratio was identified as 133. However, much of the research that examined slenderness ratio did not separate the effect of orientation.

Brumbaugh (1960) tested Douglas-fir boards made from flakes of four sizes. Longer flakes produced boards with higher MOR, whereas boards with shorter flakes had

better internal bond strength. He concluded that flake slenderness ratio should be at least 200 to obtain optimum overall board properties. Another study (Jorgensen and Murphey 1961) investigated the effects of flake dimensions on adhesive thickness and distribution. Higher frequency of overlap as length increased did not permit close contact of the particles even with thin flakes. A reason for this problem with thin flakes could be excessive curl of the flakes.

Meyers (2001) examined the effect of strand length and width separately by maintaining a single nominal thickness for three nominal strand lengths and widths, 4, 8, and 12 inches and 0.5, 0.75, and 1.0 inches respectively. In addition, the effect of strand orientation in the plane was considered apart from strand geometry by forming each geometry at two orientation levels. Meyers' study indicated that panel elastic properties were influenced primarily by strand orientation and density, thus the need for long strands is only to attain adequate orientation.

Particle Properties

The impact of wood strand quality on composite properties is manifested not only through their influence on the spatial geometry of a mat, but also through their contribution to the elastic and strength properties of a panel. Elastic properties of a wood strand are effected by the physical changes that a strand experiences during cutting of strands from lumber or a log, as well as during the composite manufacturing process (Marra 1992). In OSB or OSL manufacturing, a strand is sprayed with resin particles that penetrate into the material to a certain degree and, then, it is subjected to mechanical pressures and varying temperatures during the hot-pressing operation. These changes in physical and mechanical environment will alter wood strand elastic properties.

Densification of a mat results in densification of a strand as well. The degree of densification would vary depending on the location of the strand through the thickness of a panel. In general, strength and stiffness of wood has been found to reduce with increasing temperature due to thermal expansion of the crystal lattice of the cellulose and due to the increased intensity of the thermal molecular oscillations (Kollmann and Cote 1968, Tsoumis 1991). The duration of heat is also critical. Temperatures higher than 65° C (150° F) may have a permanent adverse effect with a long duration of heating. For instance, a temperature of 200° C (400° F) is known to reduce strength in a few minutes (Galligan 1975). A limited number of studies (Price 1976, Mahoney 1980, Jahan-Latibari 1982a, 1982b, Jahan-Latibari et. al. 1984,Geimer et. al. 1985, Gardner et. al. 1993) have been conducted to examine the influence of these processing variables on the strand properties.

Price (1976) tested sweetgum (*Liquidambar styraciflua* L.) flakes in tension before and after hot-pressing them to a target board density of 42 pcf at a press temperature of 335 degrees F. No resin was added to the boards so that the flakes could be separated after the panel was manufactured. Flakes from the outer surface, as well as from the middle of the board were tested for their tensile properties. It was reported that compared to the published Young's modulus value of small, clear solid wood specimens, the tensile modulus of the flakes were 53 to 69 percent lower. This reduction in modulus of elasticity was attributed by the author to cell damage during the flake machining process, grain angle through the thickness of the flakes, moisture content, and inability to measure correct strain by the procedure used. As per densification of flakes during the board manufacturing process, the study reported that density of outer flakes increased by

about 14%, where as the density of core flakes increased by 6.3%. A 9.8% increase in face flake and a 7.3% increase in core flake moduli of elasticity was reported.

Mahoney (1980) conducted a detailed study on the effects of press temperatures, closure rates, and target board densities on Douglas-fir flake tensile properties. He found that temperature had the greatest effect on the flake properties. He reported a reduction in ultimate tensile stress of 14 to over 40 percent; and, a reduction in the flake tensile modulus of 36 to over 50 percent. Once again, board was manufactured without any adhesive so the flakes could be separated afterwards. The mean tensile modulus of flakes, before they were hot-pressed, was reported to be less than half the published value for Douglas-fir obtained from testing small, clear samples. Flakes pressed at temperatures above 400 degrees F were reported to be significantly higher in tensile modulus than those pressed at the lower temperature, 275 degrees F. It was hypothesized by the investigator that at higher temperatures, lignin began to flow and probably filled the damaged areas, thus reinforcing them. No statistical difference in the mechanical properties tested was found between face and core flakes.

Jahan-Latibari (1982) studied the response of quaking aspen flake surface treatments with chemicals on their strength and elastic properties. He also reported a 47% lower modulus for flakes compared to the modulus of solid wood. Decreases in MOR and MOE, after hot pressing, were found to be greater than those of flakes which were exposed only to the pressing temperatures, thus indicating that a combination of pressure and temperature have a direct effect on flake mechanical properties.

Geimer, et al. (1985) found a reduction in Douglas-fir flake tensile modulus as a result of pressing by as much as 48 to 91% of the control flake depending on the flake

location in the board and the press temperature. No adhesive was used in preparing the mats used to determine the effect of temperature on flake properties. Flakes were examined under polarized light after they were manufactured to observe if there was any damage to them. Prior to hot pressing, the authors reported that they did not notice any internal damage in the form of collapsed or sheared cell walls, slip planes, or compression wrinkles in any flakes. However, after hot pressing of flakes, internal damage to the flakes was noticed. Latewood of one flake would press into the earlywood of an adjacent flake causing localized compression. Outer flakes could not be separated after hot pressing. Earlywood portions of the flakes were crushed heavily as expected, and some earlywood tracheids immediately adjacent to latewood were sheared off. Other observed damages were buckling of cell walls and tension failures in cell walls. The study indicated that high press temperatures helped flake strength, and this phenomenon was attributed to either a reduction in damage due to increased plasticization or a repair of damage by lignin flow.

Laufenberg (1984) noted that increasing the pressure during the curing process may induce some damage in the strands, but the effects of this damage is compensated and minimized by the improvements in strand-to-strand bonds. As Geimer et. al. (1985) observed, pressing boards with poor quality flakes at high temperatures considerably increased the board properties. Authors summarize that their study results suggest that pressing temperature influences the performance of damaged flakes more than either board specific gravity or press closure rate. Gardner et. al. (1993) examined the changes in polymer structure of wood flakes when heated under conditions similar to the hot pressing of wood composites. Results indicate that the cellulose crystallinity in the wood

increases slightly in response to heat treatment, supporting some of the findings of increase in elastic modulus of strands during hot pressing of wood composites by researchers discussed earlier.

Mat Formation Parameters

Packing efficiency of a mat is determined by the geometry and orientation of its elements. Ratio of particle surface area to volume is directly correlated to the packing volume. As ratio increases, the packing efficiency increases. It was shown by Milewski (1978) that intermixing particles with different area to volume ratios may lead to improved random packing. Thus, the make up of wood furnish in terms of distribution of particle size would have a direct affect on mat formation.

Structure of wood based composite, such as OSB or OSL, differs from that of laminated veneer lumber in terms of discontinuity of the laminas and extremely low usage of adhesive. The laminae are composed of adhesive coated flakes or strands that are formed to a mat by gravity deposition. Controlling certain variables of mat formation influences the internal structure of the finished product and thus its properties. These variables include the spacing between the vanes through which flakes are dropped to form a mat and height between the vanes and the top surface of the mat being formed (Geimer 1976, Barnes 2000, 2002b, Meyers 2001). Barnes (2002b) developed a model to predict the mean angular deviation of oriented strands in products such as OSB and OSL. Variables such as method of orienting, lateral gaps between discs or vanes, strand length, strand flow rate, and the free fall distance between the bottom edge of the orienting device and strand mat surface are considered in the model. Relationships between these variables and mean angular deviation or disorientation of strands are presented. Effect of

these mat formation process variables on modulus of elasticity is also discussed. McNatt et. al. (1992) from their study on panels manufactured with various combinations of random and aligned strands found that panels made with disk orienter were stronger and stiffer in bending in the aligned direction than were panels made with the vane orienter option. Primarily, these variables determine the particle orientation and particle overlap. Other variables, such as uniform deposition of particles over the mat formation area and edge or end deposition of particles, would also affect the end product properties. These undesirable characteristics during mat forming could be minimized by compressing the mat initially without causing any real compression stresses. Once the mat is formed, it is compressed in a hot press to a considerable degree of densification. Consolidation of these small particles or strands results in a three dimensional composite network that includes voids.

The fundamental variable affecting board properties is the degree of contact between particles (Suchsland 1959, 1967, Simpson 1977, Laufenberg 1984). As the mat densification takes place, the particles undergo plastic deformation and temperature and moisture transfer and gradients cause weakening of particles and a vertical density distribution. Mat spatial structure parameters discussed earlier would influence the particle densification and temperature and moisture gradients within the panel during the manufacturing process. They also influence the degree of contact between the particles, and thus the quality of the final product.

The environmental conditions in a mat affect the rate and degree of adhesive cure, the density gradient, bond quality, and consequently, the physical and mechanical properties of the resulting mat (Kelly 1977, Kamke and Casey 1988a, 1988b, Kamke and

Wolcott 1991). Therefore, platen temperature, press time, platen pressure, mat moisture content and its distribution, particle geometry, and adhesive content influence the panel properties. In conventional presses, the mode of heat transfer to the mat is conduction from heated platens, followed by convection heat transfer, with steam as the heat transfer medium (Strickler 1959). Research (Strickler 1959, Kelly 1977, Song and Ellis 1997) shows that the rate of initial heat penetration to the center of a board is directly related to the over-all board moisture content, surface moisture content, and initial platen pressure. Comprehensive discussion on the effects of manufacturing parameters on wood composite properties is presented in a paper by Kelly (1977).

Structure Characterization

Characterization of wood composite structure could be done at two stages in the panel manufacturing process: at the initial mat formation stage and at a later finished panel stage. Several researchers (Suchsland and Xu 1991, Steiner and Dai 1993, Dai and Steiner 1994a, 1994b, Lang and Wolcott 1996, Lenth and Kamke 1996, and Lu et al. 1998) had studied mat variables that would influence the physical and mechanical properties of a composite board. Effect of particle geometry on panel horizontal density variation was also investigated using computer simulations (Dai and Steiner 1994a, 1994b). As for characterization of panel structure, studies were limited to examining in-plane particle orientation and variations in horizontal and vertical density profiles (Geimer 1976, Price 1977, Geimer 1979, Suzuki and Sekino 1982, Geimer 1986, Shaler 1986, Winistorfer et. al. 1986, 1993, 1996, 1999, 2000, Shaler and Blankenhorn 1990,

Shaler 1991, Sharma and Sharon 1993, Xu and Suchsland 1998, Wang et. al. 1999, Wang and Winistorfer 2000, Barnes 2000, 2002a, Meyers 2001).

Mat Structure Characterization

Dai and Steiner (1994a, 1994b) and Lang and Wolcott (1996) applied the concepts of two-dimensional random field theory and developed mathematical models to describe the mat structure prior to consolidation. They used variables such as flake centers, number of overlapping strands, gap between adjacent strands, total flake number, flake area coverage, and average height of mat. Lenth and Kamke (1996a, 1996b) quantified structural parameters of mat sections using image analysis techniques and applied theories of cellular materials to model the consolidation of wood flake mat. Theoretical models were reported to be reasonably effective in predicting the transverse compression stress-strain relationships of strands mats at strains less than 70%. At higher strain levels, model assumptions were violated, thus making the theory of cellular materials ineffective.

Steiner and Dai (1993) and Dai and Steiner (1994) showed the importance of spatial relationship between individual wood elements in determining the ultimate density distribution in a panel. Spatial structure is governed by the manner in which the mat is formed and the size and geometry of the elements. To describe mat formation theoretically, Dai and Steiner (1994a, 1994b) applied the concepts of two-dimensional random field theory, which were originally used to describe the structure of paper sheets by Kallmes and Cortes (1960, 1961).

Dai and Steiner's (1994a, 1994b) model assumed uniform flake geometry and random packing process. Each flake was assumed to be packed independently of another

and having an equal probability of depositing at all points in the mat and having a random orientation. Mat structure was described using a Poisson or exponential distribution. Distributions of flake centers and flake area coverage were characterized by Poisson's distribution. Whereas, distribution of free flake length was an exponential distribution. The void volume was then calculated based on average mat thickness. They concluded that structural properties of a random flake layer could be satisfactorily modeled using average flake length and width, total flake number, and total layer area. By summing a series of two-dimensional randomly arranged flake layers, Dai and Steiner (1994b) modeled the mat structure of a multi-layered random flake mat. The model was applied to predict the compression behavior of a wood flake mat during pressing (Dai and Steiner 1993). The model prediction was reported to be in good agreement with experimental results except at pressure less than 1.5 MPa.

Lang and Wolcott (1996) characterized the spatial structure of randomly formed wood-strand mat with four variables: number of overlapping strands, gap between adjacent strands, location of the sampling column relative to strand length, and average height of the mat. They utilized stochastic modeling approach to simulate the structural characteristics of the mat. The model was then utilized in modeling the static stress-strain behavior of the mat during hot pressing. Because the model considered strand bending in the early stages of mat displacement to compute the cumulative stress, the model was able to predict the stress response of randomly formed mats with good accuracy over 0.01 MPa, considerably lower stress level than the model developed by Dai and Steiner (1993).

Lenth and Kamke (1996a, 1996b) conducted experimental work on formed mats to analyze the size and shape of voids and their distributions. They used digital images of small mat sample ends and edges to determine these void parameters. They examined both randomly oriented and controlled oriented mats in both directions of flake orientation. The parameters examined were all related to voids in the mat, such as void area in a given cross section, shapes and sizes of voids, and their distribution. They concluded that void size was not significantly affected by the direction of flake orientation, but void shape was by both the method of mat formation and the direction of flake orientation.

Steiner and Xu (1995) hypothesized that during hand-forming process of the mat, as flake size increases, the number of voids between adjacent elements in layers decrease in a unit area within one layer, while the size of voids increases. Moreover, element thickness, board thickness, raw material density, and board density were also shown to influence HDD.

Zombori et. al. (2001) developed a stochastic and deterministic model to simulate critical relationships between the processing parameters and the physical properties of OSB. Based on theories presented by earlier researchers (Dai and Steiner 1994a,b, Lang and Wolcott 1996) and data collected on industrial strands using an image analysis technique, a Monte-Carlo simulation model was developed for describing the spatial structure of a three-layer OSB. Simulated structural model would then serve as a basis for examining the heat and moisture transfer process during mat consolidation and predicting the physical properties of OSB.

Panel Structure Characterization

Panel structure could be described by several variables that characterize the way particles are arranged. These variables include particle orientation, void distribution and panel density, which can vary horizontally and vertically in a panel. Particle orientation should consider a particle's orientation not only in the plane of a panel, but also out of the plane. Much of the research done so far concentrated on in-plane particle orientation and panel density variation, horizontal and vertical.

Particle Orientation

Particle arrangement refers to the orientation of a particle within a composite relative to the global coordinates of the composite. The degree of orientation of the particles strongly influences the strength and stiffness of a wood composite. Influence of orientation in a wood composite, such as OSL or OSB, is at two levels: orientation of wood fiber in a strand relative to the strand coordinates, and orientation of the strand itself relative to the composite coordinates. Therefore, just as in a solid wood specimen, it is important to take into account the effects of fiber and particle orientations in a wood composite. Hearmon (1948), Kollmann and Cote (1968), Cave (1968), and Bodig and Jayne (1982) showed that most of the reduction in modulus of elasticity occurs at considerably small fiber angles. Similarly, it was found that slope of grain through the flake thickness also has significant influence on the strength of a flake-type structural particleboard (Heebink et al. 1975). Tests on ½-inch thick flakeboards made with 2-inch long flakes showed that the reduction in strength as related to slope in grain was almost identical to that in solid wood. A slope in grain of 1:5 reduced the tensile strength

parallel to the face by as much as 60 percent compared to the boards made with flakes that had no slope in grain through their thickness.

Several studies (Hse et al. 1975, Geimer 1976, 1979, 1986, Price 1977, Harris and Johnson 1982, Suzuki and Sekino 1982, Kuklewski et al. 1985, Shaler 1986, 1991, Shaler and Blankenhorn 1990, McNatt et. al. 1992, Sharma and Sharon 1993, Xu and Suchsland 1998, Barnes 2000, 2001, 2002, Xu 2002) were conducted on measuring and characterizing the in-plane alignment of particles and its effect on the strength and stiffness of structural composites. Due to the orthotropic nature of wood, each flake locally contributes to the directional properties of the board. Therefore, if most of the flakes are oriented in a particular board direction, the board will exhibit directional properties. It is generally accepted that orienting the length of the wood constituents in a structural composite product with its longitudinal axis maximizes the elastic and strength properties of the composite. McNatt et. al. (1992) tested strandboards manufactured with various combinations of random and aligned strands in static bending, uniform loading, and concentrated loading. Alignment of face strands improved the bending strength and stiffness of the boards in the direction of alignment and reduced the properties perpendicular to the direction of alignment. Degree of alignment in the core of the boards was found to have minimal effects on these properties. Internal bond strength and thickness swelling tests showed that alignment had no effect on either of the properties.

Geimer (1976) examined the effects of particle alignment machine variables, such as plate spacing and free fall distance, and particle geometry on the alignment of flakes. Flake length significantly influenced the degree of alignment, a maximum alignment of 26 percent was achieved by ¾-inch flakes while around 75 percent of alignment was

attained with 2- and 3-inch flakes. The effects of flake width and plate spacing were reported to be minimal. As free fall distance from the bottom of the alignment machine to the top of the mat increased the degree of alignment was reported to decrease. A free fall distance between 0.5-inch and 1-inch was found to optimize the flake alignment. A 1-inch increase in the free fall distance decreased particle alignment by 15 percent, and a 0.25-inch increase in vane gap decreased alignment by between 5 and 18 percent. Barnes (2000, 2001, 2002a,b) from his studies derived empirical relationships between vane gaps, height of the orienting device, and the degree of angular deviation.

From the studies conducted, Barnes (2000, 2001, 2002a) found that strength and stiffness of composite boards decreased with increasing angle of the grain to the applied stress; however, the rate of decrease, at low grain angles, was less from the cross-angled samples than for the parallel-oriented samples. It also tended to decrease with decreasing particle thickness.

Recent studies (Nishimura et. al. 2001, 2002, Nishimura and Ansell 2002) evaluated strand orientation on the surface of OSB using image analysis. Nishimura and Ansell (2002) monitored fiber orientation in OSB on a commercial factory production line using filtered image analysis technique. They reported that normal distribution described the shape of the fiber orientation distribution reasonably well.

Different methods have been used to characterize the degree of flake alignment in a structural composite, such as OSB. Geimer (1976, 1986) estimated average alignment angle from the ratio of MOE parallel to MOE perpendicular based on empirical results.

He also introduced percent flake alignment, a measure for the level of flake orientation, given by

$$percent\ flake\ alignment = [(45-A)/45]100 \qquad \textbf{Equation 2.1}$$

where A in degrees is the average of the absolute values of the flake angles measured relative to a line parallel to the long dimension of the panel. An alignment of 0% indicates a random flake alignment whereas 100% corresponds to perfect alignment. However, this measurement could be in error due to inaccuracies during trimming. In addition, percent flake alignment does not give any indication regarding the variability of flake alignment.

Xu (2002) proposed overall/effective percent alignment as a more realistic measure of strand alignment as it accounts for the variation in alignment through the thickness. Three methods, based on modulus of elasticity ratio, were presented for percent alignment measurement. These methods incorporated variation of alignment through thickness by varying the modulus of elasticity through thickness based on Hankinson's equation and volume fraction of strands oriented at angle according to the von Mises distribution. These methods were found to be sensitive to shelling ratio (total face weight/total weigth) and vertical density profile.

Other investigators (Harris and Johnson 1982, Shaler 1991) used a statistical distribution, namely von Mises distribution, to characterize particle orientation. This method is a measure of the mean flake angle and the variability in flake direction. It is specifically suited to describe axial data where directions separated by 180 degrees

represent identical physical conditions. Von Mises distribution is described by 2-parameters, μ and κ (Mardia 1972). The functional form of the von Mises probability density form is

$$f(\theta;\mu,\kappa) = \frac{1}{2\pi \mathbf{I}_o(\kappa)} e^{\kappa \cos 2(\theta-\mu)} \qquad \textbf{Equation 2.2}$$

where:

μ = mean direction,

κ = concentration parameter,

$\mathbf{I}_o(\kappa)$ = modified Bessel function of the first kind and order zero, and

θ = angle (radians) random variable ($0 \le \theta \le \pi$).

The concentration parameter, κ, is a measure of degree of concentration of the angles about the mean, μ. Therefor, if $\kappa = 0$, then the distribution of angles is uniform over 0 to π, and if $\kappa = \infty$ then all angles are concentrated at the mean angle, μ.

Density Variation

A finished panel is characterized by a non-homogeneous distribution of mass throughout the panel primarily due to forming and pressing operations. As a result, wood composite panels manifest three-dimensional density variation that can be sub-divided into a horizontal density distribution (HDD) and a vertical density profile (VDP) (Suchsland 1962). The HDD represents the density variation throughout the plane of a panel, while the VDP describes the density variation through the thickness of a panel.

An understanding of these density variations in wood composites is necessary because density influences many physical and mechanical properties of a panel (Strickler

1959, Plath and Schnitzler 1974, Steiner et. al. 1978, Zhou 1990). Some of the physical and mechanical properties which are influenced by density include: modulus of elasticity (Rice and Carey 1978, Zhou 1990, Xu and Suchsland 1998), modulus of rupture (Rice and Carey 1978, Hse 1975, Zhou 1990, Wong et. al. 1998, Kwon and Geimer 1998), tensile strength perpendicular to panel surfaces (Heebink et. al. 1972, Plath and Schnitzler 1974, Steiner et. al. 1978, Wong et. al. 1998), shear strength (Shen and Carroll 1969 and 1970), thickness swell and water absorption (Rice and Carey 1978, Zhou 1990, Winistorfer and Wang 1999, Winistorfer and Xu 1996, Xu and Winistorfer 1995a, b), linear expansion (Suzuki and Miyamoto 1998, Kelly 1977) and fastener properties (Zhou 1990).

Horizontal Density Distribution (HDD)

Horizontal density distribution is a function of particle geometry and forming. It is a result of variation in number of overlapping particles from one location to another within a mat that is pressed to a constant thickness. HDD leads to differential thickness swelling between areas of varying density resulting in damaging stresses in a panel (Suchsland 1962, 1973, Linville 2000).

Linville (2000) characterized the thickness swelling coefficients and the constitutive relations in tension and compression for an oriented strand composite and related them to density, resin content and moisture content. Increased resin content and decreased moisture content improved all panel properties, but increased density while enhancing the mechanical properties degraded the swelling properties.

Suchsland and Xu (1989, 1991) showed that large HDD variations in carefully fabricated flakeboard with controlled HDD variation would result in the development of

damaging stresses in a panel undergoing hygroscopic swelling. Steiner and Xu (1995) proved that the apparent HDD in wood composites is dependent on the size of the specimens used to measure the density variations. They observed that particle size affected the variability of the HDD, but this effect was also dependent on specimen size. Smaller specimen sizes exhibit more variability in density than larger specimen sizes. This dependency was attributed to void frequency and size. They also state that board uniformity would increase with an increase in the number of layers, thus indicating that thinner elements result in more uniform horizontal density distribution.

Dai and Steiner (1994a, b) discuss variables, such as flake centers and number of flakes, that govern the formation of a random flake mat. They note that the distribution of these variables and point density in a panel could be described by Poisson distribution. Horizontal density variation in a random flakeboard panel is a result of non-uniform flake coverage distribution. Dai (1994) presents a probability based mathematical model to describe the variances of point density and zone density averages in a flakeboard panel.

Bozo (2002) examined several statistical tools to describe horizontal density variation in panels and showed that there was an indication of spatial dependence for density, both along and across machine directions. Considering local density variation in mechanical analysis of OSB panels under concentrated static load was shown to be more appropriate than using an average global density. A clear relationship between density and mechanical properties was shown and regression model was developed between density and mechanical properties.

Vertical Density Profile (VDP)

Vertical density profile (VDP) is a result of the interaction of variables during hot pressing process. Factors affecting the formation of VDP include moisture content, temperature, and pressure in the mat during pressing (Strickler 1959, Suchsland 1962, Wolcott et. al. 1990, Winistorfer and Wang 1999, Wang and Winistorfer 2000). These parameters can be manipulated through changes in pressing schedule, method of heating, particle geometry, and particle alignment. Heat transfer to the core of the mat was found to accelerate by a short press closing time and higher moisture content face particles. Short press closing time and low moisture content face flakes also tend to increase face densities.

Temperature and moisture vary throughout the panel during pressing and change during the press cycle (Suchsland 1962, Kamke and Casey 1988, Kamke and Wolcott 1991). This results in the wood particles having a variable compressive modulus throughout the press cycle. Wood elements with low moduli will compress more than those with high moduli at a given pressure. This differential compression through the thickness of the panel results in the VDP (Kamke and Casey 1988). While it was formerly believed that VDP was formed during press closure (Kelly 1977, Suo and Bowyer 1994), recent work suggests that VDP continues to change throughout the press cycle (Wolcott et. al. 1990, Winistorfer et. al. 2000, Wang and Winistorfer 2000).

Harless et. al. (1987) and Suo and Bowyer (1994) attempted to model heat and moisture conditions in a wood composite mat during pressing and developed computer simulations to predict the VDP in a board. Their models assumed thermodynamic equilibrium at any point in the mat. Compared to the observed profiles in boards, their

model predictions of VDP were significantly different. Another model presented by Kamke and Wolcott (1991) predicted that individual flakes in the mat would not be at equilibrium moisture content, but that a significant moisture gradient would be expected in individual flakes. Inputs to the model include measured temperature and gas pressure from the mat.

Process variables, such as furnish moisture content, particle geometry, platen temperature, rate of press closure, and alternate heating methods, have an effect on vertical density profile of a composite panel. An increase in moisture content throughout the mat will cause a more pronounced difference between core and surface densities of a board (Strickler 1959, Andrews and Winistorfer 1999). Strickler (1959) showed that high moisture content in the surface layers of a particleboard, relative to the core moisture content, would cause a steeper density gradient from the surface to the core. Wong et. al. (1998) obtained higher peak densities for panels pressed with high moisture surfaces compared to panels with uniform furnish moisture content. Neither of these studies investigated the effect of high moisture in the core relative to the surface. Heebink et. al. (1972) found that the density profile could be reversed with high moisture content in the core relative to the surface.

Garcia et. al. (1999) investigated the effect of particle alignment on heat and mass flow in OSB mats during pressing. From their observations of particle alignment positively influencing longitudinal permeability and negatively influencing transverse thermal convection, they deduct that poorly aligned mats should result in flatter density profiles. Smith (1982), based on the work of Geimer et. al. (1975) and Denisov et. al.

(1975), stated that particle geometry would influence the VDP by changing the rate of moisture migration.

Suzuki and Miyamoto (1998) showed that smaller vertical density variation results in higher density boards and the peak density tends to shift inward as the overall board density increases. Increase in platen temperature was shown by Heebink et. al. (1972) to produce a more uniform density profile. However, Suchsland and Woodson (1974) found a more pronounced density gradient with higher platen temperatures.

Pressing schedule also effects formation of VDP in composite panels. Longer press closing times was shown to decrease peak density and move it inward (Strickler 1959). Supporting this observation, Suchsland and Woodson (1974) showed that long press closing times or low pressures would tend to flatten out the VDP. Their study also indicated that very short press times or high pressures, on the other hand, could actually decrease the surface density of a board compared to a moderate press closing time. Smith (1982) and Heebink et. al. (1972) found that a short press closing time would result in higher densification of the surfaces of a board. More recently Wang et. al. (1999, 2000) showed that step closing of the press could be used to effectively manipulate the VDP to produce more uniform core densities and less density variation through a section. Steam injection pressing and high frequency heating can be effectively used to minimize changes in density through the thickness of the board (Jieying et. al. 1997, Kwon and Geimer 1998, Geimer and Kwon 1999a, b, Carll 1979). As Suchsland (1962) points out if conditions through the thickness of the mat were uniform during the entire press cycle, no VDP would be formed.

As discussed earlier, since density affects several mechanical and physical properties, VDP also impacts several of these properties. Xu (1999) considered a non-uniform VDP using laminate theory to model composite MOE. He showed that the core stiffness of a composite board has little influence on MOE, and the layers near the surface control the MOE. Similarly, a panel with high densities at the surfaces should have an increased MOR because flexure of a linearly-elastic beam causes the highest stresses to be developed at the surfaces. In support of this argument, Heebink et. al. (1972) showed a strong correlation between face layer density and MOR. Several studies (Rice and Carey 1978, Hse 1975, Steiner et. al. 1978, Wong et. al. 1998, Kwon and Geimer 1998, Kelly 1977) reported that an increase in MOR and internal bond (IB) could be expected with an increase in density. Plath and Schnitzler (1974) compared the IB measured on a layer basis with its density profile and observed that IB profile trends closely followed the VDP. A uniform vertical density profile should yield maximum IB values because all layers of the board would have similar strength. In a specimen with varying VDP, internal bond behavior would be highly influenced by the layer with the lowest density value.

Prediction of Mechanical Properties, Specifically Elastic Properties

Empirical, analytical and theoretical models have been suggested by different researchers over the years to predict mechanical properties of oriented strand composites based on the arrangement of their constituents and their properties. Hoover et al. (1992) developed empirical regression models relating various properties to flake length and thickness, board density, a stress-wave timing alignment value and an error term. All

factors were experimentally determined. The models predicted some properties well and some poorly and are limited to flakes that are either 2 or 3 inches long and 0.015 or 0.025 inches thick. The models described parallel tensile modulus to within 18% of actual values with a COV of 56.2%. No practical difference existed in properties for the strand geometries evaluated. Another model developed by Lehmann (1974) with similar variables had r^2 of 0.878; however, model versatility was limited by short flake lengths of only 0.5, 1, and 2 inches. These strands are much shorter than the strands currently used in OSL manufacturing.

Geimer (1979) studied relationships between specific gravity and physical and mechanical properties of reconstituted wood flakes. He derived empirical relationships between bending, tension, and compression values of MOE or MOR and the variables of specific gravity and flake alignment for flakeboards made with uniform vertical density profiles. The equation developed described the relationship reasonably well over a broad range of specific gravity (0.4 to 1.2) and flake alignments (0 to 74%). When the relationship was used to predict the properties of a board with a vertical density profile, the accuracy was generally within the range of ± 20%.

Dong (1979) conducted a comprehensive study examining the effects of in-plane flake orientation on mechanical properties of flakeboards. He tested flakeboard specimens in tension, compression, shear, and bending at various angles of stress orientation to the axis of flake alignment. Western white pine and aspen flakes, with nominal dimensions of 1.5 by 0.5 by 0.012 inches, were used to manufacture boards. Flakeboard strength was predicted using maximum stress theory, distortional energy theory, and Hankinson's formula. Hankinson's formula was reported to be the best in

predicting the axial and bending properties for oriented flakeboards. Best fit values for the exponent, λ or n, in Hankinson's equation varied according to the properties and were different from the standard value of 2.0 for solid wood. For predicting compression modulus, he found that transformation equation fit the experimental data better than Hankinson's equation with the usual exponent of 2.0. However, the best fit λ for Hankinson's formula for compression modulus of elasticity was 2.60 for both aspen and white pine flakeboards.

Dong (1979) analyzed the failure modes under various loading conditions and reported that in longitudinal tension flakes failed such that fiber cross-section was exposed without any separation along the fiber walls. Shear failure was reported to be primarily due to lengthwise fiber fracture. In compression, he found two modes of buckling based on the degree of flake orientation. Flakeboards with flake alignment between 0 and 15 degrees failed in the "shear" mode, where as flakeboards with flake orientation greater than 30 degrees failed in the "extension" mode (Figure 1). Fibers buckling out of phase relative to one another extend or contract the matrix in the transverse direction, where as fibers buckling in phase with one another subject matrix to shearing deformation (Jones 1999).

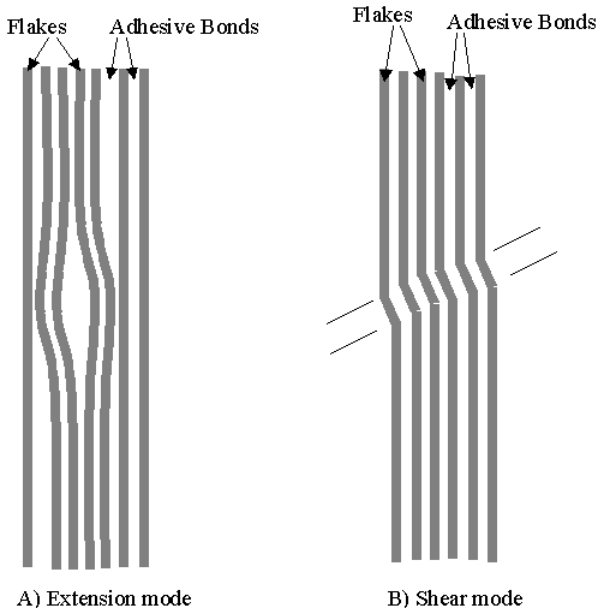

Figure 2. 1. Possible failure modes in specimens under compression parallel to the length direction (Dong 1979).

Jahan-Latibari (1982) proposed several mathematical models for MOR and MOE analysis of flakeboard based on flake property and amount of surface activator applied to flakes. Coefficient of regression (r^2) was greater than 0.90 when predicting board MOR from flake MOR; coefficients of regression were slightly lower for predicting board MOE from flake MOE; and, r^2 of models predicting board IB from flake MOR or MOE were around 0.80 and 0.75. Models proposed in this study were empirical and the results are limited to the specific data set used.

Analytical models were developed by Simpson (1977) and Triche and Hunt (1993) to predict the tensile properties of a parallel-aligned strand composite based on strand and resin properties. Simpson's model determines the tensile strength of flakeboard in the direction of flake orientation based on flake tensile strength, adhesive bond shear strength, and ratio of number of flakes that fail in tension to number of flakes

that pull out because of shear failure between flakes. The problem with this model is that it oversimplifies the failure mechanism.

Model developed by Triche and Hunt (1993) incorporated finite element method to model the strands and resin of the composite, and used a sub-structuring routine to take advantage of the composite's repeating nature. Extensive nondestructive testing was used to characterize the size and stiffness of strands. This data was then used to divide the strands into stiffness (E) classes including random (strands of random stiffness), extreme (strands of high and low stiffness), low, high, and medium. Inputs to the model included orthotropic properties of strands, resin properties, and properties of the wood-resin interface. Wood-resin interface was modeled with an addition of a layer of elements between the elements that represented wood strands and adhesive layer. A combination of experimental and finite element analysis was utilized to determine the properties of wood-resin interface. The E of the interface region was determined to be 1.69 times the E of the strand. However, the effect of manufacturing parameters on strand properties was not considered. The model accurately predicted the stiffness of hand laid laminates manufactured with certain class of strands. For laminates with different class strands, the model had a maximum error of 101.1%.

Xu and Suchsland (1998) derived a volume-based rule of mixtures model for composite modulus of elasticity by equating the total work applied to the specimen by the external force to internal energy stored in the specimen. However, they assume that the wood composite panel has a uniform vertical density profile. The initial objective of their model was to gain an understanding of the relationship between MOE and various manufacturing parameters. The conclusions drawn from their simulation were that size

of the particle does not influence MOE, out-of-plane and in-plane orientations of particles have a significant effect on MOE, and increase in board density or compaction ratio linearly increases MOE.

Suo and Bowyer (1995) presented a simulation modeling technique to predict board mechanical properties that included effective MOE, MOR, and IB. Effective MOE was modeled based on a board density profile, while MOR was modeled based on MOE values of the board layers. Internal bond strength was modeled using a modified regression equation. MOE of each layer was determined by integrating flake MOE over a full range of possible ring and grain angles of wood by applying Hankinson's formula. Board MOE was then determined based on the mechanics of composite materials by taking into account all the moduli of the layers. The model was reasonably accurate for predicting MOE and MOR.

Shaler (1986) and Shaler and Blankenhorn (1990) analyzed the quantitative influence of species, adhesive level, particle orientation, board density, and other parameters, such as volume fractions of composite constituents, to predict board elastic moduli using composite theories that have been proposed for non-wood composite materials. The composite theories investigated were longitudinal and transverse rule of mixtures, Halpin-Tsai equations, finite fiber length model, and inclusion shape model. The species they worked on were red maple (Acer rubrum) and bigtooth aspen *(Populus grandidentata*, Mich.). The researchers concluded that needle shaped inclusion and finite fiber length models worked best for predicting parallel to flake alignment elastic moduli of specimens; whereas, transverse Halpin-Tsai theory was better at estimating elastic moduli of specimens oriented perpendicular to the flake alignment direction. However,

even the models that worked the best could explain only 70% of the variation in elastic moduli. Predicted values averaged on the order of 65-70% of experimental values. From this study, one could probably conclude that the composite theories applied are not effective in estimating wood-composite elastic moduli.

Mundy and Bonfield (1998) applied short fiber composite theories to predict the short-term properties of chipboard made with Scots pine chips and urea formaldehyde resin. According to the authors, the rule of mixtures equation predicted the strength and stiffness reasonably well (differences of 28 and 34 percent from experimental results). The underlying assumptions made by the investigators was that the chips were aligned parallel to the direction of applied stress and were having cylindrical geometry. This assumption would be violated by most wood composites where strands are not perfectly aligned with the direction of applied stress either in the plane or out of the plane. The authors also calculated the critical fiber length based on the Cox model and found it to be far lower than the length of chips (0.8 mm critical fiber length); thus, majority of the chips would fracture under stress than pull out of the matrix.

Wang and Lam (1999) developed empirical relationships for MOR and MOE using three dimensional surface maps to generate quadratic regression models based on flake slenderness ratio, orientation, and board density. An integrated model was recently developed by Barnes (2000, 2001, 2002a, 2002b) that considers the effect of processing parameters on the strength properties of oriented strand products such as OSB and OSL. The model estimates the composite strength properties from the input wood property and eight parameter factors, such as wood content, adhesive content, in-plane strand orientation, strand length, strand thickness, fines content, gap between discs or vanes, and

free-fall distance of the strands while mat formation. Empirical equations were developed by the investigator to calculate these parameters. Model predictions were within ± 10% of the experimental values for both MOE and MOR.

A recent study by Meyers (2001) compared test data with predicted elastic properties of oriented strand composites from a model developed by Barnes (2000), the Hankinson equation and tensor transformation, using either the mean angle or rule of mixtures (ROM) with a distribution of angles. The study concluded that Barnes' (2000) model predicted properties best on average for the range of data used, although tensor transformation and ROM in conjunction with the normal distribution predicted properties nearly as well with more consistency. In agreement with Xu and Suchsland's (1998) model that size of the particle does not influence composite's MOE, Meyers' (2001) study also concluded that strand geometry does not significantly influence oriented strand composite properties when strand orientation is considered. Strand geometry indirectly influences the composite properties through its interaction with the mechanical orienting device. Therefore, if a method independent of strand geometry is devised to orient the strands, the mechanical properties of oriented strand composites should not be affected by strand length or width.

Summary

Modeling of wood composite structure is becoming more economical and feasible with the advent of computer technology. But, to develop effective models it is imperative to characterize the structure of wood composites and understand how they affect the composite behavior and the level of their significance. The following paper is an attempt

to review research work done in characterization of oriented strand composites and modeling of their elastic behavior. A potential benefit of developing a database of wood composites' structure and attempting to model their physical and mechanical behavior is the ability to engineer a wood composite product according to the intended end use.

References

Andrews, C. K., P. M. Winistorfer, and R. M. Bennett. 2001. The influence of furnish moisture content and press closure rate on the formation of the vertical density profile in oriented strandboard. Forest Products Journal. 51(5):32-39.

Barnes, D. 2000. An integrated model of the effect of processing parameters on the strength properties of oriented strand wood products. Forest Products Journal. 50(11/12):33-42.

_____. 2001. A model of the effect of strand length and strand thickness on the strength properties of oriented wood composites. Forest Products Journal. 51(2):36-46.

_____. 2002a. A model of the effect of strand angle and grain angle on the strength properties of oriented veneer and strand wood composites. Forest Products Journal. 52(4):39-47.

_____. 2002b. A model of the effect of orienter design and operating variables on the mean angular deviation of oriented wood strands. Forest Products Journal. 52(7/8):63-71.

Bodig, J. and J. R. Goodman. 1973. Prediction of Elastic Parameters for Wood. Wood Science. 5(4):249-264.

_____ and B. A. Jayne. 1982. Mechanics of wood and wood composites. Van Nostrand Reinhold Company, New York, NY.

Bozo, A. M. 2002. Spatial variation of wood composites. Ph.D. Dissertation. Dept. of Civil and Environmental Engineering, Washington State University. 98 pp.

Brumbaugh, J. 1960. Effect of flake dimensions on properties of particle boards. Forest Products Journal. May:243-246.

Berchem, A., I. White, and M. Gosselin. 1985. The effects of resin content and particle geometry on structural board property and production costs. Proceedings of the 19th International Particleboard/Composite Materials Symposium. Washington State University. Pullman, Washington. 349-361.

Carll, C. G. 1979. The effect of platen temperature on the pressing time and properties of dielectrically cured particleboards. Master's Thesis, University of Idaho. 69 pages.

Cave, I. D. 1968. The Anisotropic Elasticity of the Plant Cell Wall. Wood Science and Technology. 2(4):268-278.

Dai, C. and P. R. Steiner. 1993. Compression behavior of randomly formed wood flake mats. Wood Science and Technology. 25(4):349-358.

Dai, C. 1994. Modelling structure and processing characteristics of a randomly-formed wood-flake composite mat. Ph.D. Dissertation. Dept. of Forestry, The University of British Columbia. 141pp.

Dai, C. and P. R. Steiner. 1994a. Spatial structure of wood composites in relation to processing and performance characteristics: Part II. Modelling and simulation of a randomly-formed flake layer network. Wood Sci. Technol. 28:135-146.

Dai, C. and P. R. Steiner. 1994b. Spatial structure of wood composites in relation to processing and performance characteristics: Part III. Modelling the formation of multi-layered random flake mats. Wood Sci. Technol. 28(3):229-239.

Denisov, O. B., P. P. Anisou, and P. E. Zuban. 1975. Investigation of the permeability of particle mats. Holztechnologie. 16(1):10-14.

Dinwoodie, J. M. 1997. The nature and behaviour of wood-based composites. Proceedings of the First European Panel Products Symposium. Edited by Hague, Loxton, Bolton and Mott. The BioComposites Centre, UWB, Bangor, Gwynedd.

Dong, Chung-Ching. 1979. The mechanical properties of flakeboards related to flake orientation. Ph.D. Dissertation. College of Engineering, Washington State University. 157pp.

Galligan, W. L. 1975. Mechanical properties of wood. In Wood Structures, pp. 32-54. New York: Am. Soc. Civil Eng.

Garcia, P., S. Avramidis, and F. Lam. 1999. Oriented-strand-board hot-pressing and flake orientation. Proceedings of the 4th International Conference on the Development of Wood Science, Wood Technology, and Forestry. Missenden Abbey, UK. 365-373.

Gardner, D. J., D. w. Gunnells, M. P. Wolcott, and L. Amos. 1993. Changes in wood polymers during the pressing of wood-composites. In Cellulosics: Chemical, Bichemical and Material Aspects. Editors J. F. Kennedy, G. O. Phillips, and P. A. Williams. Ellis Horwood, New York, NY. pp 513-518.

Geimer, R. L., H. M. Montrey, and W. F. Lehmann. 1975. Effects of layer characteristics on the properties of three-layer particlboards. Forest Products Journal. 25(3):19-29.

_____. 1976. Flake alinement in particleboard as affected by machine variables and particle geometry. USDA Forest Service Research Paper FPL 275. 16 pp.

_____. 1979. Data basic to the engineering design of reconstituted flakeboard. In Proceedings of the 13t^{h} Washington State University International Symposium on Particleboard. pp. 105-125.

_____, R. J. Mahoney, S. P. Loehnertz, and R. W. Meyer. 1985. Influence of processing-induced damage on strength of flakes and flakeboards. USDA Forest Service Research Paper FPL 463. 15 pp.

_____. 1986. Mechanical property ratios: A measure of flake alignment. USDA Forest Service Research Paper FPL 468. 10 pp.

_____ and J. H. Kwon. 1999a. Flakeboard thickness swelling. Part I. Stress relaxation in a flakeboard mat. Wood and Fiber Science. 30(4):326-338.

_____ and J. H. Kwon. 1999b. Flakeboard thickness swelling. Part II. Fundamental response of board properties to steam injection pressing. Wood and Fiber Science. 31(1):15-27.

Generalla, N. C., E. J. Biblis, and H. F. Carino. 1989. Effect of two resin levels on the properties of commercial southern pine OSB. Forest Products Journal. 39(6):64-68.

Goodman, J. R. and J. Bodig. 1970. Orthotropic elasticity properties of wood. Journal of the Structural Division. Proceedings of the American Society of Civil Engineers. ST 11: 2301-2319.

Harless, T. E., F. G. Wagner, P. H. Short, R. D. Seale, P. H. Mitchell, and D. S. Ladd. 1987. A model to predict the density profile of particleboard. Wood and Fiber Science. 19(1):81-92.

Harris, R. A. and Johnson, J. A. 1982. Characterization of flake orientation in flakeboard by the von Mises probability distribution function. Wood and Fiber 14(4):254-266.

Hearmon, R. F. S. 1948. The elasticity of wood and plywood. Department of Scientific and Industrial Research, Forest Products Research Special Report No. 7. London. 88 pp.

Heebink, B. G., W. F. Lehmann, and F. V. Hefty. 1972. Reducing particleboard pressing time: exploratory study. Research paper FPL-180. USDA Forest Service, Forest Products Laboratory. Madison, Wisconsin.

_____. 1975. Grain angle through flake thickness: effect on properties of a structural flakeboard. USDA Forest Service Research Paper FPL 257. 5p.

Hoover, W. L., M. O. Hunt, R. C. Lattanzi, J. H. Bateman, J. A. Youngquist. 1992. Modeling Mechanical Properties of Single-Layer, Aligned, Mixed-Hardwood Strand Panels. Forest Products Journal. 42(5):12-18.

Hse, C. 1975. Properties of flakeboards from hardwoods growing on southern pine sites. Forest Products Journal. 25(3):48-53.

_____, P. Koch, C. W. McMillin, and E. W. Price. 1975. Laboratory-scale development of a structural exterior flakeboard from hardwoods growing on Southern Pine sites. Forest Products Journal. 25(4):42-50.

Jahan-Latibari, A. 1982. The response of aspen flakes and flake-board to flake surface modifications. Proceedings of 6th Washington State University International Symposium on Particleboard. pp. 331-351.

_____. 1982. The response of aspen flakes and flakeboard to flake surface modifications. Ph.D. Dissertation, Washington State University. 135pp.

_____, W. E. Johns, R. V. Subramanian. 1984. Technique for isolating flakes from the pressed mat. Forest Products Journal. 34(2):33-34.

Jones, R. M. 1999. Mechanics of Composite Materials. 2nd Edition. Taylor & Francis. Philadelphia, PA. pp. 171-183.

Jieying, W., L. Zhengtian, C. Wenbin. 1997. Comparison between steam-injection pressing and conventional hot pressing in producing poplar particleboards. Part 1: effects of steam-injection on mechanical strengths of particleboards. Journal of Beijing Forestry University (English Ed.). 6(1):72-78.

Jorgensen, R. N. and W. K. Murphey. 1961. Particle geometry and resin spread: Its effect on thickness and distribution of glue-line in oak flakeboard. Forest Products Journal. Dec.: 582-585.

Kallmes, O. and H. Corte. 1960. The structure of paper: I. Statistical geometry of an ideal two dimensional fiber network. Tappi. 43(9):737-752.

_____, _____, and G. Bernier. 1961. The structure of paper: II. The statistical geometry of a multiplanar fiber network. Tappi. 44(7):519-528.

Kamke, F. A. and L. J. Casey. 1988a. Fundamentals of flakeboard manufacture: internal-mat conditions. Forest Products Journal. 38(6):38-44.

_____ and _____. 1988b. Gas pressure and temperature in the mat during flakeboard manufacture. Forest Products Journal. 38(3):41-43.

_____ and M. P. Wolcott. 1991. Fundamentals of flakeboard manufacture: wood-moisture relationships. Wood Science and Technology. 25:57-71.

Kelly, M. W. 1977. Critical literature review of relationships between processing parameters and physical properties of particleboard. USDA Forest Service General Technical Report FPL-10. 65pp.

Knudson, R. M. 1992. PSL 300^{TM} LSL: The challenge of a new product. Proceedings of 26th Washington State University International Symposium on Particleboard. pp. 206-214.

Kollmann, F. F. P. and W. A. Cote Jr. 1968. Principles of wood science and technology: I. Solid wood. Springer-Verlag. New York, Inc., NY. pp.292-419.

Kuklewski, K. M., P. R. Blankenhorn, and L. E. Rishel. 1985. Comparison of selected physical and mechanical properties of red maple (*Acer Rubrum L.*) and aspen (*Populus Grandidentata* Michx.) flakeboard. Wood and Fiber Science. 17(1):11-21.

Kwon, J. H. and R. L. Geimer. 1998. Impact of Steam pressing variables on the dimensional stabilization of flakeboard. Forest Products Journal. 48(4):55-61.

Lang, E. M. and M. P. Wolcott. 1996. A model for viscoelastic consolidation of wood-strand mats. Part I. Structural characterization of the mat via Monte Carlo simulation. Wood and Fiber Science. 28(1):100-109.

Laufenberg, T. L. 1984. Flakeboard fracture surface observations and correlation with orthotropic failure criteria. Journal of Institute of Wood Science. 10(2):57-65.

Lehmann, W. F. 1974. Properties of Structural Particleboards. Forest Products Journal. 24(1):19-26.

Lenth, C. A. and F. A. Kamke. 1996a. Investigations of flakeboard mat consolidation. Part I. Characterizing the cellular structure. Wood and Fiber Science. 28(2):153-167.

_____ and _____. 1996b. Investigations of flakeboard mat consolidation. Part II. Modeling mat consolidation using theories of cellular materials. Wood and Fiber Science. 28(3):309-319.

Linville, J. D. 2000. The influence of a horizontal density distribution on moisture-related mechanical degradation of oriented strand composites. Master's Thesis. Dept. of Civil and Environmental Engineering, Washington State University. 121pp.

Lu, C., P. R. Steiner, and F. Lam. 1998. Simulation study of wood-flake composite mat structures. Forest Products Journal. 48(5):89-93.

Mahoney, R. J. 1980. Physical changes in wood particles induced by the particleboard hot-pressing operation. M.S. Thesis. Washington State University. 35pp.

Mardia, K. V. 1972. Statistics of directional data. Academic Press, New York, NY.

Marra, A. A. 1992. Technology of wood bonding: Principles in practice. Van Nostrand Reinhold, New York, NY.

Meyers, K. L. 2001. Impact of strand geometry and orientation on mechanical properties of strand composites. Master's Thesis. Washington State University. 115pp.

McNatt, J. D. and M. J. Superfesky. 1984. How some test variables affect bending, tension, and compression values for particle panel products. USDA Forest Service Research Paper FPL 446. 9pp.

_____ and R. C. Moody. Structural Composite Lumber. Progressive Architecture 12.90:34-36.

_____, L. Bach, and R. W. Wellwood. 1992. Contribution of flake alignment to performance of strandboard. Forest Products Journal. 42(3):45-50.

Mundy, J. S. and P. W. Bonfield. 1998. Predicting the short-term properties of chipboard using composite theory. Wood Science and Technology. 32:237-245.

Nelson, S. 1997. Structural Composite Lumber. Engineered Wood Products: A Guide for Specifiers, Designers and Users. Edited by Stephen Smulski. PFS Research Foundation, Madison, WI. pp. 147-172.

Nishimura, T., M. P. Ansell, and N. Ando. 2001. The relationship between the arrangement of wood strands at the surface of OSB and the modulus of rupture determined by image analysis. Wood Science and Technology. 35:555-562.

_____, _____, and _____. 2002. Evaluation of the arrangement of wood strands at the surface of OSB by image analysis. Wood Science and Technology. 36:93-99.

_____ and M. P. Ansell. 2002. Monitoring fiber orientation in OSB during production using filtered image analysis. Wood Science and Technology. 36:229-239.

Plath, E. and E. Schnitzler. 1974. The density profile, a criterion for evaluating particleboard. Holz asl Roh-und Werkstoff. 32:443-449.

Post, P. W. 1958. Effect of particle geometry and resin content on bending strength of oak flake board. Forest Products Journal. Oct.:317-322.

_____. 1961. Relationship of flake size and resin content to mechanical and dimensional properties of flake board. Forest Products Journal. Jan.:34-37.

Price, E. W. 1976. Determining tensile properties of sweetgum veneer flakes. Forest Products Journal. 26(10):50-53.

_____. 1977. Basic properties of full-size structural flakeboards fabricated with flakes on a shaping lathe. Proceedings of the 11th Washington State University International Symposium on Particleboard. pp. 331-332.

Rice, J. T. and R. H. Carey. 1978. Wood density and board composition effects on phenolic resin-bonded flakeboard. Forest Products Journal. 28(4):21-28.

_____. 1982. Compaction ratio and resin coverage effects on properties of thick, phenolic-bonded flakeboard. General Technical Report So-53. USDA Forest Service. Southern Forest Experiment Station. 103-118.

Shaler, M. S. 1986. The usefulness of selected polymer composite theories to predict the elastic moduli of oriented flakeboard. Ph.D. Dissertation. Penn State University. 162 pp.

_____ and P. R. Blankenhorn. 1990. Composite model prediction of elastic moduli for flakeboard. Wood and Fiber Science. 22(3):246-261.

_____. 1991. Comparing two measures of flake alignment. Wood Sci. Technol. 26:53-61.

Sharma, V. and A. Sharon. 1993. Optimal orientation of flakes in oriented strand board (OSB). Experimental Mechanics. June:91-98.

Shen, K. C. and Carroll, M. N. 1969. A new method for evaluation of internal strength of particleboard. Forest Products Journal. 19(8):17-22.

Shen, K. C. and Carroll, M. N. 1970. Measurement of layer-strength distribution in particleboard. Forest Products Journal. 20(6):53-55.

Shupe, T. F., C. Y. Hse, and E. W. Price. 2001. Flake Orientation Effects on Physical and Mechanical Properties of Sweetgum Flakeboard. Forest Products Journal. 51(9):38-43.

Simpson, W. T. 1977. Model for tensile strength of oriented flakeboard. Wood Science. 10(2):68-71.

Smith, D. C. 1982. Waferboard press closing strategies. Forest Products Journal. 32(3):40-45.

Song, D., and S. Ellis. 1997. Localized properties in flakeboards: A simulation using stacked flakes. Wood and Fiber Science. 29(4):353-363.

Steiner, P. R., L. A. Jozsa, M. L. Parker, and S. Chow. 1978. Application of x-ray densitometry to determine density profile in waferboard: relationship of density to thickness expansion and internal bond strength under various cycles. Wood Science. 11(1):48-55.

_____ and C. Dai. 1993. Spatial structure of wood composites in relation to processing and performance characteristics: Part I. Rationale for model development. Wood Sci. Technol. 28:45-51.

_____ and W. Xu. 1995. Influence of flake characteristics on horizontal density distribution of flakeboard. Forest Products Journal. 45(4):61-66.

Strickler, M. D. 1959. Effect of press cycles and moisture content on properties of Douglas-fir flakeboard. Forest Products Journal. July:205-215.

Suchsland, O. 1959. An analysis of the particle board process. Michigan Quarterly Bulletin, 42(2):350-372.

_____. 1962. The density distribution in flakeboard. Michigan Quarterly Bulletin, Agricultural Experiment Station, Michigan State University, East Lansing Michigan. 45(1):104-121.

_____. 1967. Behavior of a particleboard mat during the press cycle. Forest Products Journal. 17(2):51-57.

_____. 1968. Particle-board from Southern Pine. Southern Lumberman. December 15:139-144.

_____. 1973. Hygroscopic thickness swelling and related properties of selected commercial particleboards. Forest Products Journal. 23(7):26-30.

_____ and G. E. Woodson. 1974. Effect of press cycle variables on density gradient of medium-density fiberboard. 375-396. In Proceedings of the Eighth Washington State University Symposium on Particleboard. Washington State University, Pullman, WA.

_____ and J. D. McNatt. 1986. Computer simulation of laminated wood panel warping. Forest Products Journal. 36(11/12):16-23.

_____ and H. Xu. 1989. A simulation of the horizontal density distribution in a flakeboard. Forest Products Journal. 39(5):29-33.

_____ and H. Xu. 1991. Model analysis of flakeboard variables. Forest Products Journal. 41(11/12):55-60.

Suzuki, M. and N. Sekino. 1982. Anisotropic elasticity of oriented flakeboard. Mokuzai Gakkaishi. 28(2):91-96.

Suzuki, S. and K. Miyamoto. 1998. Effect of manufacturing parameters on the linear expansion and density profile of particleboard. Journal of Wood Science. 44:444-450.

Suo, S. and J. L. Bowyer. 1995. Modeling of strength properties of structural particleboard. Wood and Fiber Science. 27(1):84-94.

Triche, M. H. and M. O. Hunt. 1993. Modeling of parallel-aligned wood strand composites. Forest Products Journal. 43(11/12):33-44.

Tsoumis, G. 1991. Science and Technology of Wood: Structure, Properties, Utilization. Van Nostrand Reinhold, New York.

U.S. Department of Agriculture. 1987. Wood Handbook. Agriculture Handbook No. 72, Superintendent of Documents, Washington D.C. 466pp.

Wang, K and F. Lam. 1999. Quadratic RSM Models of Processing Parameters for Three-layer Oriented Flakeboard. Wood and Fiber Science. 31(2):173-186.

Wang, S. and P. M. Winistorfer. 2000. Fundamentals of vertical density profile formation in wood composites, Part II: Methodology of vertical density formation under dynamic conditions. Wood and Fiber Science. 32(2):220-238.

_____, P. M. Winistorfer, T. M. Young, and C. Helton. 1999. Step-closing pressing of medium density fiberboard, Part 1: Influences on the vertical density profile. For publication in Holz als Roh-und Werkstoff.

_____, P. M. Winistorfer, W. W. Moschler, and C. Helton. 2000. Hot-pressing of oriented strandboard by step-closure. Forest Products Journal. 50(3):28-34.

Watkinson, P. J. and N. L. van Gosliga. 1990. Effect of humidity on physical and mechanical properties of New Zealand wood composites. Forest Products Journal. 40(7/8):15-20.

Winistorfer, P. M., W. C. Davis, and W. W. Moschler, Jr. 1986. A direct scanning densitometer to measure density profiles in wood composite products. Forest Products Journal. 36(11/12):82-86.

_____, E. V. DePaula, and B. L. Bledsoe. 1993. Measuring the density profile during pressing: the method, the equipment, and the results. In Proceedings of the 27th International Particleboard Symposium. Washington State University. Pullman, WA. 45-54.

_____ and W. Xu. 1996. Layer water absorption of medium density fiberboard and oriented strandboard. Forest Products Journal. 46(6):69-72.

_____, T. M. Young, and E. Walker. 1996. Modeling and comparing vertical density profiles. Wood and Fiber Science. 28(1):133-141.

_____, W. W. Moschler, Jr., S. Wang, and E. Depaula. 2000. Fundamentals of vertical density profile formation in wood composites, Part I: In situ density measurement of the consolidation process. Wood and Fiber Science. 32(2):209-219.

_____ and S. Wang. 1999. Densification of wood composite mats during pressing: implications of mat structure and pressing schedules on density profile formation and panel properties. Proceedings of the 4th International Conference on the Development of Wood Science, Wood Technology, and Forestry. Missenden Abbey, UK. 375-382.

Wolcott, M. P., F. A. Kamke, and D. A. Dillard. 1990. Fundamentals of flakeboard manufacture: viscoelastic behavior of the wood component. Wood and Fiber Science. 22(4):345-361.

Wong, E. D., M. Zhang, Q. Wang, and S. Kawai. 1998. Effects of mat moisture content and press closing speed on the formation of density profile and properties of particleboard. Journal of Wood Science. 44:287-295.

_____, M. Zhang, Q. Wang, and S. Kawai. 1999. Formation of the density profile and its effects on the properties of particleboard. Wood Science and Technology. 33:327-340.

Wu, Q. and O. Suchsland.1997. Effect of moisture on the flexural properties of commercial oriented strandboard. Wood and Fiber Science. 29(1):47-57.

_____. 1999. In-plane dimensional stability of oriented strand panel: effect of processing variables. Wood and Fiber Science. 31(1):28-40.

Xu, D. and O. Suchsland. 1996. A modified elastic approach to the theoretical determination of the hygroscopic warping of laminated wood panels. Wood and Fiber Science. 28(2):194-204.

Xu, W. and P. R. Steiner. 1995. A statistical characterization of the horizontal density distribution in flakeboard. Wood and Fiber Science. 27(2):160-167.

_____ and P. M. Winistorfer. 1995a. A procedure to determine thickness swell distribution in wood composite panels. Wood and Fiber Science. 27(2):119-125.

_____ and P. M. Winistorfer. 1995b. Layer thickness swell and layer internal bond of medium density fiberboard and oriented strandboard. Forest Products Journal. 45(10):67-71.

_____ and O. Suchsland. 1997. Linear expansion of wood composites: a model. Wood and Fiber Science. 29(3):272-281.

_____ and O. Suchsland. 1998. Modulus of elasticity of wood composite panels with a uniform vertical density profile: A model. Wood and Fiber Science. 30(3):293-300.

_____. 1999. Influence of vertical density distribution on bending modulus of elasticity of wood composite panels: a theoretical consideration. Wood and Fiber Science. 31(3):277-282.

_____. 2002. How to analyze strand alignment of oriented strand board. Forest Products Journal. 52(4):48-52.

Zhang, M., E. Wong, S. Kawai, and J. Kwon. 1998. Manufacture and properties of high-performance oriented strand board composite using thin strands. J. Wood Sci. 44:191-197.

Zhou, D. 1990. A study of oriented structural board made from hybrid poplar: Physical and mechanical properties of OSB. Holz als Roh- und Werkstoff. 48:293-296.

Zombori, B. G., F. A. Kamke, and L. T. Watson. 2001. Simulation of the mat formation process. Wood and Fiber Science. 33(4):564-579.

Chapter 3

Elastic Properties of Wood-Strand Composites with Undulating Strands

Introduction

Structural composite lumber is rapidly replacing sawn lumber and timber for structural members, such as girders, beams, headers, joists, studs and columns. Oriented strand lumber (OSL) is a reconstituted, engineered lumber that can be substituted for high-quality structural lumber. According to McNatt and Moody (1990), the strength properties of structural composite lumber products are comparable to those of high-grade sawn lumber, and stiffness is comparable to that of a lower grade structural lumber. The importance of OSL is expected to grow as demand for highly engineered materials increase and the wood industry shifts to a greater use of small-diameter trees.

Wood-strand composites, such as oriented strand lumber (OSL) or oriented strand board (OSB), exhibit anisotropic behavior similar to solid wood, and the degree of anisotropy is determined by the spatial orientation of strands. An understanding of how spatial orientation of strands affect mechanical and physical properties of wood-strand composite is necessary to efficiently engineer its behavior.

The spatial structure of wood composites is extremely complicated and time consuming to characterize. In the past, researchers (Dai and Steiner 1994a & 1994b, Lang and Wolcott 1996, Suchsland and Xu 1991) examined key parameters to characterize the spatial structure of wood-strand mats. This information was used to model the stress-strain behavior of wood-strand mats in transverse compression during hot pressing. However, the structure of finished panels has not been studied in detail.

Previous empirical and analytical models (Geimer 1979, Suzuki and Sekino 1982, Shaler and Blankenhorn 1990, Triche and Hunt 1993, Xu and Suchsland 1998, Barnes 2000, 2001, Kristin 2001) have generally concentrated on examining the effects of in-plane orientation of particles, density of material, and certain processing parameters to predict mechanical properties of composites. All models show that particle orientation significantly influences the mechanical properties of composites, and found that its effect is non-linear with the largest influence resulting from orientations between 0 and 30 degrees. However, in wood-strand composites, such as OSL, the discontinuous strands are not bound to planes parallel to the panel surface. Rather, the strands tend to conform to density variations throughout the panel resulting in waviness or undulation through the thickness of the composite. If this out-of-plane orientation results in fiber deviations greater than three to five degrees, it could significantly reduce the mechanical properties of the composite and influence the initial failure mechanism (Figure 3.1).

Figure 3. 1. A typical compression failure in a unidirectional wood-strand composite.

Undulating strand could significantly affect the compression behavior because of the tendency of strands to buckle more readily. Current models do not account for the effects of strand undulation on wood composite properties. However, researchers (Ishikawa and Chou 1983, Hsiao and Daniel 1996, Chun et. al. 2001) have analyzed the elastic behavior of synthetic composites produced with woven fabric and unidirectional fibers with controlled fiber waviness. Ishikawa and Chou (1983) conclude that fiber undulation leads to softening of the in-plane stiffness. Their one-dimensional model was successful in evaluating the effects of fiber undulation on the elastic properties of woven fabric composites.

Hsiao and Daniel (1996) researched uniform, graded, and localized fiber waviness in unidirectional and crossply carbon/epoxy composites. A composite with repeating unit of fiber waviness is said to have uniform waviness; whereas, a composite with decaying amplitude of fiber waviness as you move away from the mid-surface to the outer surfaces is known to have a graded fiber waviness. Elastic modulus was predicted using an analytical constitutive model considering fiber waviness. The computed properties were in good agreement with the experimental results of specimens fabricated with controlled fiber waviness. Chun et. al. (2001) experimentally and theoretically examined the effects of fiber waviness on the nonlinear behavior of unidirectional graphite/epoxy composites under tensile and compressive loads. The material nonlinearity was included into the model by using the complementary energy density function. Stress-strain relations can be derived from the complementary energy density function. They found that the fiber waviness significantly affected both the elastic and inelastic behavior of specimens tested in tension and compression. They reported that rate of reduction for the E_x increases up to fiber waviness ratio (A/L) of 0.04 then decreases gradually. Fiber waviness did not influence E_y. Effect of fiber waviness was most significant for composites with uniform

fiber waviness followed by graded waviness. Research presented in this paper proposes to examine the significance of undulating strands on elastic behavior of wood-strand composites and presents a physical model to estimate their elastic properties.

Objectives

The objective of this study is to understand the effects of undulating strands on the elastic behavior of a wood-strand composite and develop a general constitutive model to predict the elastic properties as a function of strand waviness. Specific objectives of this study are to:

1. Introduce the fiber undulation model (FUM) to analyze the elastic properties of wood-strand composites,
2. Fabricate wood-strand laminates with purposefully placed undulating strands and investigate their elastic behavior in tension and compression,
3. Present a novel method to characterize strand undulation or waviness in wood strand composites, and
4. Validate the FUM to analyze the elastic properties of oriented strand composites manufactured with predetermined geometry.

Transverse Isotropy

Before presenting the theory of fiber undulation model, the assumption of transverse isotropy made regarding the oriented strand composites in this study is discussed. The labeling convention for OSL specimen axes that is followed in this study is shown in Figure 3.2. The longitudinal, transverse, and thickness direction axes of an OSL specimen are labeled x, y, and

z. LRT-axes refer to the orthotropic directions of a solid sawn wood from which strands are flaked. 123-axes of the strands refers to the principal material directions of strands obtained from stranding lumber. If the principal material directions of a strand coincide with the orthotropic axes of solid sawn wood then the 1-axis of strand coincides with L-axis of lumber and the 2-axis of strand coincides with either R- or T-axis of lumber it is flaked from.

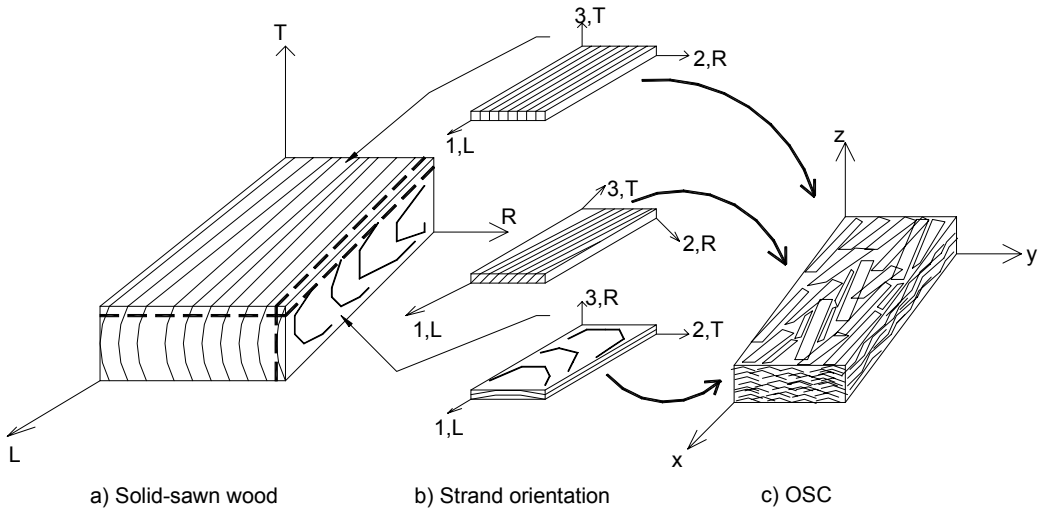

Figure 3. 2. a) Orthotropic (L, R, T) axes of a block of wood, b) strand orientation (1, 2, 3) depending on cutting direction, and c) geometric axes (x, y, z) of an oriented strand composite (OSC) specimen.

Due to the nature of flake preparation, the axis parallel to the width of the strands could either coincide with radial or tangential axis or be somewhere in between relative to the orthotropic axes of wood (Figure 3.2). In an OSC board, some strands may have their tangential surface parallel to the y- or z-axis of the board. Therefore, the final board is a conglomeration of strands with varying orientation in the width direction with respect to the orthotropic axes of the solid-sawn wood they are stranded from. Thus, the resulting composite could be assumed transversely isotropic. Modeling glued laminated beams as transversely isotropic has been experimentally validated in the past (Davalos et. al. 1991). Thus, when determining strand

constitutive matrix, it is reasonable to assume that E_R or E_2 and E_T or E_3 of a strand are approximately equal. It also follows then that $\nu_{LT} \approx \nu_{LR}$ or $\nu_{12} \approx \nu_{13}$, and $G_{LT} \approx G_{LR}$ or $G_{12} \approx G_{13}$.

Fiber Undulation Model (FUM)

The fiber undulation model (FUM) is also referred to as fiber crimp theory and has been used to analyze elastic stiffness of biaxial and triaxial woven fabric composites (Ishikawa and Chou 1983, Yang et. al. 1984, Naik and Shembekar 1992, Hsiao and Daniel 1996). A mathematical function describing the undulating shape taken by the fiber is specified.

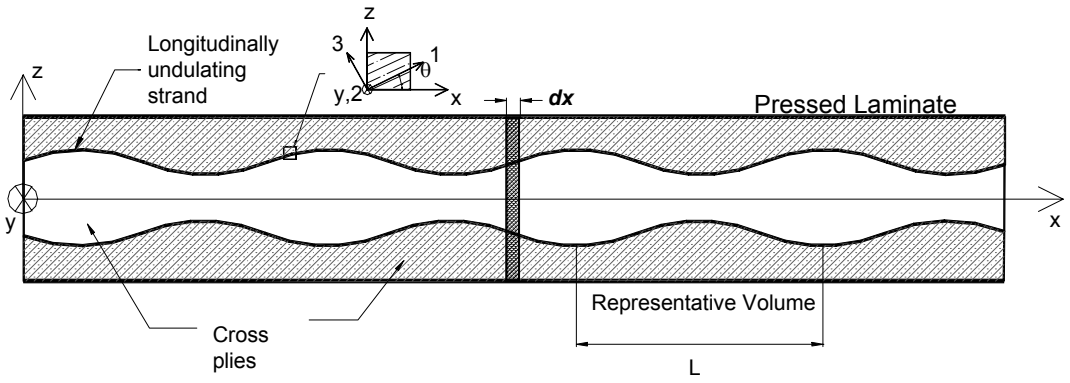

Figure 3. 3. Representative volume and coordinates for a cross-ply laminate with uniform strand undulation in the longitudinal direction.

Consider a cross-ply laminate with uniform strand undulation in the longitudinal direction as shown in Figure 3.3. Strand undulation is assumed to be plane with the xz-plane of the composite. For uniformly repeating strand undulation, it is sufficient to consider a representative volume element consisting of one period of the undulation. Let θ represent out-of-plane or undulation angle between the longitudinal laminae and the x-axis of the laminate. Let ϕ represent the angle between the fiber direction in the plane of each lamina and the x-axis of the

laminate. For the depicted uniformly undulating strand within a representative element, the undulation in the xz- plane is defined by

$$h(x) = A\sin\frac{2\pi x}{L} \qquad \textbf{Equation 3.1}$$

where A and L are the amplitude and period of the undulating strand. The out-of-plane angle (θ) between the local strand orientation and the global coordinate system can then be given as:

$$\theta(\mathbf{x}) = \tan^{-1}\left[\frac{\mathbf{dh(x)}}{\mathbf{dx}}\right] = \tan^{-1}\left[2\pi\frac{\mathbf{A}}{\mathbf{L}}\cos\frac{2\pi\mathbf{x}}{\mathbf{L}}\right] \qquad \textbf{Equation 3.2}$$

Considering the differential slice of width *dx,* the influence of θ on the elastic behavior can be determined through the transformed compliance matrix $[\bar{\mathbf{S}}]_\theta$ of the lamina or strand layer:

$$[\bar{\mathbf{S}}]_\theta = [\mathbf{T}]_\theta^{\mathbf{T}}[\mathbf{S}][\mathbf{T}]_\theta \qquad \textbf{Equation 3.3}$$

Where,

$$[\mathbf{S}] = \begin{bmatrix} \frac{1}{\mathbf{E}_1} & \frac{-\nu_{12}}{\mathbf{E}_1} & \frac{-\nu_{13}}{\mathbf{E}_1} & 0 & 0 & 0 \\ \frac{-\nu_{12}}{\mathbf{E}_1} & \frac{1}{\mathbf{E}_2} & \frac{-\nu_{23}}{\mathbf{E}_2} & 0 & 0 & 0 \\ \frac{-\nu_{13}}{\mathbf{E}_1} & \frac{-\nu_{23}}{\mathbf{E}_2} & \frac{1}{\mathbf{E}_3} & 0 & 0 & 0 \\ 0 & 0 & 0 & \frac{1}{\mathbf{G}_{23}} & 0 & 0 \\ 0 & 0 & 0 & 0 & \frac{1}{\mathbf{G}_{13}} & 0 \\ 0 & 0 & 0 & 0 & 0 & \frac{1}{\mathbf{G}_{12}} \end{bmatrix} \qquad \textbf{Equation 3.4}$$

and

$$[\mathbf{T}]_\theta = \begin{bmatrix} \cos(\theta(\mathbf{x}))^2 & 0 & \sin(\theta(\mathbf{x}))^2 & 0 & 2\cos(\theta(\mathbf{x}))\sin(\theta(\mathbf{x})) & 0 \\ 0 & 1 & 0 & 0 & 0 & 0 \\ \sin(\theta(\mathbf{x}))^2 & 0 & \cos(\theta(\mathbf{x}))^2 & 0 & -2\cos(\theta(\mathbf{x}))\sin(\theta(\mathbf{x})) & 0 \\ 0 & 0 & 0 & \cos(\theta(\mathbf{x})) & 0 & -\sin(\theta(\mathbf{x})) \\ -\cos(\theta(\mathbf{x}))\sin(\theta(\mathbf{x})) & 0 & \cos(\theta(\mathbf{x}))\sin(\theta(\mathbf{x})) & 0 & \cos(\theta(\mathbf{x}))^2 - \sin(\theta(\mathbf{x}))^2 & 0 \\ 0 & 0 & 0 & \sin(\theta(\mathbf{x})) & 0 & \cos(\theta(\mathbf{x})) \end{bmatrix} \qquad \textbf{Equation 3.5}$$

From the above relationships, transforming from the principal materials axes to the body coordinates considering the out-of-plane undulation angle (θ), the components of a two dimensional (for xy-plane) reduced stiffness matrix could be written as:

$$\begin{aligned}
&\mathbf{E_X}(\theta(\mathbf{x})) = 1/\left[\cos(\theta(\mathbf{x}))^4/\mathbf{E}_1 + (1/\mathbf{G}_{13} - 2\nu_{31}/\mathbf{E}_1)\cos(\theta(\mathbf{x}))^2\sin(\theta(\mathbf{x}))^2 + \sin(\theta(\mathbf{x}))^4/\mathbf{E}_3\right] \\
&\mathbf{G_{XY}}(\theta(\mathbf{x})) = \mathbf{G}_{12}\cos(\theta(\mathbf{x}))^2 + \mathbf{G}_{23}\sin(\theta(\mathbf{x}))^2 \\
&\mathbf{E_Y}(\theta(\mathbf{x})) = \mathbf{E_Y} = \mathbf{E}_2 \\
&\nu_{\mathbf{YX}}(\theta(\mathbf{x})) = \nu_{31}\cos(\theta(\mathbf{x}))^2 + \nu_{23}\sin(\theta(\mathbf{x}))^2
\end{aligned} \qquad \textbf{Equation 3.6}$$

Thus, the reduced stiffness matrix $\left[\overline{\mathbf{Q}}\right]_\theta$ for xy-plane accounting for undulation angle can be expressed as:

$$\overline{\mathbf{Q}}_{\mathbf{ij}}(\theta) = \begin{bmatrix} \mathbf{E_X}(\theta)/\mathbf{D_v} & \nu_{\mathbf{YX}}(\theta)\mathbf{E_Y}/\mathbf{D_v} & 0 \\ \nu_{\mathbf{YX}}(\theta)\mathbf{E_Y}/\mathbf{D_v} & \mathbf{E_Y}/\mathbf{D_v} & 0 \\ 0 & 0 & \mathbf{G_{XY}}(\theta) \end{bmatrix} \qquad \textbf{Equation 3.7}$$

where, $D_v = 1 - \nu_{yx}(\theta)^2 E_y / E_x(\theta)$ and $\theta = f(x)$.

After accounting for fiber undulation, the reduced stiffness coefficients of each lamina are further adjusted for off-axis orientation in the plane, ϕ.

$$\left[\overline{\mathbf{Q}}\right]_\phi = \left[\mathbf{T}\right]_\phi^{-1}\left[\overline{\mathbf{Q}}\right]_\theta\left[\mathbf{T}\right]_\phi^{-\mathbf{T}} = \begin{bmatrix} \overline{\mathbf{Q}}_{11} & \overline{\mathbf{Q}}_{12} & \overline{\mathbf{Q}}_{16} \\ \overline{\mathbf{Q}}_{12} & \overline{\mathbf{Q}}_{22} & \overline{\mathbf{Q}}_{26} \\ \overline{\mathbf{Q}}_{16} & \overline{\mathbf{Q}}_{26} & \overline{\mathbf{Q}}_{66} \end{bmatrix} \qquad \textbf{Equation 3.8}$$

where,

$$[\mathbf{T}]_{\phi} = \begin{bmatrix} \cos(\phi)^2 & \sin(\phi)^2 & 2\cos(\phi)\sin(\phi) \\ \sin(\phi)^2 & \cos(\phi)^2 & -2\cos(\phi)\sin(\phi) \\ -\cos(\phi)\sin(\phi) & \cos(\phi)\sin(\phi) & \cos(\phi)^2 - \sin(\phi)^2 \end{bmatrix} \quad \textbf{Equation 3.9}$$

and

$$\begin{aligned}
\overline{\mathbf{Q}}_{11} &= \left[\frac{\mathbf{E_X}(\theta)}{\mathbf{D_\nu}}\right] * \mathbf{l}_\phi^4 + 2\left[\frac{\nu_{\mathbf{YX}}(\theta) * \mathbf{E_Y}}{\mathbf{D_\nu}} + 2 * \mathbf{G_{XY}}(\theta)\right] * \mathbf{l}_\phi^2 \mathbf{m}_\phi^2 + \left[\frac{\mathbf{E_Y}}{\mathbf{D_\nu}}\right] * \mathbf{m}_\phi^4 \\
\overline{\mathbf{Q}}_{12} &= \left[\frac{\mathbf{E_X}(\theta)}{\mathbf{D_\nu}} + \frac{\mathbf{E_Y}}{\mathbf{D_\nu}} - 4\mathbf{G_{XY}}(\theta)\right] \mathbf{l}_\phi^2 \mathbf{m}_\phi^2 + \left[\frac{\upsilon_{\mathbf{YX}}(\theta)\mathbf{E_Y}}{\mathbf{D_\nu}}\right] \left(\mathbf{l}_\phi^4 + \mathbf{m}_\phi^4\right) \\
\overline{\mathbf{Q}}_{22} &= \left[\frac{\mathbf{E_X}(\theta)}{\mathbf{D_\nu}}\right] * \mathbf{m}_\phi^4 + 2\left[\frac{\nu_{\mathbf{YX}}(\theta) * \mathbf{E_Y}}{\mathbf{D_\nu}} + 2 * \mathbf{G_{XY}}(\theta)\right] * \mathbf{l}_\phi^2 \mathbf{m}_\phi^2 + \left[\frac{\mathbf{E_Y}}{\mathbf{D_\nu}}\right] * \mathbf{l}_\phi^4 \qquad \textbf{Equation 3.10} \\
\overline{\mathbf{Q}}_{16} &= \left[\frac{\mathbf{E_X}(\theta)}{\mathbf{D_\nu}} - \frac{\upsilon_{\mathbf{YX}}(\theta)\mathbf{E_Y}}{\mathbf{D_\nu}} - 2\mathbf{G_{XY}}(\theta)\right] \mathbf{l}_\phi^3 \mathbf{m}_\phi + \left[\frac{\upsilon_{\mathbf{XY}}(\theta)\mathbf{E_Y}}{\mathbf{D_\nu}} - \frac{\mathbf{E_Y}}{\mathbf{D_\nu}} + 2\mathbf{G_{XY}}(\theta)\right] \mathbf{m}_\phi^3 \mathbf{l}_\phi \\
\overline{\mathbf{Q}}_{26} &= \left[\frac{\mathbf{E_X}(\theta)}{\mathbf{D_\nu}} - \frac{\upsilon_{\mathbf{YX}}(\theta)\mathbf{E_Y}}{\mathbf{D_\nu}} - 2\mathbf{G_{XY}}(\theta)\right] \mathbf{m}_\phi^3 \mathbf{l}_\phi + \left[\frac{\upsilon_{\mathbf{YX}}(\theta)\mathbf{E_Y}}{\mathbf{D_\nu}} - \frac{\mathbf{E_Y}}{\mathbf{D_\nu}} + 2\mathbf{G_{XY}}(\theta)\right] \mathbf{l}_\phi^3 \mathbf{m}_\phi \\
\overline{\mathbf{Q}}_{66} &= \left[\frac{\mathbf{E_X}(\theta)}{\mathbf{D_\nu}} + \frac{\mathbf{E_Y}}{\mathbf{D_\nu}} - 2\frac{\upsilon_{\mathbf{YX}}(\theta)\mathbf{E_Y}}{\mathbf{D_\nu}} - 2\mathbf{G_{XY}}(\theta)\right] \mathbf{l}_\phi^2 \mathbf{m}_\phi^2 + \mathbf{G_{XY}}(\theta)(\mathbf{l}_\phi^4 + \mathbf{m}_\phi^4)
\end{aligned}$$

Note that $l_\phi = \cos(\phi)$ and $m_\phi = \sin(\phi)$. After these transformation formulas are established, assuming that the strain remains constant across the laminate thickness, they may be combined in a form convenient for plate theories as $A_{ij}(x)$, $B_{ij}(x)$ and $D_{ij}(x)$ where (Jones 1999)

$$[\boldsymbol{A_{ij}}(\boldsymbol{x}), \boldsymbol{B_{ij}}(\boldsymbol{x}), \boldsymbol{D_{ij}}(\boldsymbol{x})] = \int_{-\boldsymbol{h}/2}^{\boldsymbol{h}/2} \overline{\boldsymbol{Q}}_{\boldsymbol{ij}}(\alpha)(1, \boldsymbol{z}, \boldsymbol{z}^2)\boldsymbol{dz} \qquad \textbf{Equation 3.11}$$

Compliance coefficients, a_{ij}, b_{ij}, and d_{ij}, are obtained by inverting [**A**], [**B**], and [**D**] matrices; noting that for symmetric laminates, $B_{ij} = 0$. Then, the average in-plane compliance of the composite can be defined by:

$$\bar{a}_{ij} = \frac{1}{L}\int_0^L a_{ij}(x)dx \qquad \bar{b}_{ij} = \frac{1}{L}\int_0^L b_{ij}(x)dx \qquad \bar{d}_{ij} = \frac{1}{L}\int_0^L d_{ij}(x)dx \qquad \textbf{Equation 3.12}$$

where L is the length of one strand undulation period. Assuming in-plane loading of a symmetric balanced or symmetric cross-ply laminate, the elastic constants of the laminate with thickness t are estimated by (Hyer 1998):

$$E_x = \frac{1}{t * \bar{a}_{11}} \qquad E_y = \frac{1}{t * \bar{a}_{22}} \qquad \upsilon_{xy} = \frac{\bar{a}_{12}}{\bar{a}_{11}} \qquad G_{xy} = \frac{1}{t * \bar{a}_{66}} \qquad \textbf{Equation 3.13}$$

Materials and Methodology

Yellow poplar (*Liriodendron tulipifera* L.) veneers and lumber were bonded with polyvinyl acetate adhesive to manufacture laminates with controlled undulation amplitude to verify the proposed constitutive relations. Flat veneers were laminated between rounded cross-plies to produce specimens with sinusoidally varying orientation for internal laminae (Figure 3.3 and Appendix A).

Each laminate contained two flat strands on the outer surfaces and four internal strands (8 x 1 x 0.04-inch) with induced levels of waviness in the longitudinal direction. All of these strands were produced from the sliced veneer sheets. The fiber direction in the outer strands was oriented perpendicular to the laminate long axis. The fiber direction in the four internal strands was oriented with the longitudinal axis of the laminate. Density and fiber angle of internal strands could not be determined because they were used to manufacture the verification laminates. However, their measured elastic properties from tension tests inherently incorporated the effects of density and in-plane fiber deviations. The undulation amplitudes of the four internal layers were determined by the cross sectional shapes of the cross plies cut from 1.5 inches thick solid sawn yellow-poplar wood.

The rounded cross plies were produced by routing lumber edges with fingernail-type router bits designed to obtain the desired radii of curvature. Two fingernail-type router bits were custom manufactured with radii of curvature of 3.2 and 5.5 inches and a bead opening of 1.5 inches. After routing the lumber, the edges were ripped to a thickness of approximately 0.155 inches. The rounded strips were then cut into 1-inch long pieces and used as cross plies in manufacturing the FUM verification specimens.

Each specimen was pressed between two 1-inch thick steel plates using a screw driven universal testing machine to a maximum pressure of 500-psi. This pressure was less than the average fiber stress at proportional limit in compression perpendicular to grain for yellow poplar (Wood Handbook, 1987). The clamping pressure was applied for at least four hours after which laminates were lightly clamped by hand for an additional four hours to ensure proper bonding.

Twenty specimens were manufactured. In a set of five specimens cross plies were not rounded, thus no undulation was introduced in the longitudinally oriented plies (labeled u0 for 0-inch amplitude). Five laminates were fabricated with a maximum undulation angle of eight degrees (labeled u8), and ten laminates were manufactured with a maximum undulation angle of four degrees (labeled u4). All specimens were conditioned at 76° F and 66% relative humidity to equilibrate to average moisture content of 9%. Average specific gravity of all laminae used in the verification specimens was 0.50 with a coefficient of variation (COV) of 4%.

Prior to manufacturing the laminates, material properties of longitudinal strands and cross plies were determined experimentally. Each of the longitudinally oriented strands was tested in tension using a 2-kip screw-driven universal testing machine. The tension fixtures consisted of self-aligning mechanical grips with a constant guage-length of 6-inches. Specimens were loaded with a uniform crosshead speed of 0.015 inches/minute. A ½-inch gage length clip extensometer

(Epsilon Technology Corp., Model 3442-0050-020-ST) was mounted for strain measurements at the mid-section on the wide face of each strand. All specimens were loaded such that maximum stress applied was less than 35 percent of the proportional limit.

After testing all specimens to measure the longitudinal strains, they were tested again in tension with the extensometer reoriented to measure transverse strains. Using the measured strain, longitudinal elastic modulus, E_x, and Poisson's ratio, ν_{xy}, for each of the strands were determined. Based on E_x, strands were assigned to verification specimens such that laminates with different undulation angles had similar distribution of strand properties (Table 3.1). The measured values of E_x and ν_{xy} were used in the fiber undulation model to estimate the laminate elastic modulus in the longitudinal direction.

Solid sawn yellow-poplar, used for rounded cross ply laminae, was not wide enough to prepare small clear specimens to determine its material properties. Also, limited amount of the material was available for the study. Therefore, rectangular strips were tested in tension and transformation relationships were used to estimate cross ply properties. To determine the properties of cross ply materials, 26 thin rectangular strips (1/18-inch by 1.0-inch cross section) were cut to a length of 8 inches from solid sawn yellow-poplar. After conditioning these strips to standard conditions, they were tested in tension in the same manner as the strands. After obtaining E_x and ν_{xy}, a scribe consisting of a phonograph needle mounted on one end and a pin joint in the middle was used to mark the grain angle on the face of each of the specimens (Koehler 1943). Grain angle was subsequently measured within the gage length of each specimen using digital image analysis.

Table3. 1. Strand assignments to verification specimens based on Young's moduli of strands.

ID	Average Undulation Angle (deg.)	Strand Location	Replications Within Each Undulation Angle Set									
			Rep 1	Rep 2	Rep 3	Rep 4	Rep 5	Rep 6	Rep 7	Rep 8	Rep 9	Rep 10
			E (x10^6 psi)									
u0	0	Top	1.532	1.437	1.412	2.212	2.116	-	-	-	-	-
			1.136	1.121	1.109	1.042	1.034	-	-	-	-	-
			1.131	1.120	1.106	1.041	1.022	-	-	-	-	-
		Bottom	1.531	1.440	1.413	2.203	2.100	-	-	-	-	-
u4	4	Top	1.520	1.462	1.402	2.194	2.125	1.487	1.460	1.415	2.193	2.146
			1.131	1.120	1.113	1.059	1.021	1.151	1.119	1.102	1.076	1.017
			1.129	1.119	1.111	1.057	1.018	1.143	1.118	1.100	1.065	1.002
		Bottom	1.500	1.460	1.394	2.194	2.116	1.486	1.445	1.427	2.189	2.135
u8	8	Top	1.495	1.476	1.405	2.178	2.172	-	-	-	-	-
			1.157	1.118	1.106	1.090	1.000	-	-	-	-	-
			1.153	1.113	1.102	1.086	0.999	-	-	-	-	-
		Bottom	1.488	1.468	1.405	2.172	2.153	-	-	-	-	-

The measured E_x and ν_{xy} of strips with a grain angle of 0±1.5 degrees were averaged to obtain an estimate for E_1 and ν_{12}. Given the estimates of E_1 and ν_{12}, along with the measured values of E_x, ν_{xy}, and average in-plane grain angle (ϕ), E_2 and G_{12}, were estimated for each specimen by simultaneously solving the following two transformation equations (Jones 1999).

$$\frac{1}{\mathbf{E_x}} = \frac{1}{\mathbf{E}_1}\cos^4\phi + \left(\frac{1}{\mathbf{G}_{12}} - \frac{2\upsilon_{12}}{\mathbf{E}_1}\right)\sin^2\phi\cos^2\phi + \frac{\sin^4\phi}{\mathbf{E}_2} \qquad \textbf{Equation 3.14}$$

$$\upsilon_{\mathbf{xy}} = \frac{\upsilon_{12}(\sin^4\phi + \cos^4\phi) - (1 + \frac{\mathbf{E}_1}{\mathbf{E}_2} - \frac{\mathbf{E}_1}{\mathbf{G}_{12}})\sin^2\phi\cos^2\phi}{\cos^4\phi + (\frac{\mathbf{E}_1}{\mathbf{G}_{12}} - 2\upsilon_{12})\sin^2\phi\cos^2\phi + \frac{\mathbf{E}_1}{\mathbf{E}_2}\sin^4\phi} \qquad \textbf{Equation 3.15}$$

Mean values of E_2 and G_{12} of all specimens from solid sawn yellow-poplar then represented the material properties of the cross plies in the laminates.

Strand Orientation Through the Panel Thickness

Effectiveness of the fiber undulation model to predict the elastic coefficients of a wood-strand panel depends on accurate representation of strand undulation. If the undulation is periodic along the strand length, a simple sinusoidal function is sufficient to describe orientation (Equation 3.1). However, if a repeating pattern in the undulation cannot be identified, such as in OSL, it is necessary to use a function that can describe the undulation over the entire length of the strand. Unlike a repeating sinusoidal function used to describe fiber undulation in woven composite fabrics, a discrete Fourier series expansion is well suited to describe strand undulation with multiple modes and amplitudes. A Fourier series with a period T is defined as (Kreyszig 1999)

$$f(x) = a_0 + \sum_{n=1}^{\infty} (a_n \cos(\frac{2\pi nx}{T}) + b_n \sin(\frac{2\pi nx}{T})) \qquad \textbf{Equation 3.16}$$

Where

$$a_0 = \frac{1}{T}\int_0^T f(x)dx \qquad a_n = \frac{2}{T}\int_0^T f(x)\cos\frac{2\pi nx}{T}dx \qquad b_n = \frac{2}{T}\int_0^T f(x)\sin\frac{2\pi nx}{T}dx \qquad \textbf{Equation 3.17}$$

Digital images of verification specimen edges were taken to digitize the undulating paths of the longitudinal strands and to determine the appropriate thickness of all layers in the laminates. Figure 3.4 shows a typical digital image of an edge of a verification specimen. Coordinates of the undulating strands were digitized at an interval of 50 pixels or 0.23 inches along the laminate length. Using the coordinates, a discrete Fourier series was applied to describe strand undulations. A MathCAD worksheet that was used to fit a discrete Fourier series expansion to a given strand undulation coordinates is attached in Appendix B. This function was then used in the FUM to consider the effects of undulation on the elastic behavior of the material.

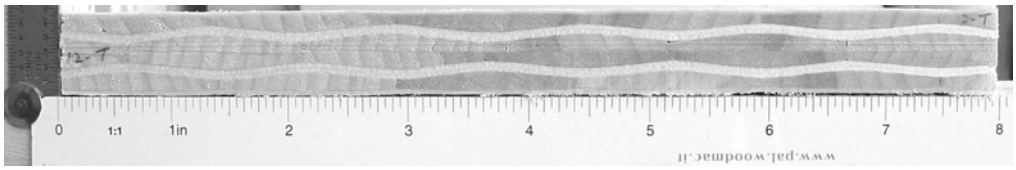

Figure 3. 4. Digital image of a verification specimen with a maximum undulation angle of eight degrees.

Mechanical Testing of Verification Specimens

All laminates were tested in tension within the elastic limit at a strain rate of 0.01 in./in./minute using a 2-kip screw-driven universal testing machine fitted with self-aligning, mechanical tension fixtures. Strain was measured using a 1-inch clip extensometer (MTS®, Model 634-12E-24).

After testing in tension, two-inch sections were cut from each end of the specimens to obtain a resulting specimen length of 4 inches for compression testing. Specimens were subsequently loaded in compression at a strain rate of 0.005 in./in./minute using a fixed bottom plate and a top plate supported by a rotating ball joint with two degrees of freedom. Strain was once again measured in the middle section using a 1-inch gage length clip extensometer. Moisture content and density of all specimens was determined in accordance with ASTM D2395-93, method A (ASTM 2001). The elastic modulus was determined by taking the slope of the linear elastic region of the stress-strain curve (Figure 3.5).

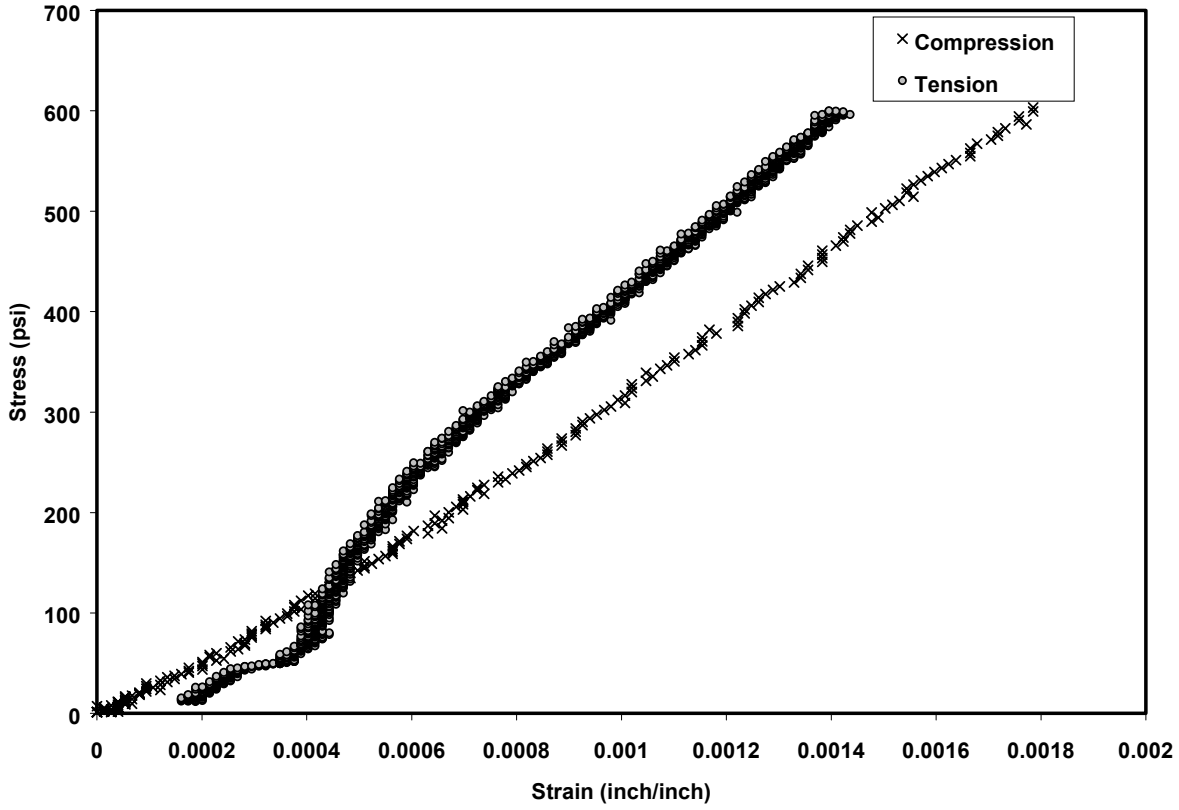

Figure 3. 5. Typical tension and compression stress-strain curves of verification specimens.

The FUM Analysis

The fiber undulation theory was applied to evaluate the longitudinal elastic modulus of the verification specimens using the Fourier series expansions describing the strand undulations and evaluated longitudinal strand and cross ply material properties. The MathCAD worksheet used to determine laminate elastic properties based on the fiber undulation theory is provided in Appendix C. Note that the average in-plane compliance (Equation 3.12) of each laminate was determined by integrating the compliance coefficients over the middle four-inch section of each specimen.

Predicted values for the elastic moduli were then compared against the experimentally determined tension and compression properties of the laminates. Because the laminates were assumed to be transversely isotropic, E_2 and E_3, G_{12} and G_{13}, ν_{12} and ν_{13} for longitudinal strands and cross plies were considered equal. As for G_{23}, a value of 22,450-psi was assumed from previously published data (Bodig and Jayne 1982). Once again invoking the assumption of transverse isotropy, the argument could be extended that ν_{21} and ν_{31} are equal as well as ν_{23} and ν_{32}. The values of ν_{21} and ν_{31} were set to 0.035 (average of ν_{RL} and ν_{TL}) and the values of as ν_{23} and ν_{32} were set to 0.50 (average of ν_{RT} and ν_{TR}), average values recommended for hardwoods by Bodig and Jayne (1982).

Results and Discussion

The mean elastic properties (E_x and ν_{xy}) of all longitudinally oriented strands used in fabricating the verification specimens in this study are presented in Table 3.1. The effect of fiber angle and density are intrinsically incorporated in these values, thus the properties of the undulating strands were transformed only for out-of-plane angles based on the undulation functions.

The measured values of E_x for the solid-sawn yellow-poplar strips with those determined using the transformation relations (Equations 3.14 and 3.15) are presented in Figure 3.6. In addition, the mean value and coefficient of variation for the estimated elastic properties in the principal material directions for the cross plies are given in Table 3.2. The coefficient of variation of E_2 and G_{12} were relatively high because of the small in-plane fiber angles in the test specimens which results in higher variations in estimates using the transformation relations.

Bodig and Goodman (1973) presented predictive equations for the elastic constants of wood based upon density. Using these equations, the predicted values of 1,730,000-psi for E_L, 124,800-psi for E_R, 56,000-psi for E_T, 97,300-psi for G_{LR}, and 70,000-psi for G_{LT} are obtained for a specific gravity of 0.40. Therefore, the calculated values for E_1 and G_{12} differ by 12% and 47% from the average predicted values of E_L and E_R and G_{LR} and G_{LT} as reported by Bodig and Goodman (1973). The measured longitudinal elastic modulus is 11.5% higher than the predicted value. The predicted equations derived by Bodig and Goodman (1973) were based on data obtained from compression specimens on small clear specimens, data obtained from other investigators, and regression equations developed by the authors. Other researchers have also found differences between values predicted using these equations and experimentally derived values (Davalos et al. 1991). Zink and et. al. (1997) reported a Poisson's ratio of 0.35 and 0.40 for ν_{LT} and ν_{LR} for yellow poplar based on measurements made using digital image correlation technique.

Table3. 2. Average elastic properties of cross plies in verification specimens.

Elastic Property	Average	COV (%)
E_1 (psi)	1929000	N/A
υ_{12}	0.50	N/A
E_2 (psi)	79570	92
G_{12} (psi)	44130	53
Specific Gravity	0.50	4

Digitized coordinates of a typical undulating strand path and a verification specimen are shown in Figure 3.7. A simple sinusoidal function and a Fourier series expansion fit of the digitized coordinates of the undulation path are also compared in the figure. Interpreting this

comparison indicates that a repeating pattern for strand undulation was not achieved. The Fourier series expansion describes the path more accurately and accounts for the slight overall slope along the length in the strand. Therefore, Fourier series expansions were used to describe the undulations of all strands in verification specimens. Coefficients of Fourier series for the top and bottom set of strands for each of the specimens are included in Table 3.3. All undulation paths could be described with either three or four terms of a Fourier series expansion with reasonable accuracy.

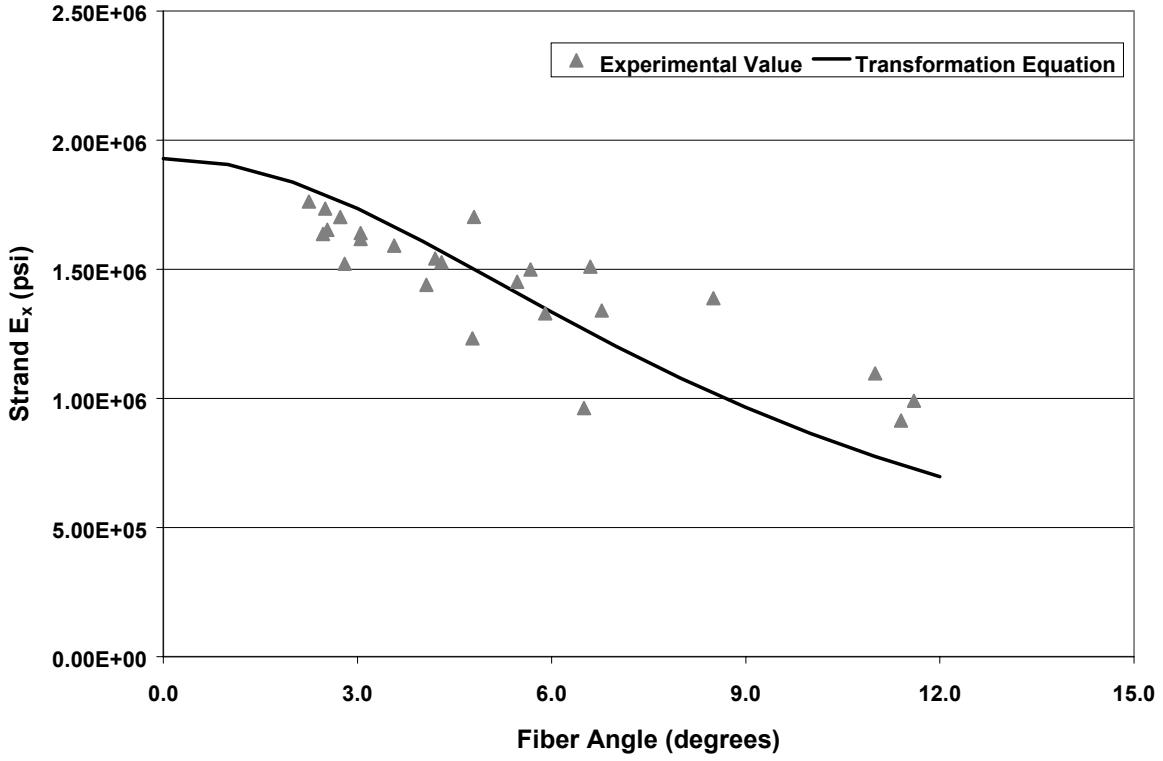

Figure 3. 6. Experimental results and transformation equation predictions of Young's modulus of yellow poplar strands with varying fiber angles.

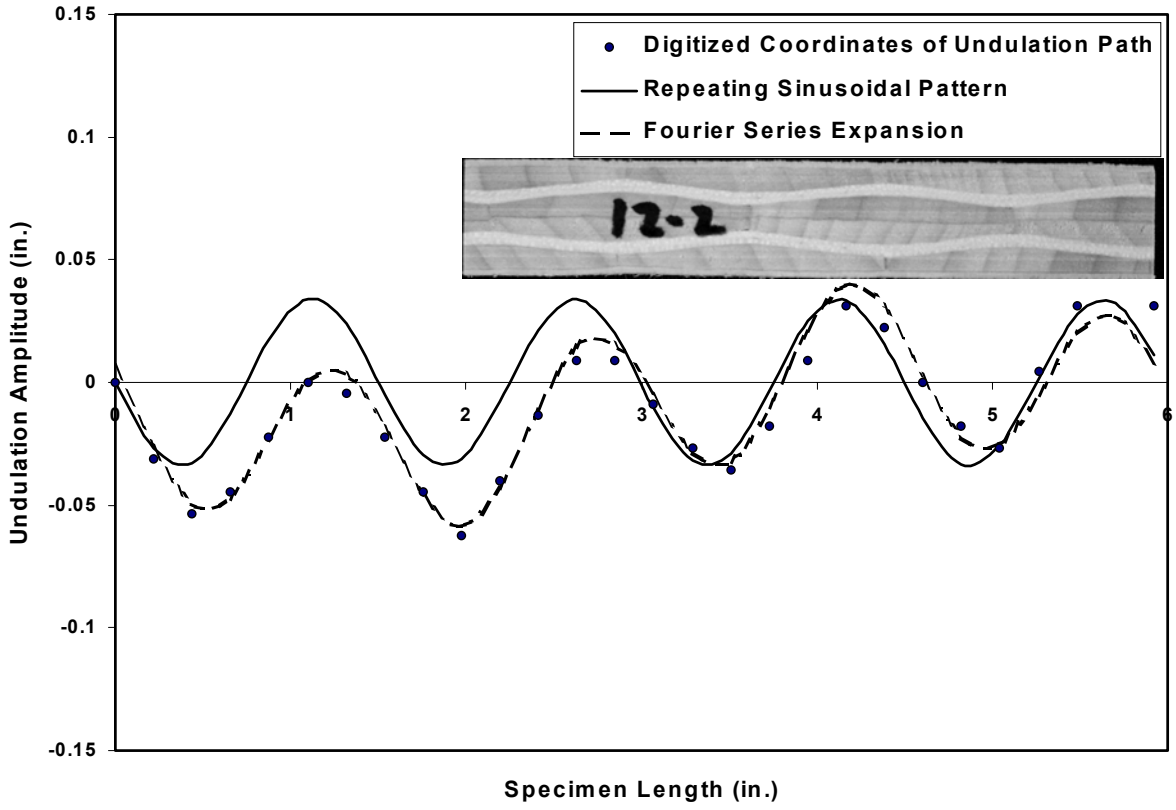

Figure 3. 7. Digitized undulation coordinates and functions describing the undulation path.

Table3. 3. Coefficients of Fourier series expansions describing strand undulations.

Specimen ID	Strand Location	Fourier Series Coefficients						
		a0	a1	a4	b1	b2	b3	b4
u4-1	Top	0.012	0.000	0.011	-0.014	0.000	0.000	0.000
	Bottom	0.033	0.000	0.000	0.000	0.000	0.000	-0.018
u4-2	Top	0.016	0.000	0.016	-0.023	0.000	0.000	-0.017
	Bottom	0.037	0.000	0.000	-0.026	-0.015	-0.012	0.000
u4-3	Top	0.019	0.000	0.013	-0.029	0.000	0.000	-0.019
	Bottom	0.022	0.010	0.000	-0.025	-0.013	0.000	0.011
u4-4	Top	0.020	0.014	0.013	-0.025	-0.015	0.000	-0.016
	Bottom	0.031	0.000	0.000	-0.026	-0.011	-0.010	0.010
u4-5	Top	0.020	0.000	0.000	-0.027	-0.011	0.000	-0.017
	Bottom	0.031	0.010	0.000	-0.027	-0.015	-0.012	0.000
u4-6	Top	0.000	0.000	0.000	-0.024	-0.014	0.000	-0.019
	Bottom	0.026	0.000	0.000	-0.023	-0.015	0.000	0.012
u4-7	Top	0.000	0.014	0.017	-0.019	0.000	0.000	-0.016
	Bottom	0.033	0.000	0.000	-0.020	-0.011	0.000	0.012
u4-8	Top	0.000	0.000	0.000	-0.021	0.000	0.000	-0.021
	Bottom	0.029	0.000	0.000	-0.025	0.000	0.000	0.010
u4-9	Top	0.019	0.011	0.000	-0.019	0.000	0.000	-0.020
	Bottom	0.017	0.000	0.000	-0.015	0.000	0.000	0.014
u4-10	Top	0.023	0.000	0.000	-0.012	0.000	0.000	-0.023
	Bottom	0.033	0.000	0.000	-0.020	-0.011	0.000	0.012
u8-1	Top	0.000	0.000	0.014	-0.016	0.000	0.000	-0.030
	Bottom	0.027	0.000	0.000	-0.020	-0.012	0.000	0.024
u8-2	Top	-0.010	0.000	0.017	-0.018	0.000	0.000	-0.028
	Bottom	0.026	0.010	-0.013	-0.017	0.000	0.000	0.024
u8-3	Top	0.011	0.000	0.000	-0.017	-0.015	0.000	0.028
	Bottom	0.034	0.000	0.000	-0.018	-0.017	0.000	-0.030
u8-4	Top	0.013	0.000	0.000	-0.023	0.000	0.000	-0.032
	Bottom	0.017	0.000	0.000	-0.024	0.000	0.000	0.028
u8-5	Top	0.031	0.000	0.000	-0.023	-0.011	0.000	-0.033
	Bottom	0.048	0.000	0.000	-0.011	0.000	-0.014	0.023

Results obtained from tension and compression tests on verification specimens along with the corresponding FUM estimations are presented in Table 3.4. Specific gravity values of the finished laminates were slightly greater than mean of lamina materials. Therefore, the laminate Young's moduli were normalized to a specific gravity of 0.5 (mean specific gravity of laminae), using a linear relationship suggested by others (Palka 1973, Kellogg and Ifju 1962), prior to comparison with the FUM predictions.

In general, compression Young's moduli were consistently lower than those determined in tension. The mean compression moduli of specimens without undulating strands differed by only 7%, however, for laminates with maximum strand undulation angles of four and eight degrees, the difference was between 14 and 15 percent. Using Tukey's mean comparison test (α=0.05) showed no significant difference between the two moduli for specimens without undulation (p=0.2894), whereas, the difference between compression and tension moduli for four and eight degree undulation angles was statistically significant (p=0.0021 and 0.0448, respectively). Interpretation of this result suggests a compounded effect of strand undulation for compression behavior as compared to tension; a result not predicted with the FUM.

Similar statistical comparisons between compression moduli of specimens with three different maximum undulation angles indicated a significant difference between the zero degree laminates and four and eight degree laminates. Statistically, the difference between compression moduli of four and eight degree laminates was not significant. However, the tension moduli of the specimens with the three different mean undulation angles were not found statistically different.

Table3. 4. Summary of verification specimens test results.

ID	Max Undulation Angle (deg.)	SG	FUM E_x ($x10^5$ psi)	Experimental Results: Unadjusted Ten. E_x ($x10^5$ psi)	Unadjusted Comp. E_x ($x10^5$ psi)	Adjusted* Ten. E_x ($x10^5$ psi)	Adjusted* Comp. E_x ($x10^5$ psi)	$FUM\_E_x/Adj\_Ten\_E_x$	$FUM\_E_x/Adj\_Comp\_E_x$
u0_1	0	0.55	5.038	5.745	5.259	5.195	4.756	0.97	1.06
u0_2	0	0.61	4.067	4.662	5.060	3.814	4.140	1.07	0.98
u0_3	0	0.63	4.029	5.847	4.997	4.652	3.976	0.87	1.01
u0_4	0	0.60	4.872	5.485	4.795	4.536	3.965	1.07	1.23
u0_5	0	0.60	4.721	5.290	5.117	4.396	4.252	1.07	1.11
Mean			**4.545**	**5.406**	**5.046**	**4.519**	**4.218**	**1.01**	**1.08**
COV (%)			**10.3**	**8.7**	**3.4**	**11.0**	**7.7**	**9.1**	**9.0**
u4_1	4.40	0.53	3.501	4.409	3.514	4.156	3.312	0.84	1.06
u4_2	2.74	0.52	3.414	4.144	3.350	3.971	3.210	0.86	1.06
u4_3	4.80	0.54	3.432	3.917	3.623	3.655	3.380	0.94	1.02
u4_4	4.30	0.56	4.181	5.167	4.052	4.646	3.643	0.90	1.15
u4_5	3.30	0.54	4.124	4.560	4.411	4.253	4.114	0.97	1.00
u4_6	4.80	0.53	3.534	5.112	4.203	4.812	3.956	0.73	0.89
u4_7	4.30	0.55	3.513	4.136	4.187	3.773	3.820	0.93	0.92
u4_8	4.00	0.56	3.508	5.247	3.927	4.654	3.483	0.75	1.01
u4_9	4.30	0.58	4.341	5.248	4.287	4.563	3.727	0.95	1.16
u4_10	4.30	0.57	4.082	5.302	4.882	4.671	4.301	0.87	0.95
Mean	**4.12**		**3.763**	**4.724**	**4.044**	**4.315**	**3.695**	**0.88**	**1.02**
COV (%)	**15.6**		**9.8**	**11.6**	**11.3**	**9.6**	**9.7**	**9.2**	**8.8**
u8_1	7.30	0.51	3.321	3.600	3.467	3.497	3.367	0.95	0.99
u8_2	7.70	0.55	3.346	4.315	3.869	3.923	3.518	0.85	0.95
u8_3	8.50	0.55	3.347	4.275	3.414	3.899	3.114	0.86	1.07
u8_4	8.30	0.54	3.933	4.793	4.431	4.417	4.083	0.89	0.96
u8_5	8.70	0.54	3.649	4.734	3.204	4.400	2.978	0.83	1.23
Mean	**8.10**		**3.519**	**4.343**	**3.677**	**4.027**	**3.412**	**0.88**	**1.04**
COV (%)	**7.2**		**7.6**	**11.0**	**13.2**	**9.6**	**12.6**	**5.3**	**11.0**

* Adjusted to SG of 0.5

Good agreement was noted between the FUM predictions and the measured compression modulus. For maximum undulation angles of four and eight degrees, the differences between the average FUM prediction and compression test results were two and four percent. As for Young's modulus in tension, the average FUM predictions were 12% lower than the experimental results. For laminates without undulating strands, the average FUM predictions differed from tension and compression moduli by one and eight percent, respectively.

The Young's moduli in tension and compression for solid wood and wood-strand composites have been shown to differ with compression modulus being generally lower than tension modulus (Kollman and Cote 1968, Dong 1979, Meyers 2001). Although these differences in Young's moduli have been experimentally shown, it cannot be claimed that the reasons for this difference in elastic behavior are yet understood. However, when tested beyond the elastic region, this difference is generally attributed to micro buckling of fibers in solid wood. Keith and Cote (1968) and Bienfait (1926) discuss microscopic failure mechanisms in solid wood subjected to compression parallel to the grain. They show that cell walls in compression tend to form slip planes and minute compression failures due to distortions in the lateral direction. Slip planes are the first indication of localized buckling of cell wall when subjected to severe longitudinal compression. After slip planes are formed, failure extends across a number of cells resulting in minute compression failure. Before buckling is noticeable to the naked eye, damage to the cell wall can be observed microscopically. These compression failures, which are not readily apparent to the eye, could be a significant source of weakness (Bienfait 1926, Keith and Cote 1968). This behavior in compression seems to manifest itself even in the elastic region.

Differences in tension and compression Young's moduli could be explained by examining the wood microstructure, as well as the distribution of internal stresses in cross plies within the laminates. When the verification specimens were subjected to compression loads, the longitudinally oriented strands could have experienced minute compressive failures contributing to lowering of modulus of elasticity in compression. These minute compressive failures could even occur in the elastic region due to the presence of voids, especially in wood-strand composites.

Dong (1979) evaluated failure mechanisms in flakeboard specimens after testing them in tension and compression. He concluded that specimens with average in-plane strand angle between 0 and 15 degrees when tested in tension exhibited a longitudinal tension failure exposing their fibers crosswise; whereas, specimens with 15 to 30 degrees of flake alignment failed in shear. In compression, he reported that flakeboards with low angles of flake alignment (between 0 and 15 degrees) failed in shear mode of the composite failure, and specimens with larger orientation angles exhibited extension mode of failure. In shear mode, matrix is subjected to shearing deformation because of in-phase buckling of fibers with one another (Jones 1999). In extension mode, the matrix extends or contracts in the transverse direction because of the out of phase buckling of fiber relative to one another.

In this study, the longitudinal strands in the laminates were already buckled out of phase relative to one another. Thus when they were subjected to compression, the cross plies, providing lateral support, were extended due to transverse tensile forces. In tension, however, larger area of cross ply layers was contracted due to compressive stresses in the transverse direction. In both cases, cross plies provided a support that is elastic in nature. Thus, the differences in elastic behavior of cross plies under transverse tension and compression loads could have contributed to the differences in laminates' Young's moduli in compression and tension. Compression modulus is lower because wood exhibits lower stiffness in tension perpendicular to grain than compression perpendicular to grain; therefore, cross plies in the laminates would tend to deform more transversely when laminates are subjected to compressive loads than tensile loads.

Undulating strands in an axially loaded wood-strand composite are not only subjected to axial forces but also moments due to p-Δ effect. Not limiting the discussion to the assumption of

small strains and displacements, it is conceivable to reason that undulating strands tend to stiffen when stretched due to their tendency to straighten and soften when compressed due to their tendency to buckle more readily. This phenomenon could also occur in the elastic region when a wood-strand composite with voids is axially loaded. Examination of strain fields in compression and tension could possibly reveal some of the clues to the differences in their elastic behavior.

Parametric Study

To examine the effects of magnitude of strand undulation on wood-strand composite's Young's modulus, E_x of a representative laminate, was predicted using the fiber undulation model at various undulation magnitudes using a periodic sinusoidal function as shown in Equation 3.1. Mean value of Young's moduli of all strands used to fabricate the 20 laminates in this study was input as strand E_x to predict laminate elastic modulus using the FUM. Strand undulation parameter, A/L (amplitude/wavelength or period), was used instead of undulation angle for these predictions. Estimated laminate E_x from the FUM was normalized by dividing it by overall mean E_x of all strands. A plot of normalized laminate moduli versus A/L ratio is shown in Figure 3.8. Experimental results from tension and compression tests on laminates are also plotted for comparison. Experimental results from compression tests follow the trend predicted by the fiber undulation model very well; however, tensile moduli follow a similar trend, but are considerably higher than the FUM predictions. The FUM estimates indicate a nonlinear degradation in laminate Young's modulus as undulation angle increases.

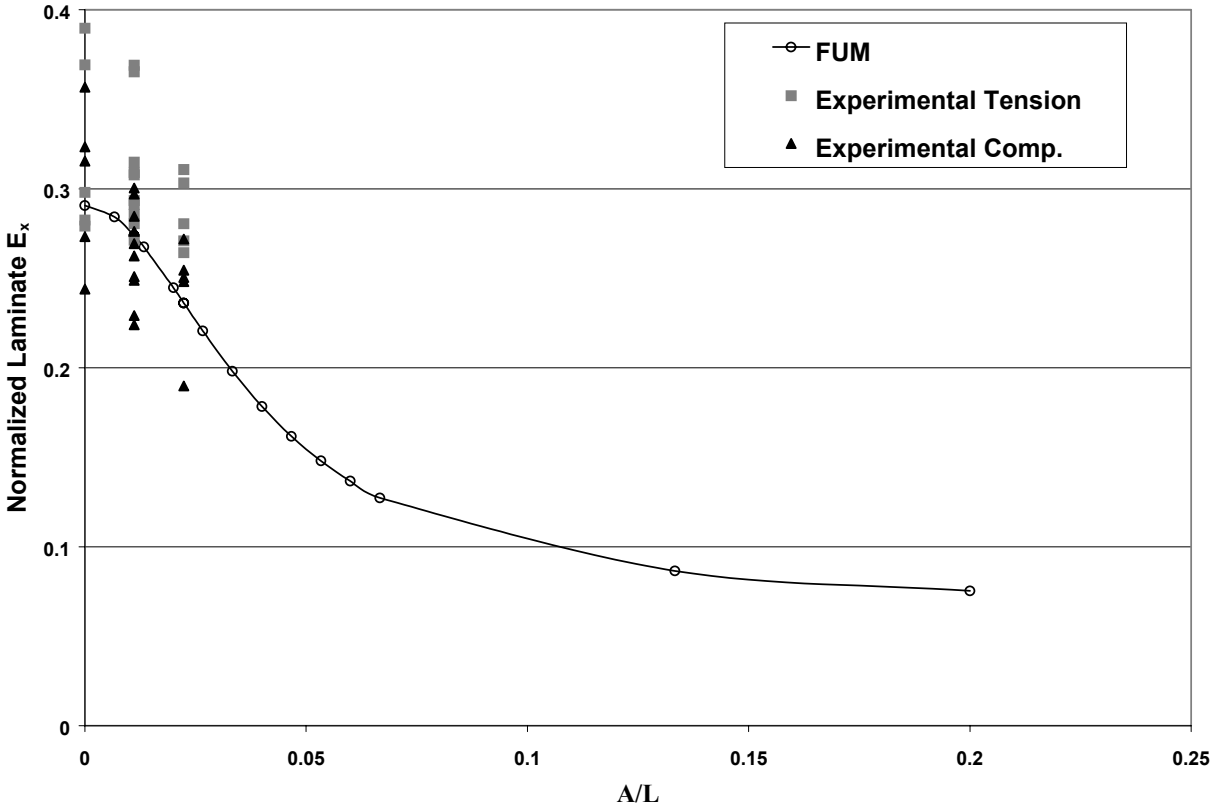

Figure 3. 8. Predicted Young's modulus as a function of undulation parameter, A/L, and experimental values for verification laminates.

Summary and Conclusions

Fiber undulation theory, an analytical approach considering fiber orientation in- and out-of-plane, was presented to predict the elastic properties of wood-strand laminates. A systematic experimental study was conducted to investigate the effects of wavy or undulating strand stands on the elastic properties of cross ply laminates. Strand undulation was shown to degrade Young's modulus of yellow-poplar laminates in both tension and compression. The effects of undulating strand were more severe when laminates were loaded in compression compared to tension. This finding was attributed to the microstructure of wood. When a wood specimen is

loaded in compression beyond the elastic region, formation of slip planes and minute compression failures at microscopic level are known to occur. This phenomenon seems to manifest itself even in the elastic region when loaded in compression. Distribution of strain field is speculated to be different when a specimen is loaded in tension versus compression. In addition, it is hypothesized that differences in compression and tension elastic behavior of the cross plies providing lateral support to undulating longitudinal strands contributed to the differences in compression and tension moduli of the laminates.

A discrete Fourier series expansion with three or four terms accurately described strand undulations in all laminates. Experimental results from compression tests were in good agreement with predictions based on the analytical model for undulatory angles of four and eight degrees (on an average, experimental values differed from the FUM predictions by 2 to 4 percent). However, in tension the experimental Young's modulus was on the average 12% greater than predictions of the FUM at the same undulation angles. In general, the tensile modulus of laminates was 7 to 14 percent greater than the compression modulus, with larger differences at higher undulation angles. In-situ strain analysis of specimen edges using nondestructive techniques, such as digital image correlation, would give more insight into reasons for differences between compression and tension moduli of wood-strand composites.

References

ASTM. 2001. Standard Test Methods for Specific Gravity of Wood and Wood-Based Materials. Standard D 2395 – 93. American Society of Testing and Materials. Volume 4.10.

Barnes, D. 2000. An integrated model of the effect of processing parameters on the strength properties of oriented strand wood products. Forest Products. J. 50(11/12):33-42.

_____. 2001. A model of the effect of strand length and strand thickness on the strength properties of oriented wood composites. Forest Products. J. 51(2):36-46.

Bienfait, J. L. 1926. Relation of the manner of failure to the structure of wood under compression parallel to the grain. Journal of Agricultural Research. 33(2):183-194.

Bodig J. and J. R. Goodman. 1973. Prediction of elastic properties for wood. Wood Science. 5(4):249-264.

_____ and B. A. Jayne. 1982. Mechanics of wood and wood composites. Van Nostrand Reinhold Company, New York, NY.

Chun H-J, J-Y Shin, and I. M. Daniel. 2001. Effects of material and geometric nonlinearities on the tensile and compressive behavior of composite materials with fiber waviness. Composites Science and Technology. 61:125-134.

Dai, C. and P. R. Steiner. 1994a. Spatial structure of wood composites in relation to processing and performance characteristics: Part II. Modelling and simulation of a randomly-formed flake layer network. Wood Sci. Technol. 28:135-146.

Dai, C. and P. R. Steiner. 1994b. Spatial structure of wood composites in relation to processing and performance characteristics: Part III. Modelling the formation of multi-layered random flake mats. Wood Sci. Technol. 28(3):229-239.

Davalos, J. F., J. R. Loferski, S. M. Holzer, and V. Yadama. 1991. Transverse isotropy modeling of 3-D glulam timber beams. Journal of Materials in Civil Engineering. 3(2): 125-139.

Dong, C-C. 1979. The mechanical properties of flakeboards related to flake orientation. Ph.D. Dissertation. College of Engineering, Washington State University. 157pp.

Geimer, R. L. 1979. Data basic to the engineering design of reconstituted flakeboard. In Proceedings of the 13t^{h} Washington State University International Symposium on Particleboard. pp. 105-125.

Hsiao, H. M. and I. M. Daniel. 1996. Elastic properties of composites with fiber waviness. Composites Part A 27A: 931-941.

Ishikawa, T. and Tsu-Wei Chou. 1983. One-dimensional micromechanical analysis of woven fabric composites. AIAA Journal 21(12):1714-1721.

Jones, R. M. 1999. Mechanics of composite materials. 2nd Edition. Taylor & Francis, Philadelphia, PA.

Keith C. T. and W. A. Cote, Jr. 1968. Microscopic characterization of slip lines and compression failures in wood cell walls. Forest Products Journal. 18(3):67-74.

Kellogg, R. M. and G. Ifju. 1962. Influence of specific gravity and certain other factors on the tensile properties of wood. Forest Products Journal. 12(10):463-470.

Koehler, A. 1955. Guide to determining slope of grain in lumber and veneer. Forest Products Laboratory Report 1585, Madison, WI.

Kollmann, F. F. P. and W. A. Cote, Jr. 1968. Principles of Wood Science and Technology, I. Solid Wood. Springer-Verlag, New York, NY.

Kreyszig, E. 1999. Advanced Engineering Mathematics, 8th Edition. John Wiley & Sons, Inc., New York, NY.

Lang, E. M. and M. P. Wolcott. 1996. A model for viscoelastic consolidation of wood-strand mats. Part I. Structural characterization of the mat via Monte Carlo simulation. Wood and Fiber Science. 28(1):100-109.

McNatt, J. D. and R. C. Moody. 1990. Structural Composite Lumber. Progressive Architecture 12.90:34-36.

Meyers, K. L. 2001. Impact of strand geometry and orientation on mechanical properties of strand composites. Master's Thesis. Dept. of Civil and Environmental Engineering, Washington State University. 115pp.

Naik, N. K. and P. S. Shembekar. 1992. Elastic behavior of woven fabric composites: I – Lamina analysis. Journal of Composite Materials. 26(15):2196-2225.

Palka, L. C. 1973. Predicting the effect of specific gravity, moisture content, temperature and strain rate on the elastic properties of softwoods. Wood Science and Technology. 7:127-141.

Shaler, S. M. and P. R. Blankenhorn. 1990. Composite model prediction of elastic moduli for flakeboard. Wood and Fiber Science. 22(3):246-261.

Suchsland, O. and H. Xu. 1991. Model analysis of flakeboard variables. Forest Prod. J. 41(11/12):55-60.

Suzuki, M. and N. Sekino. 1982. Anisotropic elasticity of oriented flakeboard. Mokuzai Gakkaishi. 28(2):91-96.

Triche, M. H., and M. O. Hunt. 1993. Modeling of parallel-aligned wood strand composites. Forest Prod. J. 43(11/12):33-44.

Wood Handbook: wood as an engineering material. 1987. Forest Products Laboratory. Agriculture Handbook 72. U.S. Dept. of Agriculture. 466pp.

Xu, W., and O. Suchsland. 1998. Modulus of elasticity of wood composite panels with a uniform vertical density profile: A model. Wood and Fiber Science. 30(3):293-300.

Yang, J. M., C. L. Ma, and Tsu-Wei Chou. 1984. Elastic stiffness of biaxial and triaxial woven fabric composites. 29th National SAMPE Symposium. pp. 292-303.

Zink, A. G., R. B. Hanna, and J. W. Stelmokas. 1997. Measurement of Poisson's ratios for yellow-poplar. Forest Products Journal. 47(3):78-80.

Chapter 4

Elastic Properties of Hot Pressed Aspen Strands

Introduction

Oriented strand composites such as OSB or OSL can be viewed as laminated composites where individual laminae are composed of adhesive coated strands of varying orientation. During hot pressing, the strands undergo considerable densification. The pressing conditions and location in the mat govern the environmental conditions surrounding each strand, which in turn influence the adhesive cure and final strand density. When assembled into the composite, the strand properties and the bond quality connecting the strands dictate the physical and mechanical properties of the resulting composite (Kamke and Casey 1988).

The *in-situ* elastic constants of a wood strand are affected by the physical changes that it experiences during the manufacturing process. These physical changes occur during cutting of strands and during hot pressing. Several studies (Price 1976, Mahoney 1980, Jahan-Latibari 1982a, 1982b, Geimer et. al. 1985, Casey 1987) have examined the influence of processing variables on strand properties.

In general, past researchers (Price 1976, Mahoney 1980, Jahan-Latibari 1982) have found that tensile moduli of strands were approximately 50% lower than Young's modulus values published for small, clear wood specimens. Although it has not been formally studied, this reduction might be attributed to damage induced during strand production. Studies addressing the change in Young's modulus after hot pressing conflict to some degree. Mahoney (1980) and Geimer et al. (1985) report a reduction in

modulus of elasticity after hot pressing; whereas, Price (1976) noted an increase in strand's Young's modulus. In all these studies, mats were pressed without resin, to facilitate isolating the strands for subsequent testing. Mahoney (1980) reported that strands subjected to higher temperatures influenced strand density and yielded significantly higher tensile moduli than those pressed at lower temperatures. Casey (1987) also reported that the dynamic bending moduli of test strands, normalized for density, increased with hot pressing. The magnitude of the increase was positively correlated to both the platen temperature and furnish moisture during pressing. In this study, resin was applied to strands, but the amount of resin on individual strands was not quantified.

Despite the numerous studies addressing strand properties, none have systematically examined the changes in elastic constants due to strand density, location, and/or resin content. This data is paramount to accurately model structure-property relationships in wood strand composites or to systematically study the role of pressing variables on altering strand properties.

Objectives

The goal of this study is to characterize the elastic properties of strands used in manufacturing oriented strand composites and to determine the effects of hot pressing on these properties. Specifically, the objectives leading towards this goal are to:

1. Determine the in-plane elastic constants of strands prior to the hot pressing process,
2. Investigate the influence of strand location and resin content on changes in strand density and elastic properties within a pressed panel, and
3. Develop a response model to predict the *in-situ* elastic constants of strands.

Materials and Methodology

The strands used in this study were produced from 65-70 years old quaking aspen (*Populus tremuloides* Mich.) trees harvested locally. The harvested logs were sawn into 0.5, 0.75, 1.0-inch thick lumber which were subsequently stranded using a laboratory-scale ring strander (CAE Model 12/48) equipped with 12-inch long knives. The lumber was oriented in the strander such that strand width was determined by the thickness. Knife projection and the ring advance speed were set to produce strands with average thickness of 0.03 inches. The mean strand length was 8 inches and the width varied between 0.5 and 1 inch.

Strand Selection and Treatment

A total of 114 strands were conditioned to mean moisture content of 7.4% with a coefficient of variation (COV) of 7%. After testing the strands, which will be discussed in the following section, all strands were oven dried to determine their moisture content

(MC) and density (ρ) according to ASTM D2395, Method A (ASTM 2001). Three sets of 27 strands were randomly selected from the entire set of stands to investigate the effects of hot pressing on elastic properties and density of strands. These strands were then conditioned to equilibrate to 3% MC, which was the moisture content of the furnish used for the hot pressing effects study.

A technique to isolate strands from a pressed mat using thin perforated Teflon® sheets as discussed by Jahan-Latibari et al. (1984) was employed in this study. This technique was shown not to significantly disturb the mechanisms of board manufacture, while yielding properties that are statistically similar to mats hot pressed without the use of Teflon®.

Three oriented strand test panels, each with three different target resin contents (0%, 4%, and 6% based on dry weight of furnish), were hot pressed under similar manufacturing conditions as the test panels made for an experimental study conducted by Meyers (2001). For board without any resin, furnish at 3% moisture content was taken through the same process as the furnish that was sprayed with resin, however no resin was applied. All panels were pressed to a thickness of 0.75 inches and a target density of 37 pounds per cubic feet (pcf). A 15-minute cycle was used with one-minute press closing time, eight-minute hold time, and two-minute degassing time. The platen temperature was 360 degree F and the mean core temperature was 275 degrees F. The peak pressure applied was around 750-psi.

Twenty-seven test strands were embedded in each test panel through their thickness at three different locations (Figure 4.1). Thus, each location consisted of nine test strands. A predetermined mass of liquid PF resin (GP® 130C44, 45% solids) was

sprayed on each face of test strands using an air-brush operated with 25-psi of air pressure. Strands were weighed immediately prior to and after spraying to determine the actual percentage of resin applied. These test strands were then enclosed in perforated Teflon® pouches and carefully distributed through the depth of the hand-formed mat at the three predetermined locations (Figure 4.1). To ensure that strands were distributed through the mat depth at approximately identical coordinates at all three locations in all three panels, the furnish for each panel was distributed into eight equal parts.

After forming a one strand thick layer, test strands were placed at the three locations with their longitudinal axis parallel to the mat's long direction (machine direction). Then, the remaining furnish was distributed followed by placement of another three test strands. This process was continued through the mat forming process. Another three test strands were placed on the top of the mat before distributing one strand thick layer of furnish at the end to finish forming the entire mat.

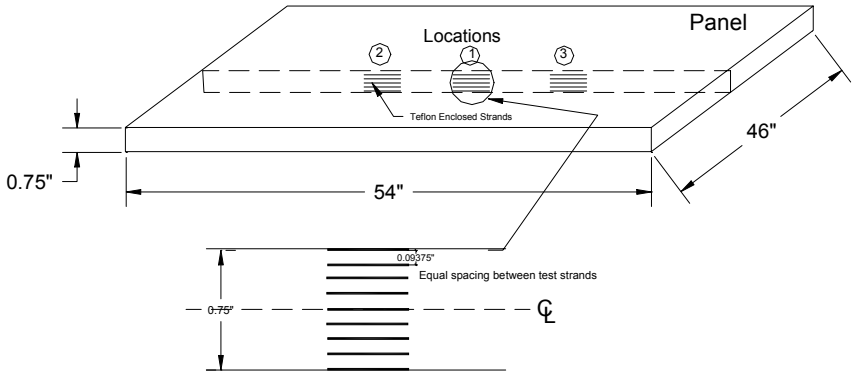

Figure 4. 1. Distribution of test strands within a test panel to study the effects of hot pressing on strand properties.

Upon completion of making the test panels, they were conditioned to reach an equilibrium moisture content at a relative humidity of 55% and temperature of 75 degrees F for over four months. After the panels equilibrated to a MC of approximately 8 to 9 percent, the test strands were carefully isolated from the panels using a wood chisel and tested.

Mechanical Testing

Prior to hot pressing

All strands, prior to being prepared to be embedded in the test panels, were tested in tension parallel to the longitudinal axis using a 2-kip screw-driven universal testing machine. The tension fixtures were self-aligning mechanical grips with a constant length separating the grips. Specimens were loaded at a uniform crosshead speed rate of 0.015 inches/minute. A ½-inch gage length clip extensometer (Epsilon Technology Corp., Model 3442-0050-020-ST) was used to measure strain at the mid-section of each strand. Load was applied such that the maximum stress applied was well within the lower part of the elastic region of the stress-strain curve.

After measuring longitudinal strain, each specimen was unloaded and the extensometer was reoriented to measure transverse strain while loading the specimen in tension. Using the measured strain in the longitudinal and transverse directions, the longitudinal elastic modulus, E_x, and Poisson's ratio, ν_{xy}, were determined for each of the strands. A Mathematica® program was written to determine the Young's modulus of the strands, which was the slope of the linear elastic region of the stress-strain curve. Poisson's ratio was determined using the method recommended in ASTM D638-99 (ASTM 2000).

Considering a plane-stress state, the engineering constants of a unidirectional lamina when geometric and material axes are not aligned with each other can be expressed as functions of the off-axis angle, ϕ, and the transformation relations are as follows (Jones 1999):

$$\frac{1}{\mathbf{E_x}} = \frac{1}{\mathbf{E}_1}\cos^4\phi + \left(\frac{1}{\mathbf{G}_{12}} - \frac{2\upsilon_{12}}{\mathbf{E}_1}\right)\sin^2\phi\cos^2\phi + \frac{\sin^4\phi}{\mathbf{E}_2} \qquad \textbf{Equation 4.2}$$

$$\upsilon_{xy} = \frac{\upsilon_{12}(\sin^4\phi + \cos^4\phi) - (1 + \frac{\mathbf{E}_1}{\mathbf{E}_2} - \frac{\mathbf{E}_1}{\mathbf{G}_{12}})\sin^2\phi\cos^2\phi}{\cos^4\phi + (\frac{\mathbf{E}_1}{\mathbf{G}_{12}} - 2\upsilon_{12})\sin^2\phi\cos^2\phi + \frac{\mathbf{E}_1}{\mathbf{E}_2}\sin^4\phi} \qquad \textbf{Equation 4.3}$$

Prior to being subjected to the hot pressing process, the Young's modulus and Poisson's ratio of aspen strands that had a grain angle closest to zero (between 0 and 1) were averaged to obtain an estimate for E_1 and ν_{12}. The remaining strands were grouped based on their fiber angles and average E_x and ν_{xy} values were computed. Using the computed mean values of E_1, ν_{12}, E_x, ν_{xy} and ϕ, tensor transformation relations (Equations 4.2 and 4.3) were simultaneously solved to determine the transverse modulus, E_2, and shear modulus, G_{12}, for each fiber angle category. Then E_2 and G_{12} of all fiber angle groups were averaged to represent the corresponding E_2 and G_{12} of the strands prior to being hot pressed.

After hot pressing

Immediately after isolating the strands from test panels their cross section dimensions were re-measured, and they were weighed and tested in tension following the procedures described earlier to determine E_x and ν_{xy}. After testing the strands, they were

oven dried to calculate their moisture content and density. The strands were then scribed with a needle (Yadama, 2002) to determine the fiber angle within the gage length.

Besides the grain angle, the elastic properties of these strands are also affected by the degree of densification as well as the temperature and moisture conditions they are exposed to depending on their relative location within a panel. Therefore the transformation equations should be applied with caution to determine the changed E_1 and ν_{12} of these strands. Because of lack of published information, it was assumed in this study that the relationships between E_1 and E_2 and E_1 and G_{12} of the strands prior to being subjected to hot pressing would still be valid after the strands were subjected to the hot pressing process. With this assumption, E_2 and G_{12} can be replaced with $c1E_1$ and $c2E_1$ in Equations 4.2 and 4.3, where c1 and c2 are constants of proportionality relating E_1 to E_2 and E_1 to G_{12} (c1 = 1/21 and c2 = 1/24 as shown later). Then, knowing E_x, ν_{xy}, and ϕ of the strands after hot pressing, their E_1 and ν_{12} can be calculated using Equations 4.4 and 4.5.

$$\nu_{12} = \frac{\nu_{xy}(\cos^4\phi + \frac{1}{c2}\sin^2\phi\cos^2\phi + \frac{1}{c1}\sin^4\phi) + \sin^2\phi\cos^2\phi(1 + \frac{1}{c1} - \frac{1}{c2})}{(\sin^4\phi + \cos^4\phi + 2\nu_{xy}\sin^2\phi\cos^2\phi)} \quad \textbf{Equation 4.4}$$

$$E_1 = E_x\left[\cos^4\phi + \frac{1}{c2}\sin^4\phi\cos^4\phi - 2\nu_{12}\sin^2\phi\cos^2\phi + \frac{1}{c1}\sin^4\phi\right] \quad \textbf{Equation 4.5}$$

Based on the oven dry weights of strands prior to hot pressing and their new cross section dimensions after hot pressing, strand densities were calculated. With the information generated regarding strand elastic properties after hot pressing, the data was analyzed using the simplex method (Cornell 1981, Breyfogle III 1992) to develop a response

model to predict E_1 and ν_{12} of strands in a hot pressed panel based on their constituent ratios.

Response Surface – Simplex Model

The objective of the simplex method is to develop an empirical model to estimate strand properties based on the composition of its constituents. To empirically model the properties of a strand with varying levels of density and resin, the system can be considered as mixture of three ingredients: cell wall material (C), void space (V), and resin content (R). In this case, the sum of the volume fraction for all the components will always sum to equal unity. The simplex method is a fractional factorial statistical design and analysis method that is ideally suited to develop response models for products that are a mixture of two or more ingredients (Cornell 1981).

Specific gravity, G, of the material that constitutes the cell walls is a constant, about 1.5 on the basis of oven-dry weight and volume (Bodig and Jayne 1982). Therefore, for all strands in this study, wood and void volume fractions were determined using the measured density and assuming a specific gravity of 1.5 for the cell wall material. Past research (Johnson and Kamke 1992) indicates that PF resin typically used in manufacturing of composite panels penetrates primarily into the cell lumens and vessel elements. Thus, assuming that the resin primarily occupies void space in the strands, the percent void volume was adjusted by subtracting the corresponding percent resin added.

In the simplex method, a mathematical equation is fit to model the response surface over the entire simplex factor space so that the empirical prediction of the response to any mixture over the entire simplex is possible (Cornell 1981). The ternary plot for the three components (C, V, and R), relevant to this study is shown in Figure 4.2.

The partial region, depicted in the plot, is determined by the volume fraction limits of the components of the mixture. A general form of regression function that can be fit to the data collected at the points of a {q,m} simplex lattice is the canonical form of the polynomial, which is derived by applying a restriction that the terms in a standard polynomial of a mixture design sum to one (Cornell 1981). In matrix notation, the equation can be written as

$$\{y\} = [X]\{\beta\} + \{\varepsilon\} \qquad \textbf{Equation 4.6}$$

Estimates of the β_i parameters are determined using the method of least squares which minimizes the square of the error. Knowing strand density and the amount of resin used, the proportions of the components of each of the test strands were determined. Knowing proportions of the three constituents, the ADX module in the statistical package SAS (SAS Institute Inc. 1999) was utilized to analyze the data and fit a response model, as per the mixture design, to predict E_1 and ν_{12} of strands after subjecting them to the hot pressing process. This response model is only valid for the manufacturing parameters and ranges of strand constituents examined in this study.

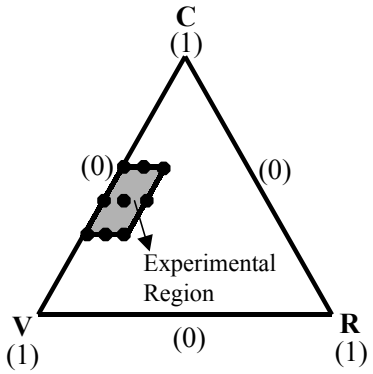

Figure 4. 2. {3,2} simplex factor space. Shaded area is the experimental region for this study, and the points are the design points where response was measured (C = cell wall, V = void volume, and R = resin content).

Results and Discussion

Original Strand Properties

Transformation equations along with strand fiber angle, E_x, and ν_{xy}, were utilized to determine original strand properties. The mean specific gravity of all strands was 0.39 with a COV of approximately 9%. Since, the variation in density of strands is significant, measured strand elastic properties were normalized to the average specific gravity of 0.39 using a linear relation suggested by others (Palka 1973, Kellogg and Ifju 1962). Then, strands were grouped by their fiber angles and transformation equations were applied based on average E_x and ν_{xy} to determine E_2 and G_{12} for each of the groups. The grouped normalized tensile test results on strands prior to the hot pressing process are summarized in Table 4.1. E_2 and G_{12} determined for each of the angle groups were averaged to obtain mean elastic constants for all strands ($E_2 = 8.316 \times 10^4$-psi and $G_{12} = 7.161 \times 10^4$-psi). There is, however, a lot of variation in the values of E_2 (COV of 61%) and G_{12} (COV of 39%), which could be a result of the high degree of variation in ν_{xy} of strands and relatively small fiber angles within strands.

The longitudinal Young's modulus in the material direction, E_1, of aspen strands was 1.75×10^6-psi with a COV of 13%. A published value (Bodig and Jayne 1982) for E_L of aspen at an average specific gravity of 0.35 and 12% moisture content is 1.293×10^6-psi. When the published value is adjusted to mean specific gravity (0.39) and MC (7.4%) of the test strands, it differs from the experimental value by approximately 8%. Note also that the published value was based on regression models developed from compression tests conducted on a limited number of species (Bodig and Goodman 1973). Poisson's ratio, ν_{12}, for strands with fiber angles near zero averaged 0.5, as compared to published

average values of 0.37 for ν_{LR} and 0.5 for ν_{LT} for hardwoods (Bodig and Jayne 1982). The mean ν_{xy} for all strands was 0.39 with a COV of 9%.

Table 4. 1. Summary of normalized test results on strands prior to hot pressing.

Mean. Fiber Angle (deg.)	Mean E_x (10^6 psi)	COV (%)	Mean ν_{xy}	E_2 (10^5 psi)	G_{12} (10^5 psi)
0.0	1.750	13	0.50		
2.2	1.585	13	0.42	0.187	0.247
3.4	1.467	14	0.47	0.449	0.300
4.4	1.614	13	0.39	0.618	1.016
5.2	1.394	12	0.36	0.458	0.518
6.2	1.352	16	0.33	0.534	0.616
7.3	1.262	17	0.36	0.709	0.649
10.4	1.174	17	0.48	1.880	0.957
11.3	0.982	N/A	0.23	0.738	0.751
12.0	1.099	N/A	0.40	1.533	1.039
13.0	0.975	N/A	0.22	0.932	0.941
17.0	0.702	N/A	0.29	1.111	0.844
			Mean	0.832	0.716
			COV (%)	61	39

In order to compare E_2 and G_{12} of strands to published values, it is necessary to invoke the assumption of transverse isotropy (Yadama 2002). With this assumption, E_2 could be compared against mean E_R and E_T values (75,800-psi), and G_{12} against mean G_{LR} and G_{LT} values (71,250-psi) as published by Bodig and Jayne (1982). Values of E_2 and G_{12} determined in the present study differ from published values by about 16.5% and 0.5%, respectively. Typically, considering all the variations in wood, the moduli of all woods are related according to the following ratios (Bodig and Jayne 1982):

$$E_L:E_R:E_T \approx 20:1.6:1 \quad \text{and} \quad E_L:G_{LR} \approx 14:1$$

In this study, the following relationships were established between E_1, E_2, and G_{12} of aspen strands:

$$E_2 = E_1/21 \qquad \text{and} \qquad G_{12} = E_1/24$$

The E_1:E_2 ratio is similar to the published ratios, whereas the E_1:G_{12} ratio is off by a factor of 2. For this study in transformation equations (Equations 4.4 and 4.5) c1 and c2 are set equal to 1/21 and 1/24.

A plot of normalized Young's modulus, E_x, against the fiber angle for all tested strands, as well as mean normalized Young's modulus for strand groups based on fiber angles is shown in Figure 4.3. The plot also shows the theoretical curve relating fiber angle to E_x based on the tensor transformation relationship (Equation 4.2) assuming E_1 = 1.750×10^6-psi, $E_2 = 8.316 \times 10^4$-psi, $G_{12} = 7.161 \times 10^4$-psi, and $\nu_{12} = 0.5$. The results indicate that tensor transformation is an effective way to describe the effect of fiber angle on the longitudinal elastic modulus of aspen strands. It is well established in the literature that E_x rapidly decreases with an initial increase in fiber angle. As the graph indicates, E_x at a 10-degree fiber angle is about 60% of its value at a zero degree fiber angle. Using equation 4.3, Poisson's ratio, ν_{xy}, was plotted against changing fiber angle in Figure 4.4. Variation in measured Poisson's ratio is very high, illustrating the degree of difficulty in determining Poisson's ratio experimentally. As the tensor transformation equation indicates, the value of Poisson's ratio, ν_{xy}, becomes relatively small (0.02) at very high fiber angles. This corresponds well to an average of ν_{RL} and ν_{TL} values of 0.044 and 0.027 published for hardwoods (Bodig and Jayne 1982).

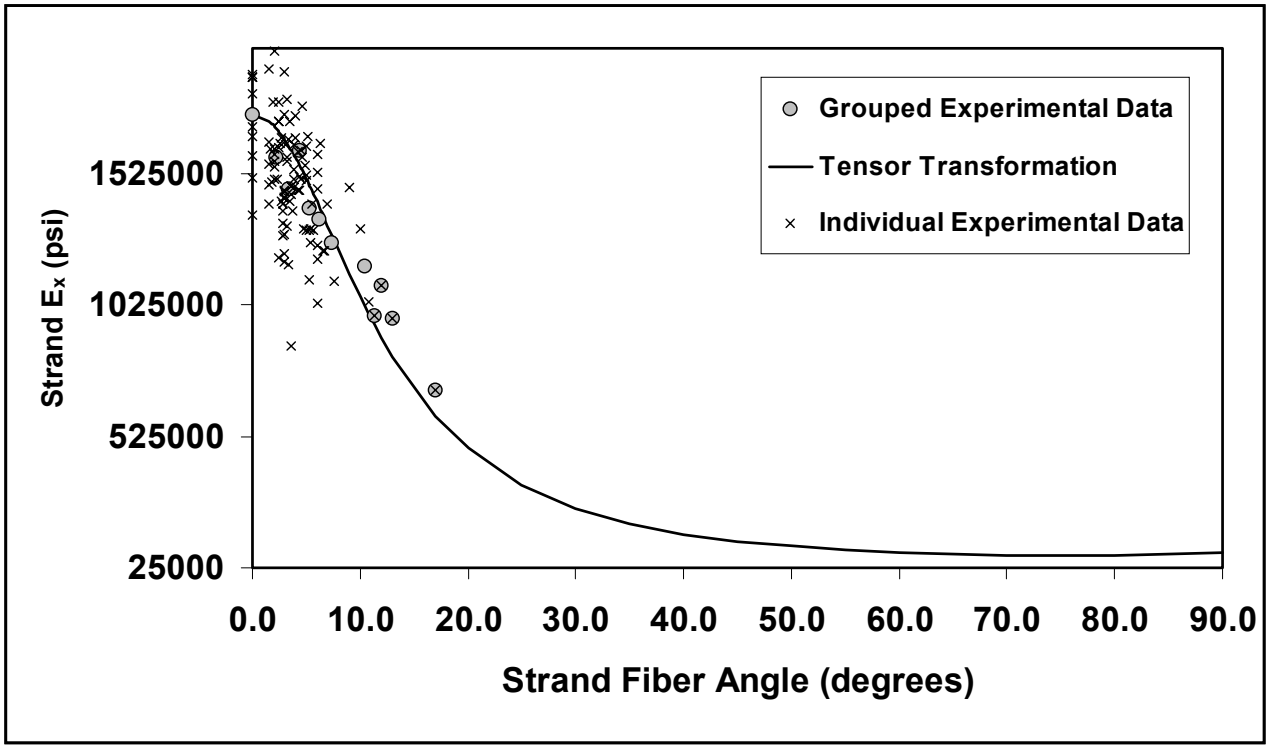

Figure 4. 3. Normalized Young's modulus versus strand fiber angle – experimental data and theoretical fit using tensor transformation.

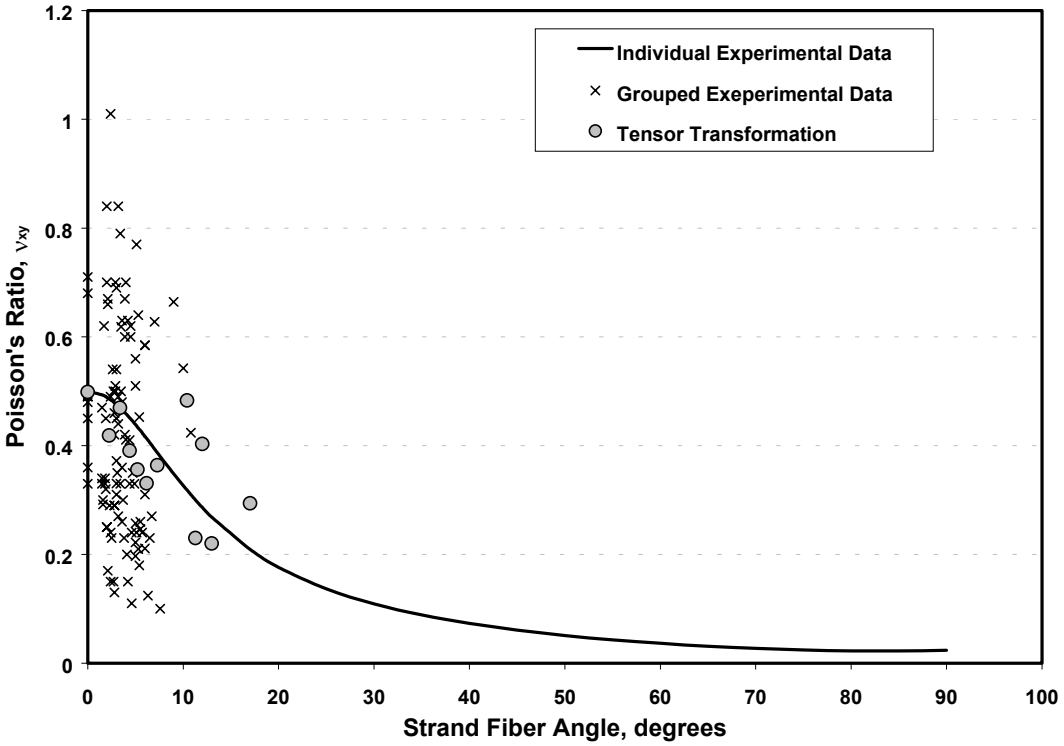

Figure 4. 4. Poisson's ratio of strands versus strand fiber angle – experimental data and tensor transformation fit.

The histogram of 116 strand fiber angles measured in this study is shown in Figure 4.5. Statistical analysis indicated that a 2-parameter lognormal probability density function (shape parameter, σ, of 0.637 and scale parameter, μ, of 1.201) describes the fiber angle distribution well. Chi-square test for goodness of fit yielded a p-value of 0.245 indicating a good fit.

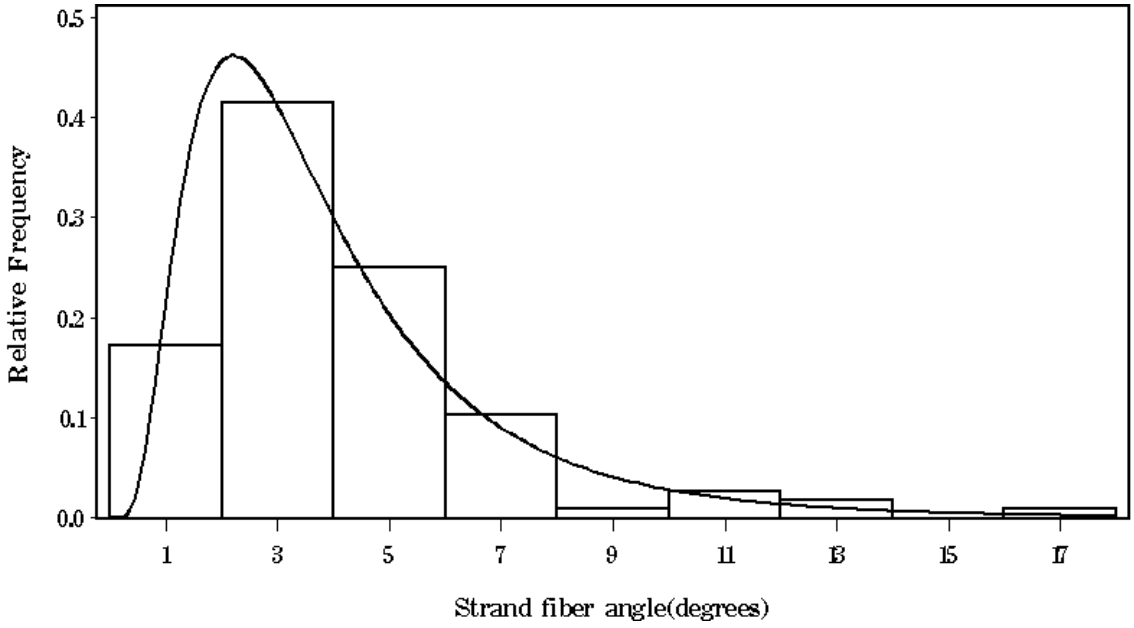

Figure 4. 5. Distribution of strand fiber angle and lognormal probability density function describing the distribution.

Hot Pressing Effects

To study the influence of hot pressing on physical and mechanical properties, the property ratio was computed as the ratio of that property after and before hot pressing. This ratio was computed separately for strand density ($\hat{\rho}$), Young's modulus ($\hat{\mathbf{E}}_x$) and Poisson's ratio ($\hat{\nu}_{xy}$). Mean changes in densification ratio through the thickness of the

three panels for three different resin levels are illustrated in Figure 4.6. Determination of actual resin contents gave a mean resin content of 5% and 7.5% with COV of 3%.

A relative strand location through the panel thickness corresponds to the top and bottom (1,-1) surfaces and panel center (0). As expected, the densification ratio profile is similar to the vertical density profile one would expect in an oriented strand composite panel (Figure 4.6). In general, strands with resin experienced higher densification ($\hat{\rho}$ = 2.15) compared to those without resin ($\hat{\rho}$ = 1.9) near the panel surfaces. A logical explanation for this difference could be the differences in the amount of springback or recovery from compression in strands with and without resin. The resin penetrating the strand is curing and restraining springback. At the core, the density ratio for strands averaged 1.3 to 1.45 for strands with and without resin, respectively. An earlier study by Casey (1987) supports these findings.

Scatter plots of $\hat{\mathbf{E}}_{\mathbf{x}}$ and $\hat{\nu}_{xy}$ versus the densification ratio for all strands in each resin percent category are shown in Figures 4.7 and 4.8. The $\hat{\mathbf{E}}_{\mathbf{x}}$ for the strands is positively correlated to densification ratio; whereas, $\hat{\nu}_{xy}$ remains invariant or indicates a slight tendency to decrease with increase in densification ratio for strands with resin.

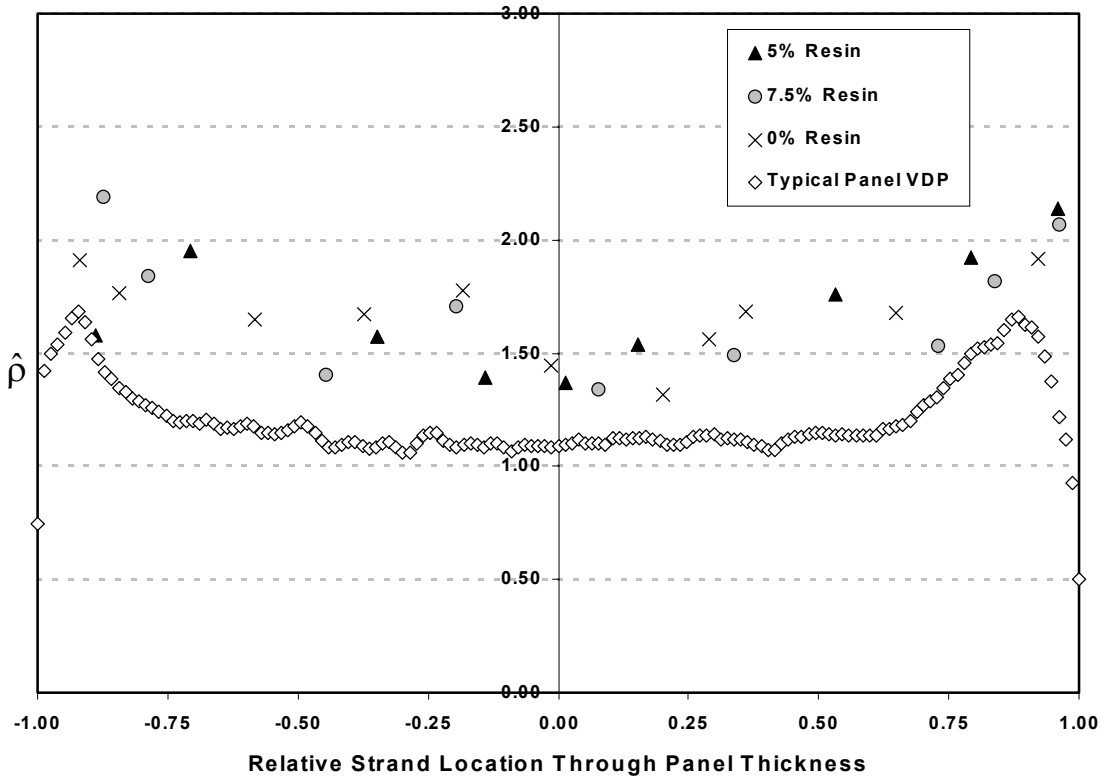

Figure 4. 6. Mean strand densification ratios through panel thickness for three resin levels. Also included is a typical panel vertical density profile.

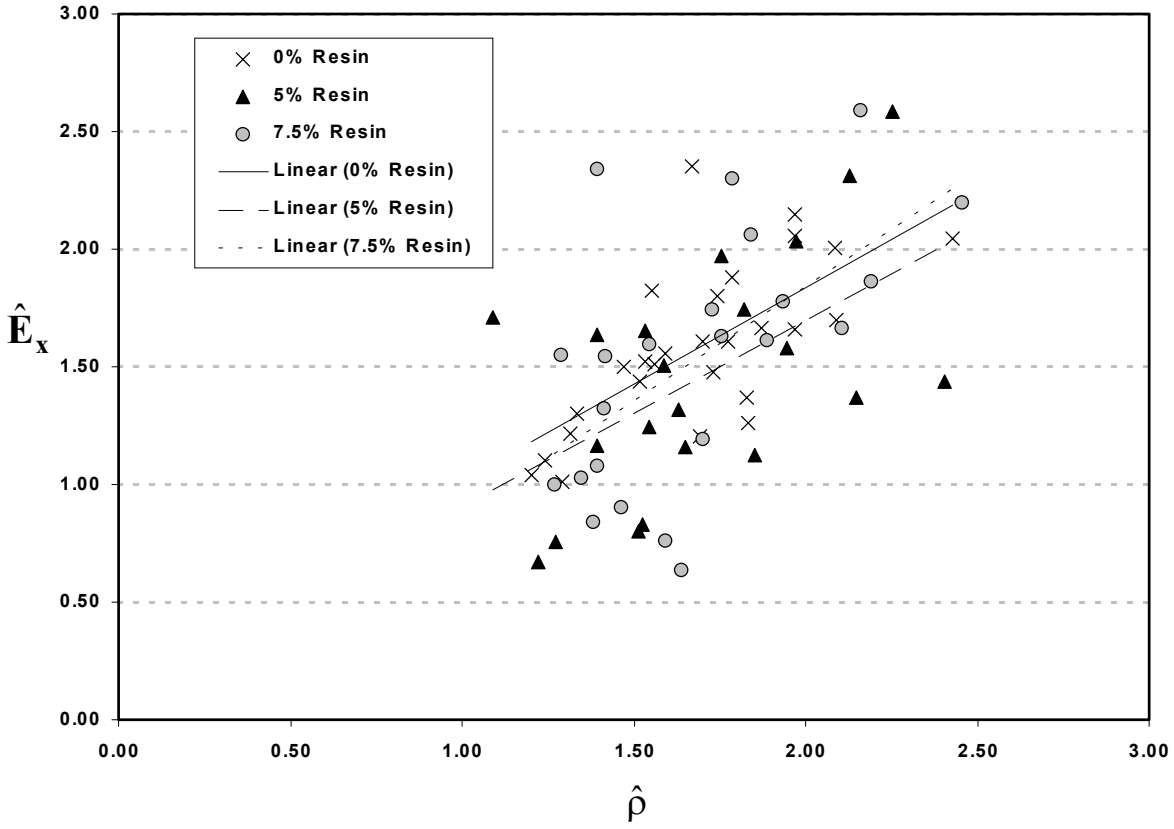

Figure 4. 7. Scatter plot of $\hat{E}_x$ versus densification ratio for all strands.

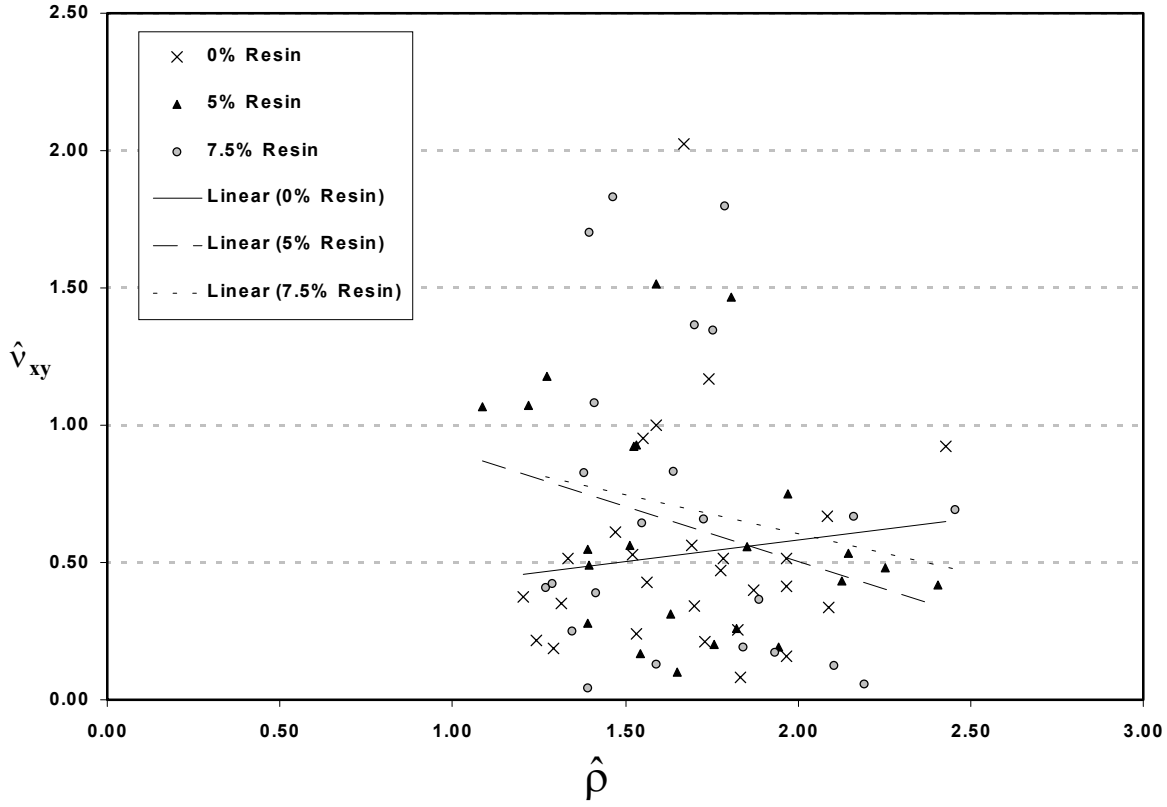

Figure 4. 8. Scatter plot of $\hat{\nu}_{xy}$ versus densification ratio for all strands.

The thickness of a panel was divided into three regions as illustrated in Figure 4.9: outer region (Region A) closer to the surfaces, middle region (Region C) closer to the mid-plane, and intermediate region (Region B) between the outer and middle regions. The mean $\hat{\mathbf{E}}_x$ for these regions were calculated within each resin level (Figure 4.9). In panels without resin, $\hat{\mathbf{E}}_x$ does not vary significantly between Regions A and B; whereas, in panels with resin, $\hat{\mathbf{E}}_x$ decreases substantially moving from Region A to B. This trend reinforces the role of resin in strand recovery and also suggests that the cured resin may act to repair strand damage or defect induced during pressing. On average, $\hat{\mathbf{E}}_x$ in the region around mid-plane is significantly lower than in the other two regions in panels

with or without the resin. The average moisture content of all strands isolated from pressed panels was 6.4% with a COV of 10%.

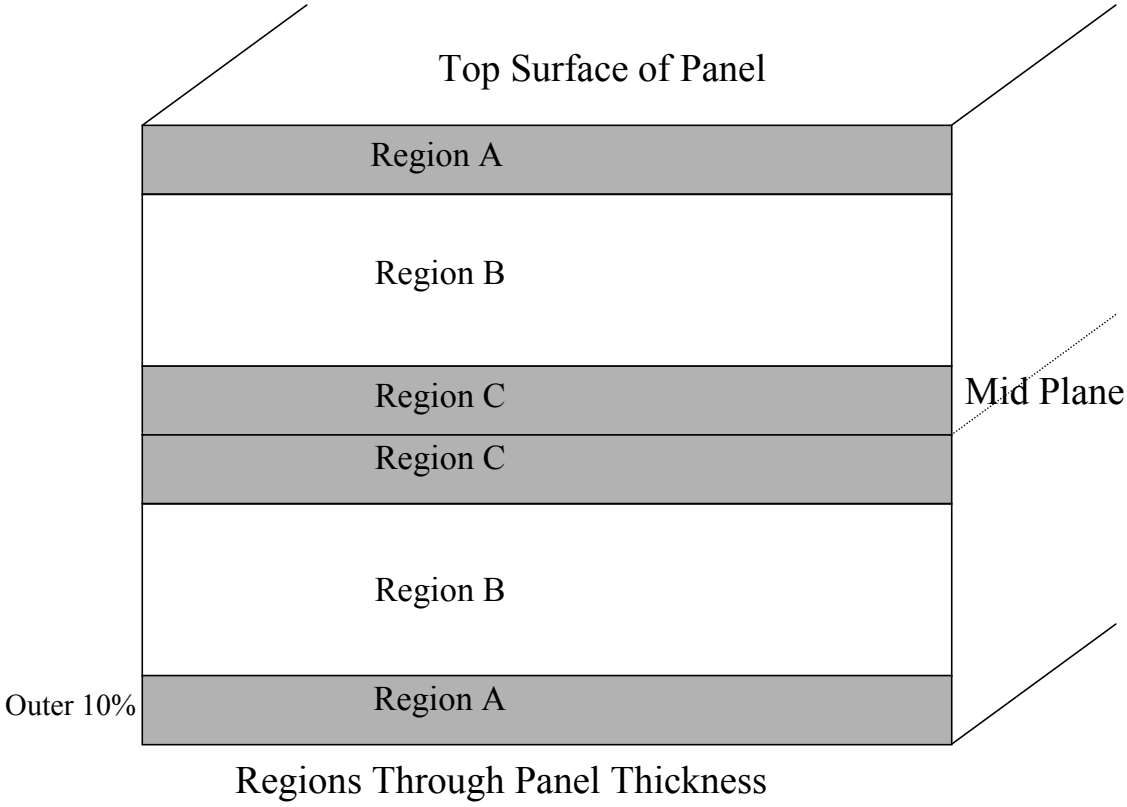

Regions Through Panel Thickness

	0% Resin	5% Resin	7.5% Resin
	$\hat{E}_x$	$\hat{E}_x$	$\hat{E}_x$
Region A	1.69	1.79	1.89
Region B	1.62	1.46	1.46
Region C	1.10	1.34	1.19

Figure 4. 9. Mean $\hat{E}_x$ for different regions through thickness of a test panel at three resin levels investigated in this study.

The intention of this study was to obtain a relationship between densification of strands during hot pressing and E_1 and ν_{12} while considering the effects of resin content. Therefore, to normalize for the effects of fiber angle in strands, E_1 and ν_{12} for all strands were calculated using Equations 4.4 and 4.5. As a first step, to describe the relationship between the combinations of density and Young's modulus, E_1, within each of the resin levels the exponential relationship, often used by researchers (Bodig and Goodman 1973, Bodig and Jayne 1982), was examined.

$$E_1 = a\,\rho^b \qquad \textbf{Equation 4.7}$$

This equation can be made linear for determining values of a and b by $\ln \mathbf{E}_1 = \ln \mathbf{a} + \mathbf{b} \ln \rho$. For the three resin levels, Figure 4.10 graphically shows the linear regression relationships between $\ln(E_1)$ and $\ln(\rho)$. The regression parameters for E_1 along with the corresponding correlation coefficients, r^2, are summarized in Table 4.2.

An analysis of covariance was performed to investigate whether there was a statistical difference between E_1 and ν_{12} values at different resin contents while density was introduced as a covariate into the model. Since analysis of covariance accounts for the linear effect of the covariate, $\ln(\rho)$ was taken as a covariate. Results indicated that the effect of resin content was not statistically significant for either of the response variables (E_1: p-value = 0.0916 and ν_{12}: p-value = 0.6222). The regression method was not well suited to obtain an estimate of the elastic property, ν_{12}, as density changes since the dependency of ν_{12} on density was not significant.

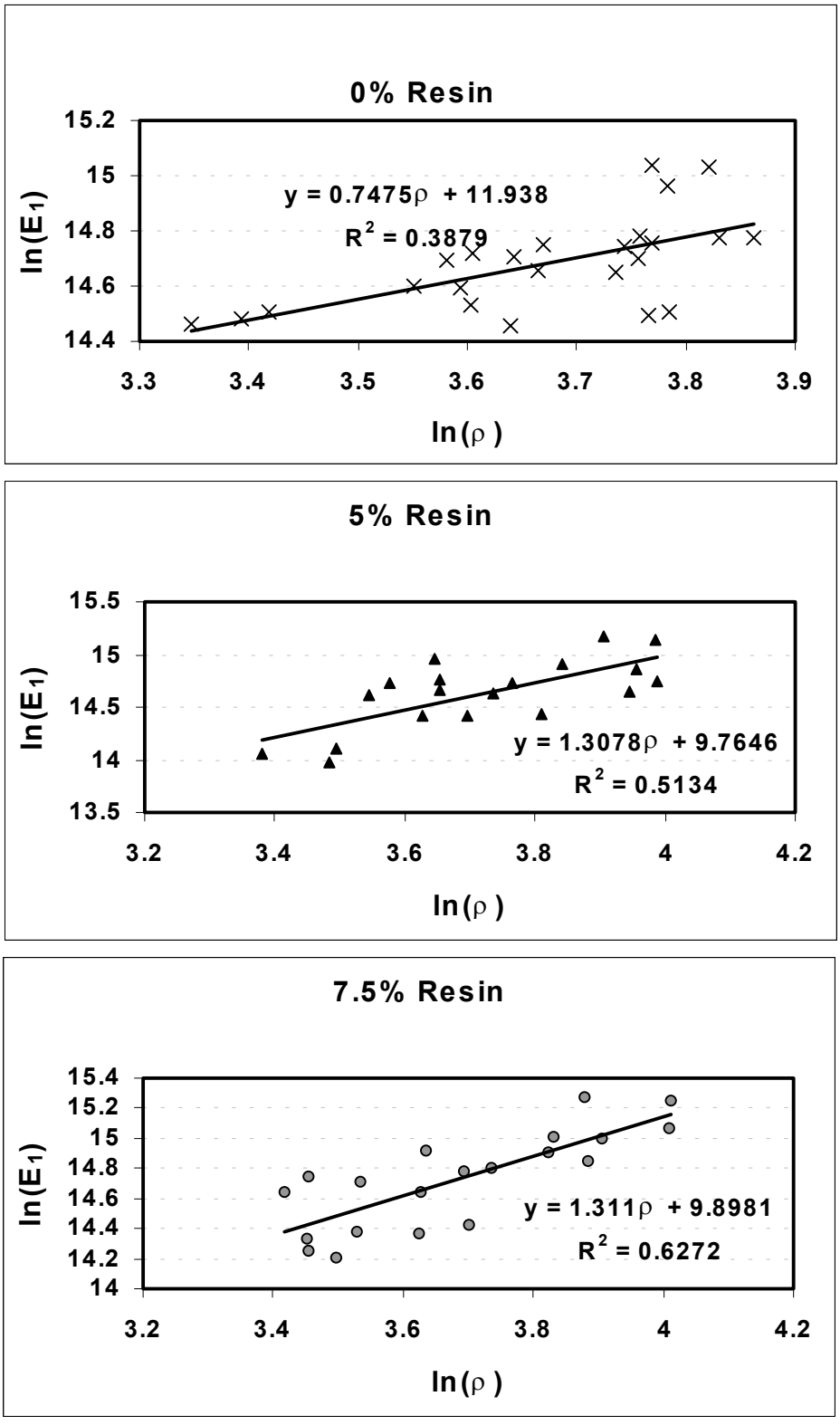

Figure 4. 10. Plots of $\ln(E_1)$ versus $\ln(\rho)$ for each of the resin levels.

Table 4. 2. Values of coefficients in the exponential relationship based on a regression analysis of $\ln(E_1)$ and $\ln(\rho)$.

Avg. Resin Level	a	b	r^2
0%	152970	0.7475	0.39
5%	17406	1.3078	0.51
7.5%	19892	1.311	0.63

A more suitable method would be one that describes the trends in response variables over an experimental region as control variables vary, even when their effects are not statistically significant. Therefore, as discussed earlier, data was analyzed using the simplex method (Cornell 1981, Breyfogle III 1992) to develop a response model to predict E_1 and ν_{12} of strands based on their constituent ratios, namely percent cell wall material, percent voids, and percent resin.

Simplex Analysis

Based on the post-pressing strand density, volume fractions for each of the three constituents were determined.

Resin volume fraction = R = 0, 0.05, or 0.075 **Equation 4.8a**

Void volume fraction = $V = (1 - G_{OD}/1.50) - R$ **Equation 4.8b**

Cell wall volume fraction = $C = 1-(1 - G_{OD}/1.50)$ **Equation 4.8c**

These proportions of constituents must be non-negative and sum to unity. Based on the calculated proportions of the three mixture components in this study, the constraints for each of the components were:

$$0.35 \leq C \leq 0.50$$

$$0.42 \leq V \leq 0.65$$

$$0 \leq R \leq 0.08$$

The response surface for strand E_1 and ν_{12} after hot pressing in the experimental region (Figure 4.2) can be expressed with the following best fit canonical polynomials:

$$E_1 = \beta_1 * C + \beta_2 * V + \beta_3 * R + \beta_4 * V * R \qquad \textbf{Equation 4.9}$$

$$\nu_{12} = \beta_1 * C + \beta_2 * V + \beta_3 * R \qquad \textbf{Equation 4.10}$$

The values of coefficients along with the corresponding correlation coefficients are given in Table 4.3. Contour plots of the response variables, E_1 and ν_{12}, over the area of interest within the simplex model are shown in Figure 4.11. The response surfaces within the experimental region for both response variables are graphically illustrated in Figures 4.12 and 4.13.

Table 4. 3. Values of coefficients for canonical polynomials to predict the response of E_1 and ν_{12}.

Elastic Constant	Estimates of Coefficients				r^2
	β_1	β_2	β_3	β_4	
E_1	4711775	678475	46125091	-89340000	0.54
ν_{12}	0.007272	0.572264	0.132851	0	0.02

The correlation coefficient for Poisson's ratio is extremely low indicating that the reduction in ν_{12} is basically a constant due to hot pressing and not strongly dependent

upon either the amount of densification or percent resin content. The mean reduction in ν_{12} was 38% irrespective of the densification and resin content. This phenomenon is reflected in the response surface obtained using mixture design (Figure 4.13), where the regression model for ν_{12} was not statistically significant. However, this method of analysis provides an insight into trends in changes in response variable as control variables are changed. For instance, the ν_{12}-response surface is a flat surface with a slight decrease in slope as cell wall and resin percents increased, indicating an increase in transverse stiffness of strands with increased densification and higher resin content. These results suggest that changes in strand structure during hot pressing are taking place with temperature changes and the presence of moisture introduced by the addition of resin. The ν_{12} varied between 0.25 and 0.4 within the region. The variations in ν_{12} and E_1, along with 95% prediction intervals, as each of the three constituents are varied within their constraints are shown in Figure 4.14.

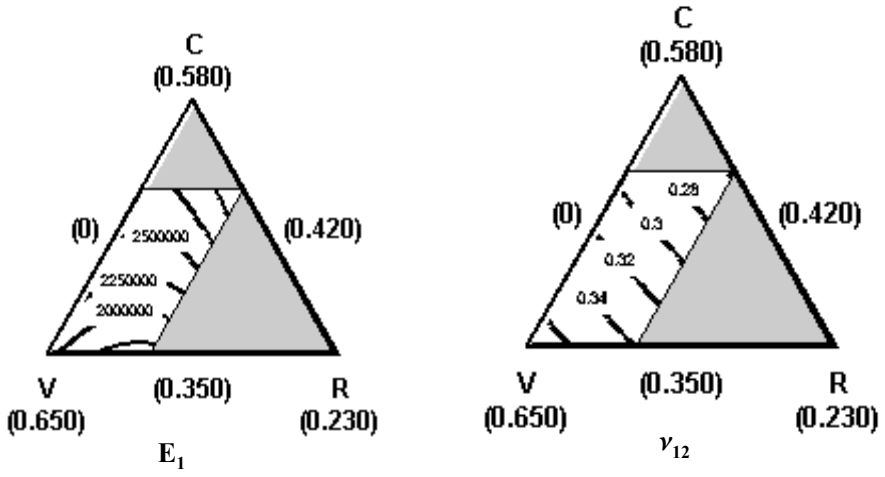

Figure 4. 11. Contour plots of response variables over the experimental region. Values in parenthesis are the constraints on control variables -- cell wall (C), void volume (V), and resin content (R).

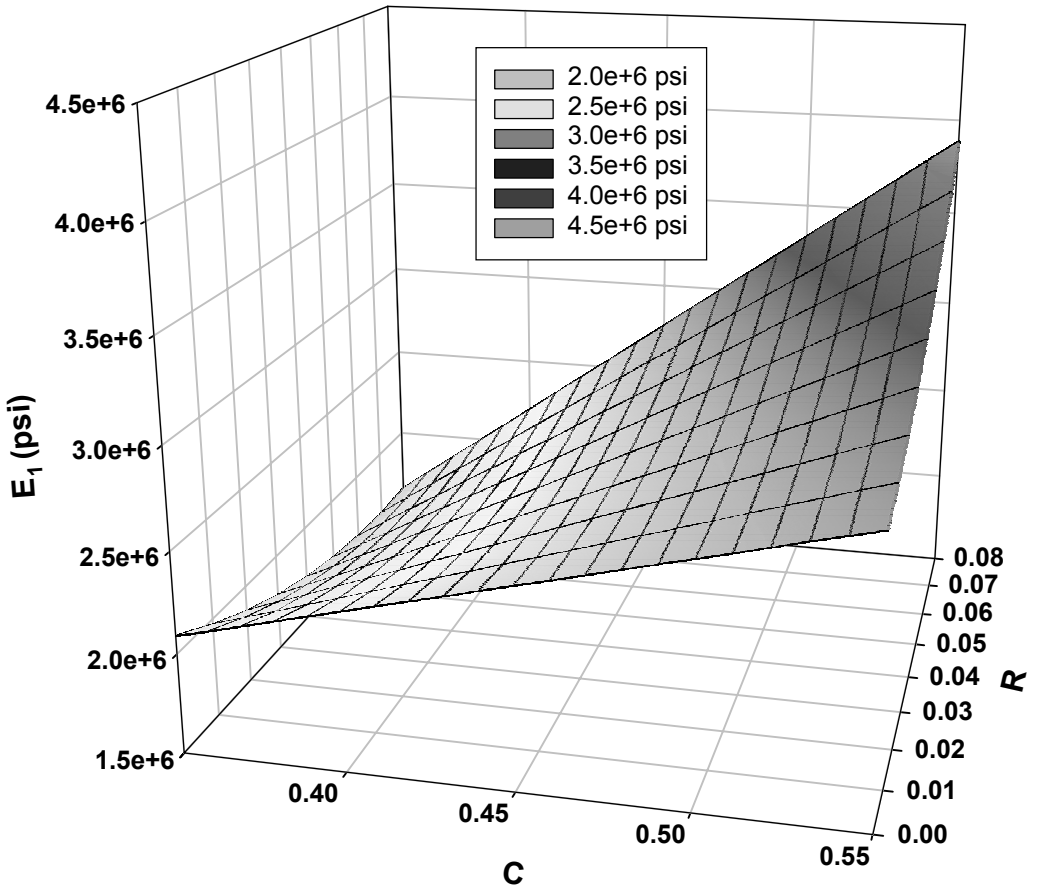

Figure 4. 12. Graphical representation of strand E_1 response equation accounting for the effects of hot pressing based on mixture design.

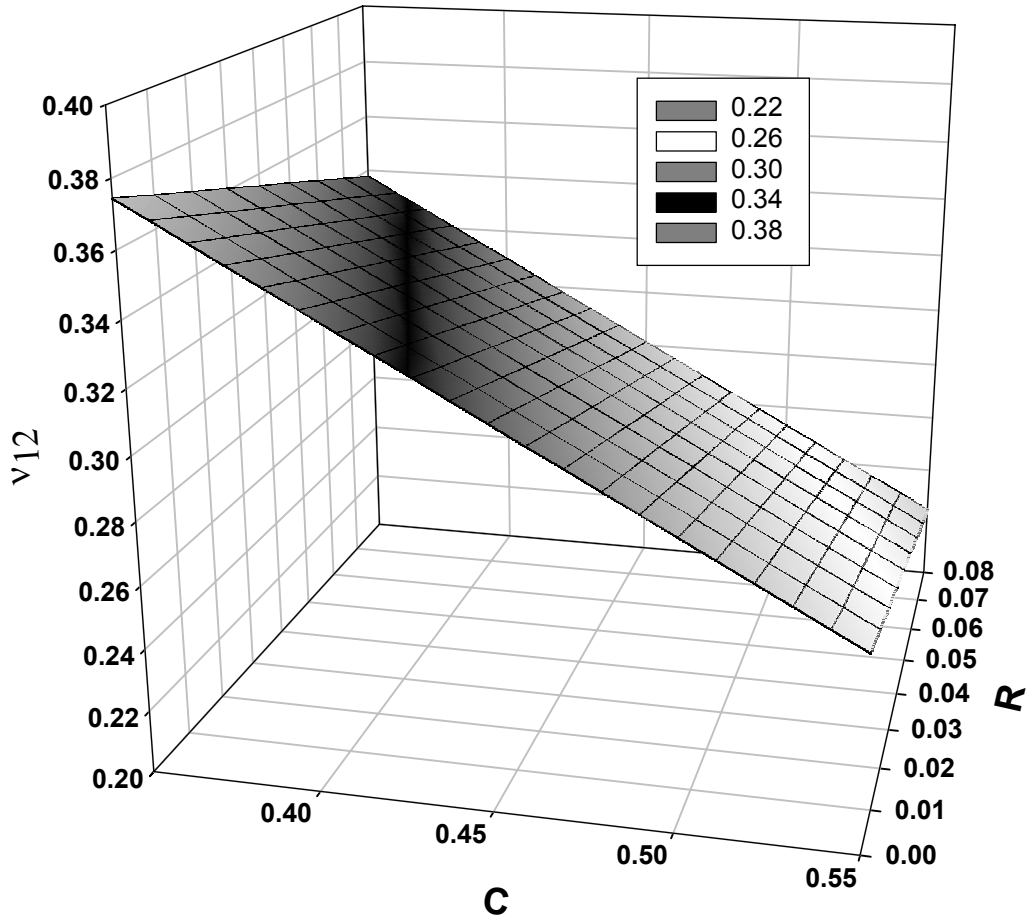

Figure 4. 13. Graphical representation of strand ν_{12} response equation accounting for the effects of hot pressing based on mixture design.

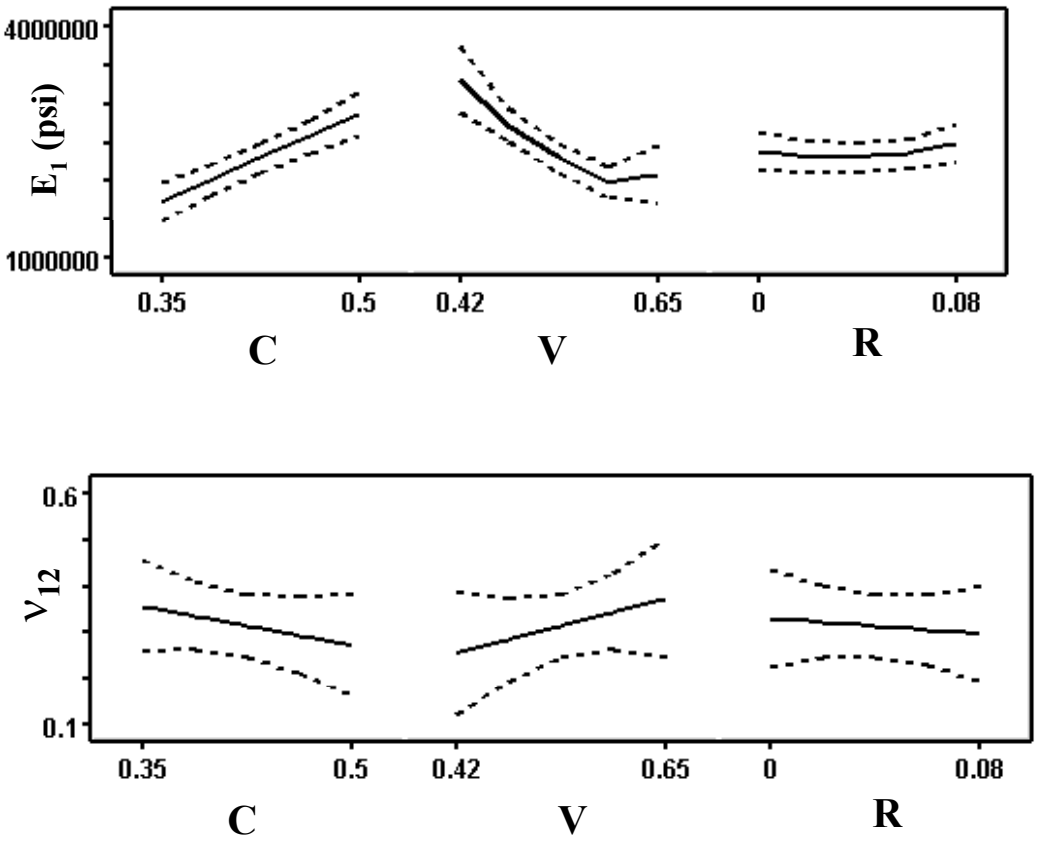

Figure 4. 14. Variation in strand E_1 and ν_{12} as its constituent fractions varied within the experimental region. Dashed lines indicate 95% prediction intervals.

Examination of the E_1 response surface (Figure 4.12) indicates a decrease with decreasing densities and increasing resin content. However, at high density levels, this trend is reversed. A possible explanation for this effect of resin content on E_1 could be stiffening of the strands as resin interacts with cell wall material with increasing densification ratios due to more penetration of resin into cell wall. This interaction between resin and cell wall material is probably initiated due to an increase in wood plasticization at higher densification ratios (Laborie 2002). More research is needed in this area to establish definite trends and interactions. An increase in densification has

direct impact on strand elastic modulus. A similar trend was also found with increase in resin content, however it was not statistically significant. Casey (1987) also reported an increase in dynamic bending modulus with increase in flake densification. Although she reported that increases in mat moisture content increased the dynamic bending modulus of strands, she did not examine the effects of changes in resin amounts.

Gardner et. al. (1993) examined changes in polymer structure of wood strands when heated under conditions similar to the hot pressing of wood composites. Results indicated that the cellulose crystallinity in the wood increases slightly in response to heat treatment, thus supporting the findings of this study that hot pressing of wood strands increases their elastic modulus. This effect is further magnified with an increasing presence of moisture. The addition of adhesive has a dual effect on strand properties. It influences the strand stiffness and affects the heat and moisture movement within the mat through adding more water to the furnish. Moisture added to furnish through adhesive plays an important role in determining the dynamics of heat and moisture transfer within the mat during hot pressing. Also, it affects the properties of strands since wood is a viscoelastic material. Andrews et. al. (2001) showed in their study that furnish moisture influences the amount of densification in all zones through the thickness of a panel.

Summary & Conclusions

Material properties, E_1 and ν_{12}, of aspen strands were experimentally evaluated in tension. E_2 and G_{12} were estimated using tensor transformation relations. Estimated values agreed well with the published values. Tensor transformation is an effective way to relate fiber angle and Young's modulus of aspen strands, however large variations in

estimated properties could result with smaller fiber angles. A lognormal probability density function fit the distribution of strand fiber angles well.

Investigation of hot pressing effects on strand properties indicated a direct relation between densification during hot pressing and E_1. Response models based on mixture design, considering the hot pressing effects, were developed to predict E_1 and ν_{12} of aspen strands. Even though the effect of resin content on strand elastic properties was not statistically significant, results of the simplex analysis suggested a positive trend for E_1 and a negative trend for ν_{12}. The results of this study support findings by other researchers that hot pressing increases strand elastic properties due to densification and plasticization, and this effect is further enhanced as resin content is increased due to addition of moisture. The addition of adhesive has a dual effect on strand properties. It influences the strand stiffness and affects the heat and moisture movement within the mat through adding more water to the furnish. Resin content tends to show a positive affect on strand's Young's modulus. A possible explanation for this effect of resin content on E_1 could be stiffening of the strands as resin interacts with cell wall material with increasing densification ratios due to more penetration of resin into cell wall. This interaction between resin and cell wall material is probably initiated due to an increase in wood plasticization at higher densification ratios (Laborie 2002).

References

Andrews, C. K., P. M. Winistorfer, and R. M. Bennett. 2001. The influence of furnish moisture content and press closure rate on the formation of the vertical density profile in oriented strandboard. Forest Products Journal. 51(5):32-39.

ASTM. 2000. Standard Test Methods for Tensile Properties of Plastics. Standard D 638-99. American Society of Testing and Materials. Volume 8.01.

ASTM. 2001. Standard Test Methods for Specific Gravity of Wood and Wood-Based Materials. Standard D 2395 – 93. American Society of Testing and Materials. Volume 4.10.

Bodig J. and J. R. Goodman. 1973. Prediction of elastic properties for wood. Wood Science. 5(4):249-264.

_____ and B. A. Jayne. 1982. Mechanics of wood and wood composites. Van Nostrand Reinhold Company, New York, NY.

Breyfogle III, F. W. 1992. Statistical Methods for Testing, Development, and Manufacturing. John Wiley & Sons, Inc., New York, NY.

Casey, L. J. 1987. Changes in wood-flake properties in relation to heat, moisture, and pressure during flakeboard manufacture. Master's Thesis, Dept. of Forestry and Forest Products, Virginia Polytechnic Institute and State University, Blacksburg, VA. 162pp.

Cornell, J. A. 1981. Experiments with mixtures: Designs, Models, and the Analysis of Mixture Data. John Wiley & Sons, New York, NY.

Gardner, D. J., D. w. Gunnells, M. P. Wolcott, and L. Amos. 1993. Changes in wood polymers during the pressing of wood-composites. In Cellulosics: Chemical, Bichemical and Material Aspects. Editors J. F. Kennedy, G. O. Phillips, and P. A. Williams. Ellis Horwood, New York, NY. pp 513-518.

Geimer, R. L., R. J. Mahoney, S. P. Loehnertz, and R. W. Meyer. 1985. Influence of processing-induced damage on strength of flakes and flakeboards. USDA Forest Service Research Paper FPL 463. 15 pp.

Jahan-Latibari, A. 1982a. The response of aspen flakes and flake-board to flake surface modifications. Proceedings of 6th Washington State University International Symposium on Particleboard. pp. 331-351.

_____. 1982b. The response of aspen flakes and flakeboard to flake surface modifications. Ph.D. Dissertation, Washington State University. 135pp.

_____, W. E. Johns, R. V. Subramanian. 1984. Technique for isolating flakes from the pressed mat. Forest Products Journal. 34(2):33-34.

Johnson, S. E. and F. A. Kamke. 1992. Quantitative analysis of gross adhesive penetration in wood using fluorescence microscopy. Journal of Adhesion. 40:47-61.

Jones, R. M. 1999. Mechanics of composite materials. 2nd Edition. Taylor & Francis, Philadelphia, PA.

Kamke, F. A. and L. J. Casey. 1988a. Fundamentals of flakeboard manufacture: internal-mat conditions. Forest Products Journal. 38(6):38-44.

Kellogg, R. M. and G. Ifju. 1962. Influence of specific gravity and certain other factors on the tensile properties of wood. Forest Products Journal. 12(10):463-470.

Laborie, M-P. G. 2002. Investigation of the wood/phenol-formaldehyde adhesive interphase morphology. Ph.D. Disseration. Virginia Polytechnic Institute and State University.

Mahoney, R. J. 1980. Physical changes in wood particles induced by the particleboard hot-pressing operation. M.S. Thesis. Washington State University. 35pp.

Marra, A. A. 1992. Technology of Wood Bonding Principles in Practice. Van Nostrand Reinhold, New York, NY.

Meyers, K. L. 2001. Impact of strand geometry and orientation on mechanical properties of strand composites. Master's Thesis. Dept. of Civil and Environmental Engineering, Washington State University. 115pp.

Palka, L. C. 1973. Predicting the effect of specific gravity, moisture content, temperature and strain rate on the elastic properties of softwoods. Wood Science and Technology. 7:127-141.

Price, E. W. 1976. Determining tensile properties of sweetgum veneer flakes. Forest Products Journal. 26(10):50-53.

SAS Institute Inc. 1999. SAS for Windows Version 8. Cary, North Carolina.

Yadama, V. 2002. Characterization and modeling of oriented strand composites: Chapter 3. Ph.D. Dissertation. Washington State University.

Chapter 5

Characterization of Oriented Strand Composite Panels

Introduction

Oriented strand composites can be engineered to meet service requirements. The mat structure formed through the manufacturing process gives rise to different degrees of anisotropic behavior in the product. In practice, the directional properties can be controlled through the size and orientation of the anisotropic wood elements. A model predicting the behavior of an OSC must incorporate a description for the directional properties of the wood elements comprising the particle network. However, the spatial structure of wood composites is extremely complex, time consuming to characterize, and complicated by the inherent variability of wood. To accurately model wood-strand composites and efficiently engineer them, it is critical that a database of wood composite structure, factors influencing it and the effects of structure on composite stiffness and strength be developed.

In the past, researchers (Dai and Steiner 1994a & 1994b, Lang and Wolcott 1996, Lenth and Kamke 1996, and Suchsland and Xu 1991) have developed models that incorporated key parameters contributing to the structure of a wood-strand mat. The result has largely been statistical and probabilistic methods describing the horizontal density distribution. Analyses of spatial structure for the mats have been used primarily to model stress-strain behavior of wood-strand mats in transverse compression during hot pressing. However, the focus for studying the structure of finished panels has been directed primarily towards the vertical density profile that is established during hot

pressing. To aid the micro- or macro-mechanic modeling of OSC performance, certain key parameters characterizing the finished panels must be determined.

Previous studies (Geimer 1976, Geimer et. al. 1979, Harris and Johnson 1982, Shaler and Blankenhorn 1990, Shaler 1991, Barnes 2000, Meyers 2001) have generally concentrated on examining in-plane orientation of particles and how it affects composite properties. However, there is a third dimension to the structure of a wood composite panel. The out-of-plane orientation of particles can significantly influence the mechanical and physical behavior of particleboard (Maloney 1993). In long strand composites, the waviness along the strand length can potentially reduce mechanical properties in a similar manner. Under compressive loading in the longitudinal direction the effect of strand waviness becomes an important issue because of their tendency to buckle more readily.

Besides particle orientation, another inherent feature of a wood composite panel is voids present between and within the wood elements. Voids within a strand vary with the *in situ* particle density; however, between strand voids are developed from mat structure and must be accounted for separately. Very little work has been done to characterize these random and incidental features of oriented strand composites. A finished wood-strand panel could be characterized with three key parameters: in-plane orientation of particles, out-of-plane or through thickness undulation of particles, and between strand void volume fraction. Where Meyers (2001) has characterized the in-plane orientation of oriented strand composites fabricated for this study, this research concentrates on strand undulation and void distribution.

Objectives

The objectives of this study are to contribute to the characterization of the three dimensional structure of an oriented strand composite panel with key random variables. Specific objectives of the study are to:

1. Determine the between strand void volume of single layer, oriented strand composites,
2. Quantify strand orientation through the thickness of oriented strand panels in the longitudinal and transverse directions, and
3. Examine the influence of manufacturing variables such as strand geometry and vane spacing, on these structural variables.

Materials and Methodology

Specimens for this study were obtained from laboratory manufactured oriented strand composites as described elsewhere (Meyers 2001, Yadama 2002). To summarize, panels were manufactured with aspen (*Populus tremuloides)* strands with multiple geometries and levels of orientation. Three nominal strand lengths (4, 8, and 12 inches) and widths (0.5, 0.75, and 1.0 inches) were manufactured with a single average strand thickness of 0.03 inches. Three boards were made within each length and width category and during mat formation, these strands were oriented using two vane spacings (1.5 and 3.0 inches) with three replicate panels resulting in a total of 45 boards (Table 5.1). Panels were trimmed to final dimensions of 41" by 35". Three 2 by 14-inch specimens were cut from each panel within each strand length, strand width, and vane spacing category for

determination of void volume fractions and strand undulations in both directions (see specimen cutting scheme figure in Appendix D).

Table 5. 1. Summary of panels manufactured for this study.

Strand Length(in.)	Vane Spacing(in.)	Strand Width (in.) 0.5	0.75	1
4	1.5	3 panels	3 panels	3 panels
	3	3 panels	3 panels	3 panels
8	1.5	3 panels	3 panels	3 panels
	3	3 panels	3 panels	3 panels
12	3	3 panels	3 panels	3 panels

Determination of Void Volume Fraction

Total void volume (V_t) in any given cross section of an oriented strand composite is a sum of void volume within each strand (V_w) and void volume between strands (V_b). To determine V_b, two 2-inch by 2-inch samples were obtained from each of the three 2-inch by 14-inch specimens cut from test panels. After oven drying all specimens, their oven dry specific gravity (G) values were determined by dividing their weight by volume. The total percentage of void volume, V_t, was then calculated based on the assumption that the cell wall specific gravity of any wood is approximately 1.5 (Bodig and Jayne 1982).

$$\mathbf{V_t} = 1 - \frac{\mathbf{G}}{1.5} \qquad \textbf{Equation 5.1}$$

After determining V_t, vertical density profiles of all specimens were obtained using an x-ray density profiler at increments of 0.005". In general, the density profiles

were symmetric with an average face to core density ratio of 1.5 (Meyers 2001). A representative density profile for the boards fabricated for this study is given in Figure 5.1. A digital image of the specimen edge was used to count the number of strands in one plane of the specimen and determine their relative locations through the depth of the specimen. Using the digitized locations and the density profile data, approximate strand void volumes within each strand through the thickness of a specimen were determined using:

$$\mathbf{V_w^i} = 1 - \frac{\mathbf{G_i}}{1.5} \qquad \textbf{Equation 5.2}$$

where $\mathbf{V_w^i}$ = void volume within i^{th} strand and G_i is the specific gravity of i^{th} strand obtained from vertical density profile data. Then V_w for a specimen was then estimated using

$$\mathbf{V_w} = \frac{1}{\mathbf{N}} \sum_{\mathbf{i}=1}^{\mathbf{N}} \mathbf{V_w^i} \qquad \textbf{Equation 5.3}$$

where, N = number of strands through the thickness of a specimen. The between strand void volume for a specimen could then be determined as:

$$V_b = V_t - V_w \qquad \textbf{Equation 5.4}$$

An analysis of variance was performed to determine the statistical significance of strand geometry and vane spacing on V_w.

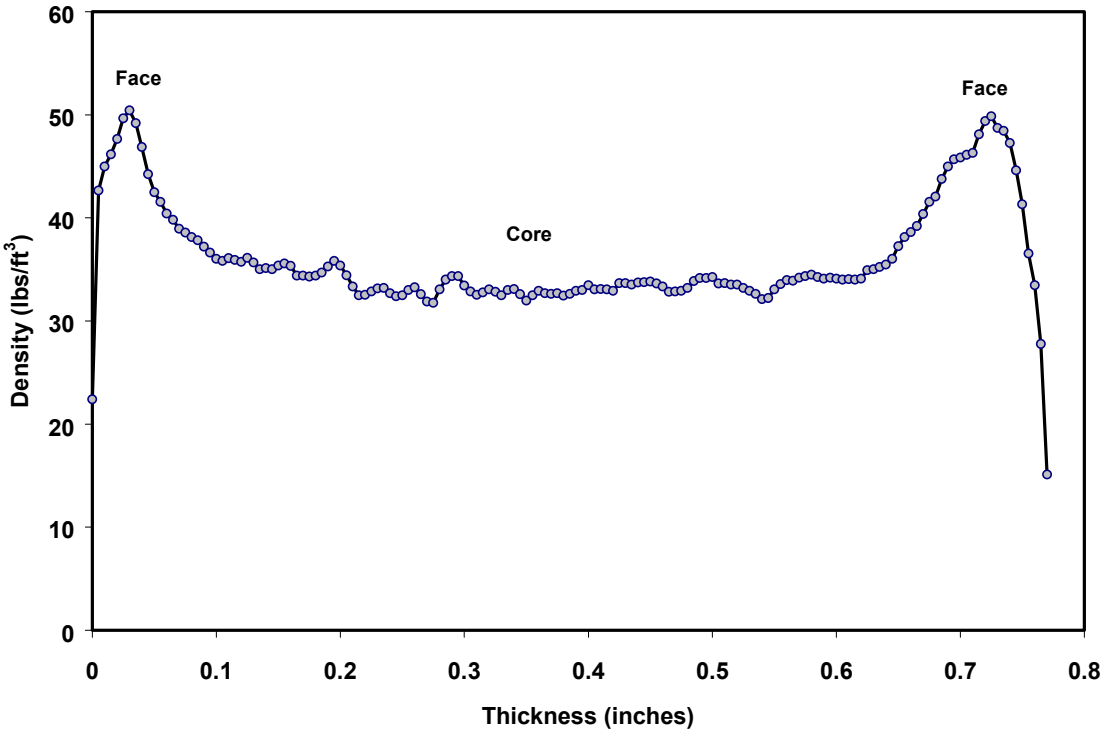

Figure 5. 1. A representative vertical density profile from the test panels.

Strand Orientation Through Panel Thickness

After examining the edge and end of an oriented strand composite panel (Figure 5.2), it is evident that strands weave or undulate along their length and width. The resulting strand undulation varies with vertical position within a panel. Generally, the panel faces are of higher density then the core (Figure 5.1). Therefore, the degree of undulation could be more pronounced around the mid-section of a panel in the thickness direction.

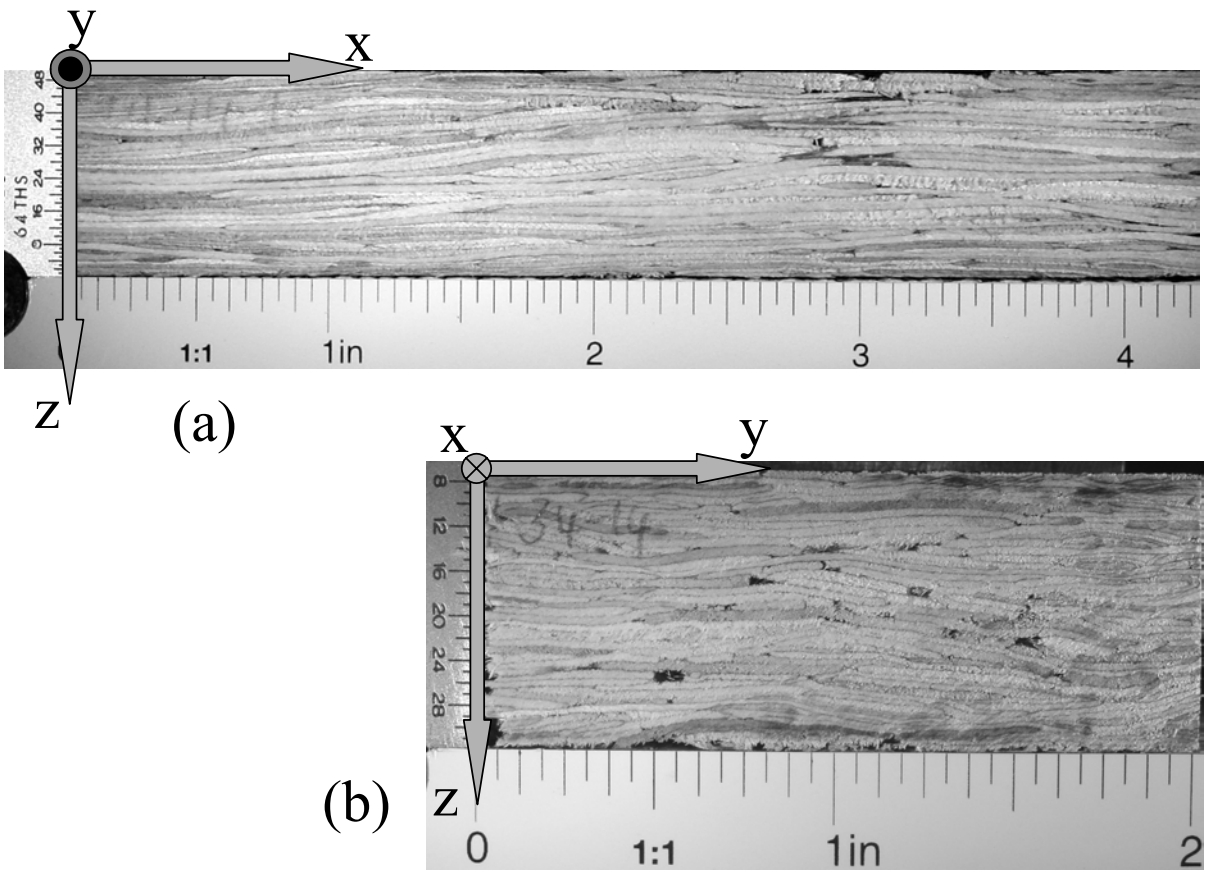

Figure 5. 2. Digital images of an oriented strand composite specimen (a) edge and (b) end along with the corresponding coordinate systems.

The experimental plan for characterizing strand undulation angles in longitudinal and transverse directions to study the effects of strand geometry and vane spacing is summarized in Table 5.2. One specimen (2" x 12") was taken from each of the panels to make up three replicates for each of the cells in the experimental plan.

Table 5. 2. Experimental plan to study the effects of strand geometry and vane spacing on longitudinal and transverse direction strand undulations. Number in each of the cells represents number of specimens.

(a) Experimental plan for strand geometry effects on longitudinal undulation

Vane Spacing = 3.0"	Strand Width (in.)		
Strand Length (in.)	0.5	0.75	1
4	3	3	3
8	-	3	-
12	3	3	3

(b) Experimental plan for vane spacing effects on longitudinal undulation

Strand width = 0.75"	Vane Spacing (in.)	
Strand Length (in.)	1.5	3
4	3	3
8	3	3

(c) Experimental plan for strand geometry effects on transverse undulation

Vane Spacing = 3.0"	Strand Width (in.)	
Strand Length (in.)	0.5	1
4	3	3
12	3	3

In this study, longitudinal and transverse strand undulation was characterized separately for face and core sections of panels. Henceforth, strands in the surface zones (1/8-inch from top and bottom surfaces) will be referred to as "surface strands" and strands in the core zone (area between the outer 1/8-inch sections) will be referred to as "core strands." It is noted through the vertical density profiles that density changes rapidly in the panel faces and gradually decreases towards the relatively constant middle section (Figure 5.1).

Digital images of specimen edges were used to obtain coordinates of an undulating strand in both directions. For longitudinal undulation (Figure 5.2), coordinates along the lengths of four strands from the surface zones and six strands from the core zone were digitized at even spacings of 50 pixels (approximately 0.115 inches).

Similarly, for transverse strand undulation (Figure 5.2), coordinates along the widths of six strands from the surface zones and six strands from the core zone of each specimen were digitized at even spacings of 25 pixels (approximately 0.03 inches). Since the width of the strands was relatively small compared to the length, additional strands were chosen for transverse direction undulation to obtain more data points.

Using the digitized coordinates, a discrete Fourier series expansion was obtained to describe the undulation of each of the digitized strands. A Fourier series with a period or total length of a digitized strand, T, is defined as

$$f(x) = a_0 + \sum_{n=1}^{\infty} (a_n \cos(\frac{2\pi nx}{T}) + b_n \sin(\frac{2\pi nx}{T})) \qquad \textbf{Equation 5.5}$$

where, $a_0 = \frac{1}{T}\int_0^T f(x)dx$ $\qquad a_n = \frac{2}{T}\int_0^T f(x)\cos\frac{2\pi nx}{T}dx$ $\qquad b_n = \frac{2}{T}\int_0^T f(x)\sin\frac{2\pi nx}{T}dx$

Then, the undulation angles, θ (in the longitudinal direction) and ψ (in the transverse direction), were determined by taking the inverse tangent of the Fourier series expansion functions' derivatives.

$$\theta = \tan^{-1}\left[\frac{df(x)}{dx}\right] \qquad \textbf{Equation 5.6}$$

$$\psi = \tan^{-1}\left[\frac{df(y)}{dy}\right] \qquad \textbf{Equation 5.7}$$

Strand undulation angle, θ, was determined at increments of 0.1-inch in the longitudinal direction (x-axis); whereas, strand undulation angle, ψ, was determined at an increment of 0.03 inches in the transverse direction (y-axis).

Once the undulation angles were obtained, data from all the replicates were combined for surface and core zones to form distributions of undulation angles within

each group. These distributions were then compared with the Kolmgorov-Smirnov (KS) test (SAS 1999). For surface and core zones within each group, an appropriate statistical distribution was fit to the experimental data to describe the out-of-plane angular distributions in the longitudinal and transverse directions.

Results and Discussion

Void Volume Fraction

The void volume fractions between strands, V_b, for each of the strand geometry and vane spacing groups is summarized in Table 5.3. A large variation in void volume exists within each of the categories. In general, the mean V_b for all groups ranged between about 0.01 and 0.03. The statistical analysis to examine the influence of vane spacing within each length and width category indicated no significant differences between vane spacing in each of the categories, except for 1-inch wide by 8-inch long strands (p-value = 0.0085). For all other width and length combinations, p-values were greater than 0.16, indicating no significant differences in mean void volumes due to differences in vane spacing.

The analysis of variance for the 3-inch vane spacing to examine the effects of varying strand width indicated no statistically significant differences in V_b for all three strand lengths (p-values were greater than 0.28). This statistical result is likely to arise from the high variability within each void volume sample. Therefore, within each strand length, data was combined for the three widths and statistical analysis was performed. Further analysis indicated that the effect of length on void volume for the 3-inch vane spacing was not statistically significant (minimum p-value = 0.25).

Table 5. 3. Summary of void volume fraction results.

Vane Spacing (in.)	Strand Length (in.)	Strand Width (in.)	N	Mean V_b Void Volume Fraction	COV (%)
1.5	4	0.5	9	0.009	106.5
		0.75	9	0.011	91.5
		1	9	0.014	75.8
	8	0.5	9	0.010	56.7
		0.75	9	0.018	62.9
		1	9	0.028	43.4
3	4	0.5	9	0.009	69.4
		0.75	9	0.011	91.2
		1	9	0.014	72.6
	8	0.5	9	0.013	53
		0.75	9	0.011	60.2
		1	9	0.012	80.1
	12	0.5	9	0.020	69.8
		0.75	9	0.015	56.1
		1	9	0.012	66.1

Based on the experimental results for a vane spacing of 1.5 inches, the mean V_b increased as strand width increased in each of the length categories, however, this increase became increasingly evident for longer strand lengths. It appears that as strand length and width increase, the probability of overlapping strands increases, resulting in an increase in void size and volume. However, this trend is not evident for the 3-inch vane spacing suggesting that wide vane spacing may facilitate strand rotation and packing.

Results from this study provided mean void volumes for oriented strand composite panels, but a more rigorous study is necessary to examine the variations due to strand geometry and vane spacing.

Strand Orientation Through The Panel Thickness

Typical strand undulation paths and angles in the longitudinal and transverse directions are shown in Figures 5.3 and 5.4. In general, longitudinal undulation angles in the core zones for all specimens ranged between 0 and 30 degrees. In contrast, angles in the surface zones ranged between 0 and 18 degrees. Comparison of core and surface undulation angle distributions in both directions, for all categories, resulted in statistically significant distributions (KS test p-values ranged between 0.0001 and 0.01).

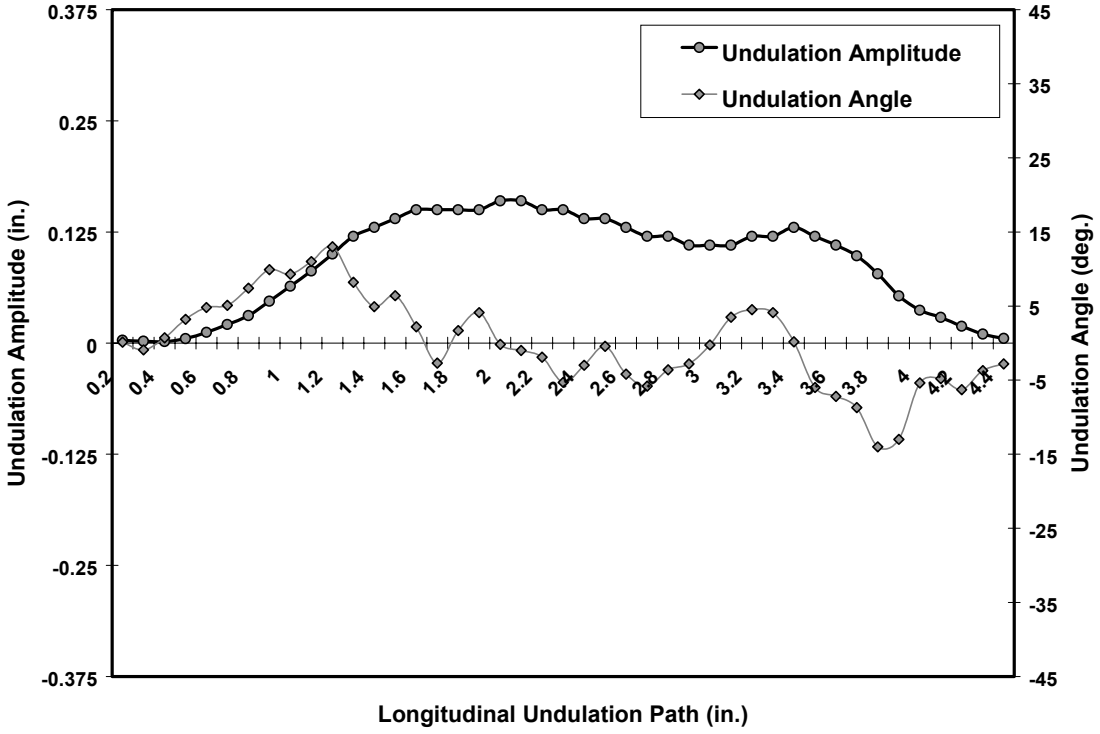

Figure 5. 3. Strand undulation amplitude and angle in the longitudinal direction.

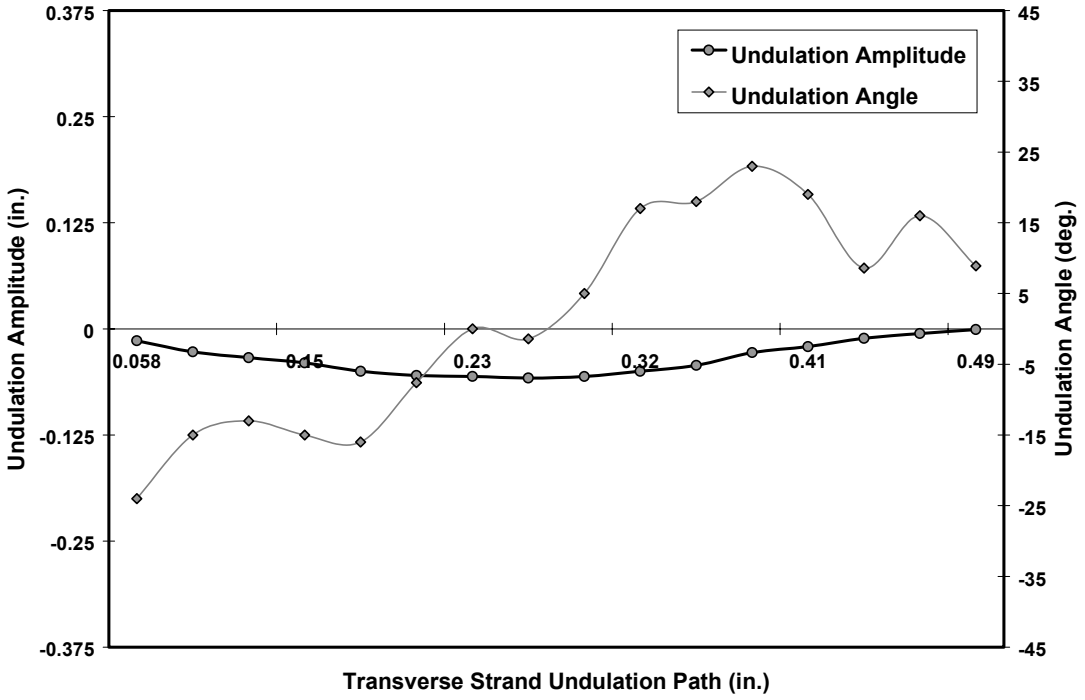

Figure 5. 4. Strand undulation amplitude and angle in the transverse direction.

Further comparisons of undulation distributions were performed separately for core strands and surface strands. The results of the KS tests comparing the angle distributions in the longitudinal direction for all strand geometry combinations for surface and core strands are presented in Tables 5.4 and 5.5. P-values of distributions that are not statistically significant are denoted with bold type. Similarly, the KS test results for transverse direction distributions for surface and core strands are summarized in Tables 5.6 and 5.7.

For 4-inch long strands, the effect of varying strand width in both directions was not significant for vane spacing of 3 inches. However, for 12-inch strands the angle distribution of 0.5-inch wide strands was significantly different than 0.75-inch and 1.0-

inch wide strands. Results also show that there is no statistically significant difference between undulation angle distributions as vane spacing is varied between 1.5 and 3.0 inches while keeping strand length and width constant. To examine the effects of strand geometry and vane spacing on variations in angle distributions, cumulative density plots of different strand geometry and vane spacing combinations are presented in Appendix E.

For 3-inch vane spacing, narrow strands (0.5") tend to result in higher percentages of larger undulation angles than 0.75-inch or 1.0-inch wide strands for 4-inch and 12-inch long strands (Figures E.1 and E.2). Surprisingly, 0.75-inch wide strands seemed to result in smaller undulation angles than 1-inch wide strands even though the difference is not statistically significant. Comparing the effect of strand length as width (0.75") was kept constant indicated that shorter strands (4-inch long) yield higher percentages of large angles than longer strands (8-inch or 12-inch), however, this difference seems to diminish as strands became longer (Figure E.3). Similar length effects were also found for 1.5-inch vane spacing and 0.75-inch strand width (Figure E.4). However, vane spacing does not seem to influence the angular distribution even as strand length and width are kept constant.

In transverse direction, the strand width and length seem to affect the undulation angle distributions (Figure E.5). Cumulative distribution plots indicate that narrow and long strands tend to give rise to higher percentage of larger angles than wide and short or long strands. This could be attributed to potentially larger rotations that strands undergo when they are short or long but narrow. Differences in transverse undulation angle distributions were not as prominent as for the longitudinal direction angle undulations, which could be attributed to the smaller differences in undulation periods, namely strand

widths. However, it should be noted that transverse undulation angles are large and could play a significant role in the reduction of transverse elastic properties. In the core zone, undulation angles ranged between 0 and 60 degrees, whereas for surface strands they ranged between 0 and 50 degrees. The mean undulation angle of the core strands varied from 11 to 16 degrees, and the mean undulation angle of surface strands varied from 7 to 10 degrees.

Several factors are responsible for causing strands to weave through the thickness of a panel. It is speculated that the key factors are presence of voids and overlapping of strands during mat formation. Conceptually, it is possible to visualize that this degree of overlap also increases as strand width increases. Voids and strand overlap in panels also influence the local densities throughout the panel resulting in horizontal density variation. Dai (1994) modeled the effects of strand geometry on horizontal density variation in randomly formed flakeboards. The model predicted that as strand width and length are increased, there is an increase in horizontal density variation. Therefore, in this study, as the strand length and width increased, the horizontal density variation in the panels could have increased leading to greater variation in strand undulation angles.

Table 5. 4. Comparison of longitudinal undulation distributions of surface strands (bold text denotes similar distributions).

Units: inches		Vane Spacing	1.5	1.5	3	3	3	3	3	3	3
		Length	4	8	4	4	4	8	12	12	12
Vane Spacing	Length	Width	0.75	0.75	0.5	0.75	1	0.75	0.5	0.75	1
1.5	4	0.75	1	**0.6961**	-	**0.0575**	-	**0.58**	-	-	-
1.5	8	0.75		1	-	0.0016	-	**0.3913**	-	-	-
3	4	0.5			1	0.0134	**0.2321**	0.0001	0.0001	0.0001	0.0001
3	4	0.75				1	**0.3269**	0.0059	**0.2217**	0.0001	0.0001
3	4	1					1	0.0001	0.0249	0.0001	0.0001
3	8	0.75						1	**0.0783**	0.034	**0.2722**
3	12	0.5							1	0.0001	0.0062
3	12	0.75								1	**0.4171**
3	12	1									1

Table 5. 5. Comparison of longitudinal undulation distributions of core strands (bold text denotes similar distributions).

Units:inches		Vane Spacing	1.5	1.5	3	3	3	3	3	3	3
		Length	4	8	4	4	4	8	12	12	12
Vane Spacing	Length	Width	0.75	0.75	0.5	0.75	1	0.75	0.5	0.75	1
1.5	4	0.75	1	0.0001	-	**0.1599**	-	0.0001	-	-	-
1.5	8	0.75		1	-	0.0001	-	**0.3364**	-	-	-
3	4	0.5			1	**0.2082**	**0.3383**	0.0001	0.0001	0.0001	0.0001
3	4	0.75				1	**0.5071**	0.0001	0.0007	0.0001	0.0001
3	4	1					1	0.0001	0.0001	0.0001	0.0001
3	8	0.75						1	**0.2912**	0.0001	0.0022
3	12	0.5							1	0.0001	0.0001
3	12	0.75								1	0.0001
3	12	1									1

Table 5. 6. Comparison of transverse undulation distributions of surface strands (bold text denotes similar distributions).

Units: inches		Vane Spacing	3	3	3	3
		Length	4	4	12	12
Vane Spacing	Length	Width	0.5	1	0.5	1
3	4	0.5	1	**0.1052**	**0.9293**	**0.2205**
3	4	1		1	0.0228	0.0139
3	12	0.5			1	**0.1644**
3	12	1				1

Table 5. 7. Comparison of transverse undulation distributions of core strands (bold text denotes similar distributions).

Units: inches		Vane Spacing	3	3	3	3
		Length	4	4	12	12
Vane Spacing	Length	Width	0.5	1	0.5	1
3	4	0.5	1	**0.144**	0.0001	**0.6673**
3	4	1		1	0.0001	**0.319**
3	12	0.5			1	0.0006
3	12	1				1

Probability Density Functions

Normal, lognormal, beta, and Weibull probability density functions were explored to describe the undulation angle distributions. Two-parameter Weibull distributions described the longitudinal and transverse undulation angle data very well. The probability density function (pdf) for the two-parameter Weibull distribution is given as

$$f(x) = \alpha\beta^{-\alpha} x^{\alpha-1} e^{-(x/\beta)^{\alpha}} \qquad \text{for x > 0} \qquad \textbf{Equation 5.8}$$

where α is the shape parameter and β is the scale parameter. Since the sign of the angle did not matter in this study as only in-plane loads (tension and compression) are considered, absolute value of all angles was taken to give a range of angles from 0 to 90 degrees. Representative probability density functions describing strand undulation angle in longitudinal and transverse directions for different strand length, width, and vane spacing combinations are shown in Figures 5.5 through 5.7. The two-parameter Weibull distribution parameters and the Chi-square goodness of fit statistics (p-values) for undulation angle distributions for surface and core strands in the longitudinal and transverse directions are presented in Tables 5.8 through 5.11.

Probability density functions of surface strands are skewed more to the left and more area is included in the smaller angle intervals reflecting shallow undulation angles in the denser outer regions versus the less dense core region. Note that in Table 5.9, three of the distributions have a low p-value (less than 0.05) indicating that the 2-parameter Weibull distribution is not a very good fit. However, visual inspection indicates that the Weibull probability density function indeed fits the data distribution better than any other density function.

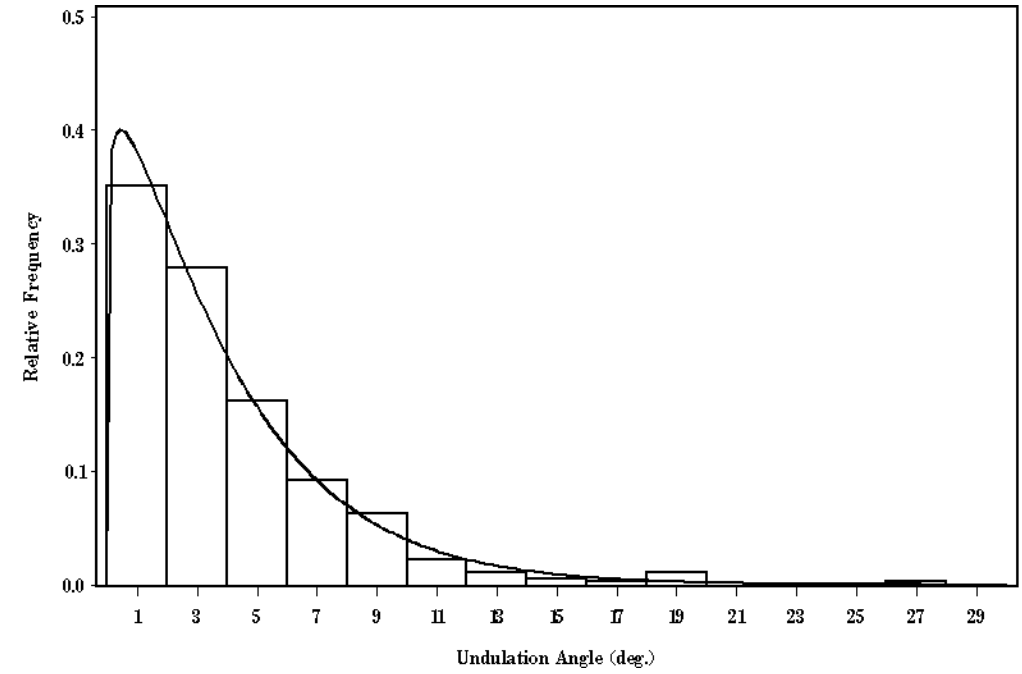

(a) Surface Strands

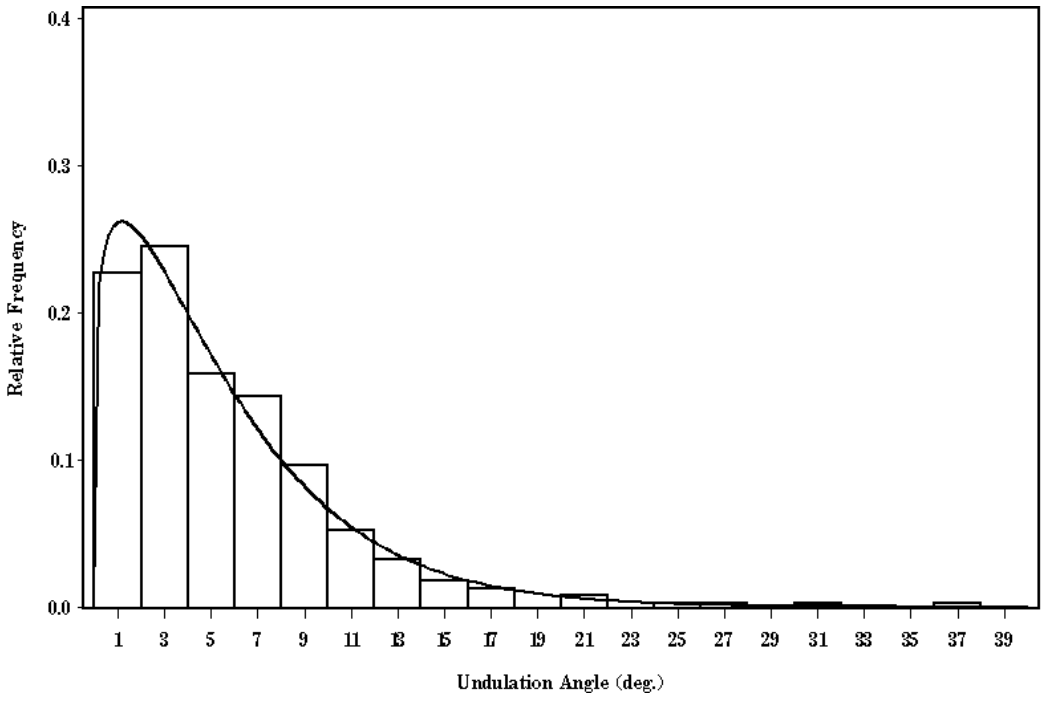

(b) Core Strands

Figure 5. 5. Longitudinal direction surface and core strand undulation angle distributions: 4” by 0.75” and vane spacing of 3.0”.

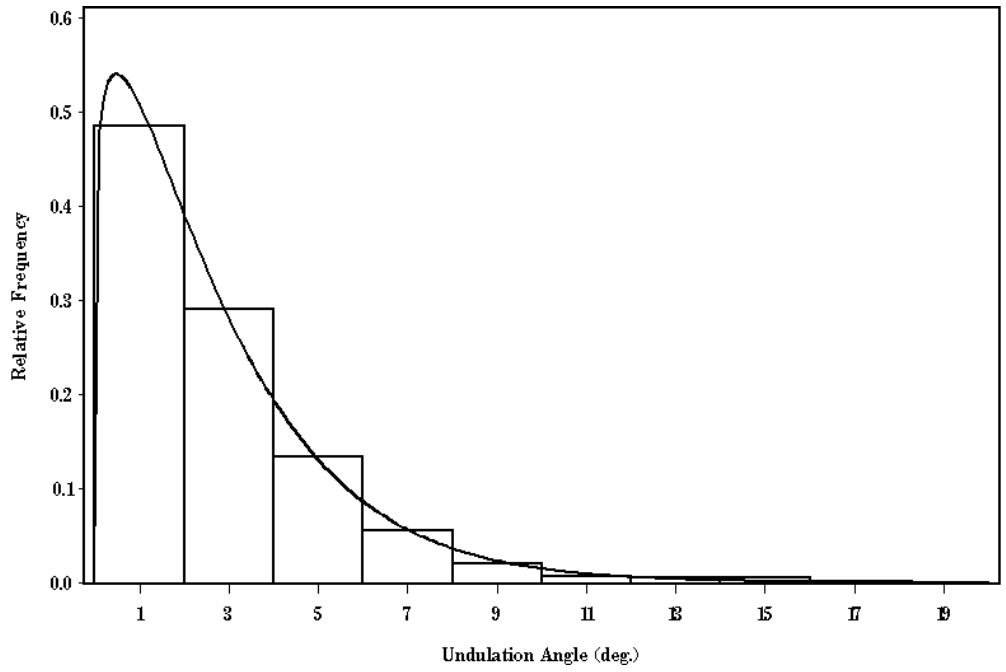

(a) Surface strands

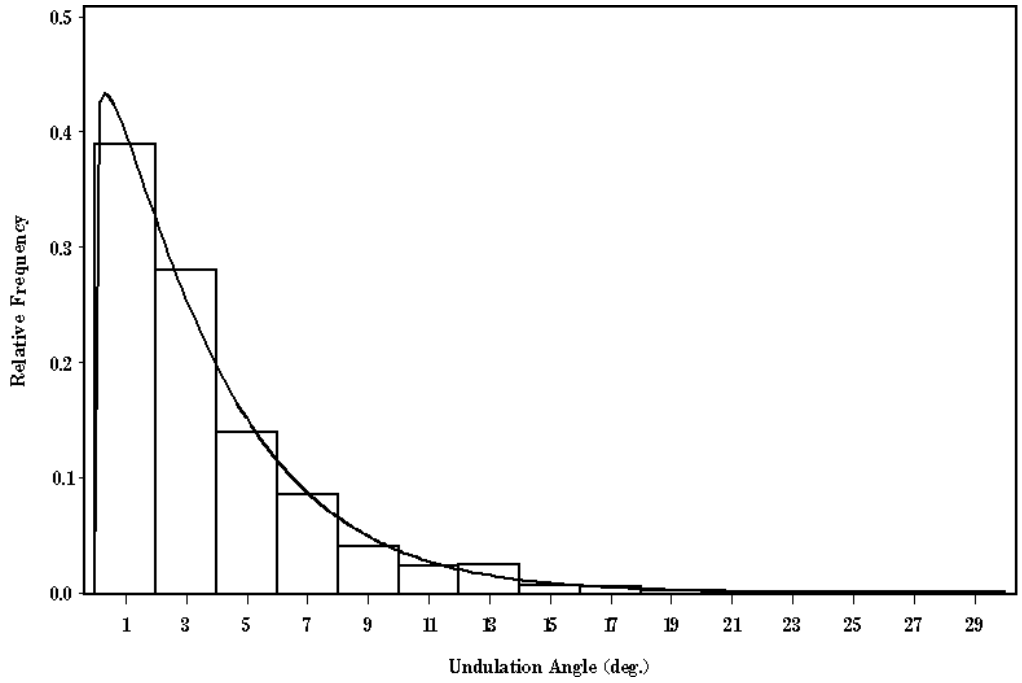

(b) Core strands

Figure 5. 6. Longitudinal direction surface and core strand undulation angle distributions: 12” by 1.0” and vane spacing of 3.0”.

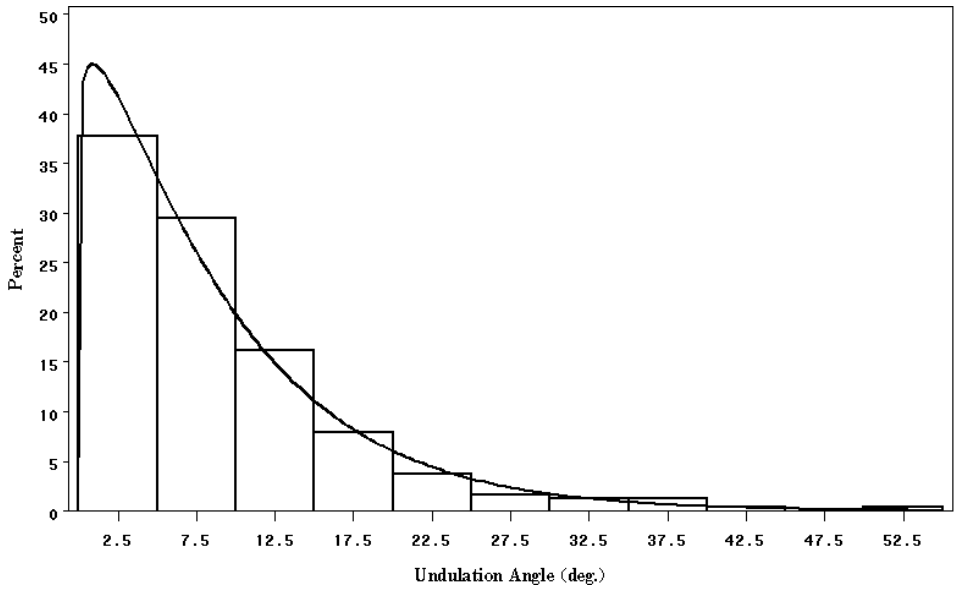

(a) Surface strands

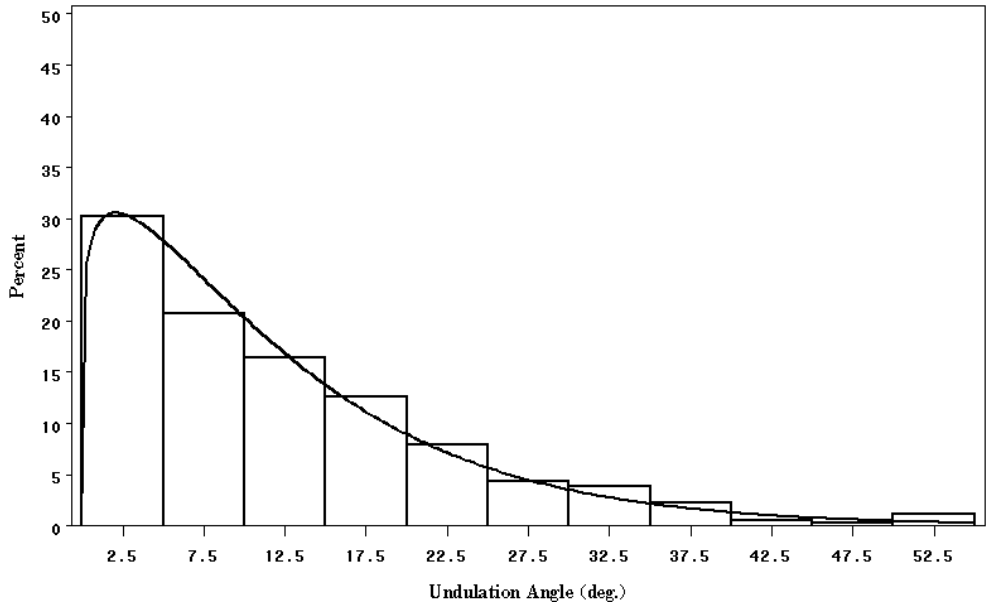

(b) Core strands

Figure 5. 7. Transverse direction surface and core strand undulation angle distributions: 4” by 0.5” and vane spacing of 3.0”.

Table 5. 8. Distribution parameters and goodness of fit statistics for longitudinal undulation angle distributions of surface strands (bold text denotes good fit).

Vane Spacing (in.)	Length (in.)	Width (in.)	Weibull Parameter Estimates		Chi-Square p-Value
			Scale	Shape	
1.5	4	0.75	3.249	1.218	**0.36**
	8	0.75	3.159	1.252	**0.326**
3	4	0.5	4.955	1.314	**0.94**
		0.75	4.047	1.098	**0.087**
		1	4.337	1.254	**0.822**
	8	0.75	3.096	1.11	**0.753**
	12	0.5	3.515	1.146	**0.181**
		0.75	2.624	1.154	**0.801**
		1	2.866	1.149	**0.636**

Table 5. 9. Distribution parameters and goodness of fit statistics for longitudinal undulation angle distributions of core strands (bold text denotes good fit).

Vane Spacing (in.)	Length (in.)	Width (in.)	Weibull Parameter Estimates		Chi-Square p-Value
			Scale	Shape	
1.5	4	0.75	6.232	1.204	**0.162**
	8	0.75	4.318	1.096	0.001
3	4	0.5	6.742	1.202	**0.675**
		0.75	5.809	1.18	0.026
		1	5.924	1.225	**0.525**
	8	0.75	4.512	1.104	**0.469**
	12	0.5	4.833	1.147	**0.075**
		0.75	3.121	1.179	0.001
		1	3.841	1.076	**0.139**

Table 5. 10. Distribution parameters and goodness of fit statistics for transverse undulation angle distributions of surface strands (bold text denotes good fit).

Vane Spacing (in.)	Length (in.)	Width (in.)	Weibull Parameter Estimates		Chi-Square p-Value
			Scale	Shape	
3	4	0.5	9.098	1.087	**0.181**
		1	7.848	1.109	**0.352**
	12	0.5	9.018	1.21	**0.157**
		1	10.63	1.004	**0.409**

Table 5. 11. Distribution parameters and goodness of fit statistics for transverse undulation angle distributions of core strands (bold text denotes good fit).

Vane Spacing (in.)	Length (in.)	Width (in.)	Weibull Parameter Estimates		Chi-Square p-Value
			Scale	Shape	
3	4	0.5	12.71	1.145	**0.152**
		1	11.42	1.094	**0.416**
	12	0.5	17.12	1.162	**0.058**
		1	12.7	1.009	**0.769**

Summary and Conclusions

Volume fractions of between strand voids were determined for oriented strand composite boards manufactured for this study. In general, between strand void volume ranged from 0.01 to 0.03. For a vane spacing of 1.5 inches, void volume showed a tendency to increase as strand width was increased. However, this trend was not so apparent for a vane spacing of 3.0 inches. Very high coefficients of variation indicate that more data is needed to observe conclusive trends between strand geometry, vane spacing and void volume fractions.

Strand orientations through the thickness of oriented strand panels in the longitudinal and transverse directions were quantified and the effects of strand geometry and vane spacing on out-of-plane strand undulations in both directions were investigated. Undulation angle distributions of surface strands (0.125 inches from top and bottom surface of panels) were significantly different than those of core strands in both directions. Vane spacing did not significantly influence the distribution when strand length and width were kept constant. Short strands tend to result in larger undulation angles than long strands, however this effect diminishes beyond certain strand length.

For 4-inch strands, both surface and core strand undulation distributions did not vary significantly as strand width was varied, but results indicated a tendency for larger undulation angles as width of long strands decreased. Strand undulation angles were found to range between 0 and 30 degrees in the core region and between 0 and 20 degrees in the surface regions. In the transverse direction, strand deviation angles ranged between 0 and 60 degrees for the core strands and between 0 and 50 degrees for surface strands. Cumulative distribution plots indicate that smaller strand widths tend to result in

higher percentages of larger undulation angles in the transverse direction for long strands. A two-parameter Weibull probability density function adequately fits both longitudinal and transverse direction strand undulation data. Distribution parameters for all strand length, width and vane spacing combinations are presented.

Results of this study support the trends found by Dai (1994) with horizontal density variation. He found that as strand width and length increased there is more variation in the horizontal density variation of a panel. Horizontal density variation is directly correlated with void volume and degree of overlapping between strands as their lengths and widths vary. Results on between strand void volume and out-of-plane strand deviations indicate an increase in these values as strand length and width increase. Results of this study indicate that random and incidental strand undulations in longitudinal and transverse directions, which are inherent attributes of oriented strand composites, are significant and could potentially influence their physical and mechanical behavior.

References

Barnes, D. 2000. An integrated model of the effect of processing parameters on the strength properties of oriented strand wood products. Forest Products Journal. 50(11/12):33-42.

Bodig, J. and B. A. Jayne. 1982. Mechanics of wood and wood composites. Van Nostrand Reinhold Company, New York, NY.

Dai, C. 1994. Modelling structure and processing characteristics of a randomly-formed wood-flake composite mat. Ph.D. Dissertation. Dept. of Forestry, The University of British Columbia. 141pp.

_____ and P. R. Steiner. 1994a. Spatial structure of wood composites in relation to processing and performance characteristics: Part II. Modelling and simulation of a randomly-formed flake layer network. Wood Sci. Technol. 28:135-146.

_____ and P. R. Steiner. 1994b. Spatial structure of wood composites in relation to processing and performance characteristics: Part III. Modelling the formation of multi-layered random flake mats. Wood Sci. Technol. 28(3):229-239.

Geimer, R. L. 1976. Flake alinement in particleboard as affected by machine variables and particle geometry. USDA Forest Service Research Paper FPL 275. 16 pp.

_____. 1979. Data basic to the engineering design of reconstituted flakeboard. In Proceedings of the 13t^{h} Washington State University International Symposium on Particleboard. pp. 105-125.

Harris, R. A. and Johnson, J. A. 1982. Characterization of flake orientation in flakeboard by the von Mises probability distribution function. Wood and Fiber 14(4):254-266.

Lang, E. M. and M. P. Wolcott. 1996. A model for viscoelastic consolidation of wood-strand mats. Part I. Structural characterization of the mat via Monte Carlo simulation. Wood and Fiber Science. 28(1):100-109.

Lenth, C. A. and F. A. Kamke. 1996a. Investigations of flakeboard mat consolidation. Part I. Characterizing the cellular structure. Wood and Fiber Science. 28(2):153-167.

Maloney, T. M. 1993. Modern Particleboard & Dry-Process Fiberboard Manufacturing. Updated Edition. Miller Freeman Inc., San Francisco, CA.

Meyers, K. L. 2001. Impact of strand geometry and orientation on mechanical properties of strand composites. Master's Thesis. Dept. of Civil and Environmental Engineering, Washington State University. 115pp.

SAS Institute Inc. 1999. SAS for Windows Version 8. Cary, North Carolina.

Shaler, M. S. and P. R. Blankenhorn. 1990. Composite model prediction of elastic moduli for flakeboard. Wood and Fiber Science. 22(3):246-261.

_____. 1991. Comparing two measures of flake alignment. Wood Sci. Technol. 26:53-61.

Suchsland, O. and H. Xu. 1991. Model analysis of flakeboard variables. Forest Products Journal. 41(11/12):55-60.

Yadama, V. 2002. Characterization and modeling of oriented strand composites: Chapter 4. Ph.D. Dissertation. Washington State University.

Chapter 6

Fiber Undulation Model to Predict Oriented Strand Composite Elastic Properties

Introduction

The physical and mechanical properties of oriented strand composites are influenced by their structure. Examination of a panel surface reveals that the orientation of strands in the plane of the panel has a certain distribution and is not parallel to the longitudinal edge of the panel. The effects of the variation in strand orientation in the plane of a panel has been investigated by several researchers in the past and modeled reasonably well (Geimer 1976, Geimer et. al. 1979, Shaler and Blankenhorn 1990, Barnes 2000, Meyers 2001). Other important structural characteristics include vertical density profile, within strand void volume, and deviation of strands in the longitudinal and transverse directions through the thickness of a panel (Figure 6.1). Due to differential densification through the depth of a panel, elastic properties of strands through a panel depth vary (Yadama 2002c). Strand undulations could play a significant role in determining the compression behavior of a composite because of the tendency of the strands to buckle more readily. Out-of-plane strand deviations could also potentially reduce the strength of a composite and resistance to dimensional changes due to exposure to varying environmental conditions.

a) strand undulation in the longitudinal direction

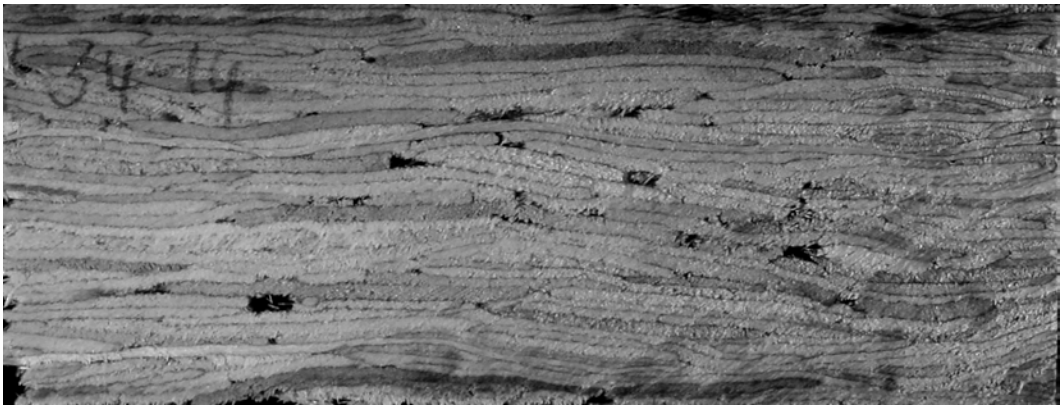

b) strand undulation in the transverse direction

Figure 6. 1. Strand undulations in the longitudinal and transverse directions. Note the presence of voids between strands in (b).

Empirical, analytical, and theoretical models have been suggested by past researchers to predict the mechanical properties of oriented strand composites based on the arrangement and properties of their constituents (Hoover et al. 1992, Geimer 1979, Dong 1979, Triche and Hunt 1993, Xu and Suchsland 1998, Shaler 1986, Shaler and Blankenhorn 1990, Barnes 2000, 2001, 2002a, 2002b, Meyers 2001). A review of these

studies has been conducted by Yadama (2002a). In general, these models highlight the role of strand orientation in developing mechanical properties; however, in-plane alignment is the only factor considered. Strand undulation angles were shown to range between 0 and 30 degrees in the longitudinal direction and between 0 and 60 degrees in the transverse direction (Yadama 2002d). In compression, it was shown by Yadama (2002b) that a maximum undulation angle of four degrees could reduce the Young's modulus by approximately 12%. The fiber undulation model (FUM) predictions of carefully manufactured wood-strand laminates indicated a nonlinear degradation in the Young's modulus of the composite as undulation angle increased. Therefore, consideration of strand undulation angles could be critical in examining the mechanical behavior of an oriented strand panel. In addition, many of the earlier models do not consider the changes in strand properties during the hot pressing process, which were found to be significant (Yadama 2002c).

Objectives

In this study, the investigator predicts the mechanical properties of laboratory manufactured oriented strand panels using the fiber undulation model. This approach incorporates hot pressing effects on strand properties, strand deviations in the plane of a panel, and strand undulations through the panel thickness in the longitudinal direction. The effects of strand undulation in the transverse direction are not included because of the assumption that the composite panels manufactured for this study are transversely isotropic (Yadama 2002b). The objective of this study is to confirm the validity of the

fiber undulation model to predict the elastic properties of oriented strand composite panels. Specific objectives to achieve this task are to:

1. Present a method to include the effects of out-of-plane strand undulations along with the in-plane strand deviations on the elastic behavior of a panel,
2. Experimentally determine the shear modulus of oriented strand panels, and
3. Predict the elastic properties, E_x, E_y, G_{xy}, and ν_{xy}, of panels fabricated with a range of strand geometries using the FUM and compare them with the experimental results compiled by Meyers (2001).

Method to Include Strand Orientation Angles in FUM

The fiber undulation model will be used to predict the elastic properties of oriented strand panels, namely E_x, E_y, G_{xy}, and ν_{xy} (Yadama 2002b). The panel and material coordinate axes of a strand with three-dimensional orientation in a composite panel are shown in Figure 6.2. The off-axis orientation of a strand in the plane of a panel is designated ϕ, and the strand undulation angle through panel depth in the longitudinal direction is designated θ. Strand undulation angle in the transverse direction is designated ψ.

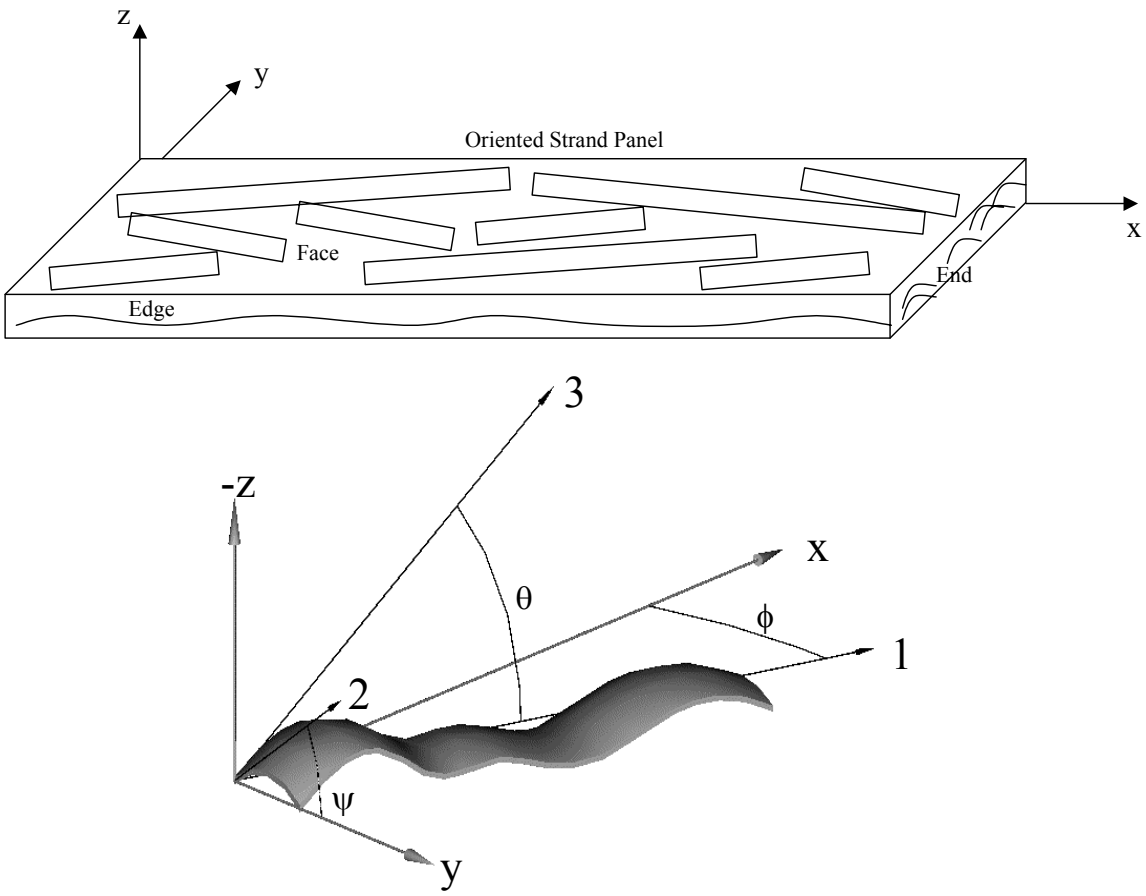

Figure 6. 2. Panel coordinate system and strand orientation angles with respect to the panel coordinate axes.

In a previous study (Yadama 2002b), strand undulation paths were described with a discrete Fourier series expansion. These functions were subsequently utilized in the fiber undulation model to determine the effects of undulation angles on laminate elastic properties. This method, however, is not practical when a laminate consists of 35 to 45 layers and each layer could potentially be described by functions that involve over 10 terms of a Fourier series. A solution to this problem is to consider statistical distributions of strand angles in the fiber undulation model.

Meyers (2001) previously characterized the in-plane orientation of strands for the oriented strand composite panels fabricated for this study. Table 6.1 summarizes the Weibull distribution parameters for in-plane orientation of strands based on her study. Absolute values of all measured angles were taken to give a range of angles from 0 to 90 degrees.

Table 6. 1. Weibull distribution parameters for in-plane strand angle distributions.

Vane Spacing (in.)	Length (in.)	Width (in.)	Weibull Parameter Estimates	
			Scale	Shape
1.5	4	0.75	19.81	1.28
	8	0.75	13.9	1.18
3	4	0.5	31.34	1.41
		0.75	31.34	1.41
		1	31.34	1.41
	8	0.75	19.81	1.28
	12	0.5	14.85	1.17
		0.75	17.82	1.13
		1	13.9	1.18

Since the distributions of strand angles, θ and ϕ, were determined in previous studies (Yadama 2002d, Meyers 2001), a series rule of mixtures approach was considered to incorporate these statistical distributions into the FUM in determining the transformed stiffness matrix. The compliance matrix, **[S]**, was adjusted for strand undulation effects by calculating $\left[\overline{\mathbf{S}}\right]_{\theta}^{n}$ at the mean angle for each of n^{th} bin of the Weibull probability density distribution of an appropriate panel type (based on the strand geometry and vane

spacing). The transformation matrix used to adjust for the strand undulation angle in the xz-plane is given as:

$$[\mathbf{T}]_\theta = \begin{bmatrix} \cos(\theta)^2 & 0 & \sin(\theta)^2 & 0 & 2\cos(\theta)\sin(\theta) & 0 \\ 0 & 1 & 0 & 0 & 0 & 0 \\ \sin(\theta)^2 & 0 & \cos(\theta)^2 & 0 & -2\cos(\theta)\sin(\theta) & 0 \\ 0 & 0 & 0 & \cos(\theta) & 0 & -\sin(\theta) \\ -\cos(\theta)\sin(\theta) & 0 & \cos(\theta)\sin(\theta) & 0 & \cos(\theta)^2 - \sin(\theta)^2 & 0 \\ 0 & 0 & 0 & \sin(\theta) & 0 & \cos(\theta) \end{bmatrix} \qquad \textbf{Equation 6.1}$$

After determining the transformed compliance matrices for each two-degree wide bin, the compliance matrix of each bin was multiplied by the corresponding bin probability values to account for bin's contribution to the undulation effects. The average transformed compliance matrix could then be determined by integrating over the range of the transformation angles (0 to 90 degrees in this study) as follows:

$$(\bar{\mathbf{S}}_{\mathbf{ij}})_\theta = \frac{2}{\pi}\int_0^{\pi/2} (\bar{\mathbf{S}}_{\mathbf{ij}})_\theta \Pr(\theta)\mathbf{d}\theta \qquad \textbf{Equation 6.2}$$

Since the transformed compliance matrix and Pr(θ) are constants within each bin, their product for each bin of a probability density distribution can be summed over the total number of bins, n, to determine an average transformed compliance matrix, $[\bar{\mathbf{S}}]_\theta$, accounting for strand undulation effects as follows:

$$[\bar{\mathbf{S}}]_\theta = \sum_{\mathbf{i}=1}^{\mathbf{n}} [\bar{\mathbf{S}}]_\theta^{\mathbf{i}} \Pr(\theta_{\mathbf{i}}) \qquad \textbf{Equation 6.3}$$

Then, $[\bar{S}]_{\theta}$ was transformed again to account for off-axis strand deviations in the plane of a panel to obtain $[\bar{S}]_{\theta\phi}$. Subsequently, $[\bar{S}]_{\theta\phi}$ may be inverted to obtain averaged stiffness matrix of the laminate to determine its effective elastic constants in the fiber undulation model. Thus, the effects of both undulation angle and in-plane deviation angle of a strand on the constitutive matrix of each lamina were included in the model.

Model Flow

A flow chart of the fiber undulation model to predict the elastic properties of the oriented strand panels is presented in Figure 6.3. The MathCAD® worksheet of the model is given in Appendix F. Every panel was modeled as a symmetric laminate consisting of eight laminae (Figure 6.4). The laminate lay-up was determined based on vertical density profiles of the panels. Close examination of the density profiles shows that each of the high-density regions on panel surfaces could be divided into three sections with the thickness of each section equal to 0.04 inches. Densities within each of these sections were averaged to determine the mean density for each of the regions. Density values in the core section of the panels (between the outer 1/8-inch thick surface regions) were averaged to yield a mean value for the middle two laminae in each of the laminates. Based on the density profiles of a specimen from each panel group, average strand densities for the top four laminae were assigned. These values were assigned accordingly to the bottom four laminae to produce a symmetric laminate.

Knowing the densities of each lamina, the volume fraction of the strand constituents, namely the cell wall and void content, were determined (Yadama 2002c). The volume fraction of resin was taken to be that of the target resin content, 0.06, and

was subtracted from the void volume fraction to satisfy the condition that the sum of the three components (cell wall, voids, and resin) is one. The E_1 and ν_{12} of each lamina were computed using the simplex model developed earlier (Yadama 2002c). Based on the proportionality constants relating E_1 to E_2 and G_{12} (Yadama 2002c), the corresponding material properties were computed. Values for ν_{23} and ν_{21} were taken to be 0.5 and 0.035 based on published values (Bodig and Jayne 1982). G_{23} was taken to be one half of G_{12} based on the ratio of these properties found in the literature. The remaining material properties were determined based on the assumption of transverse isotropy.

The model computes the transformed compliance and stiffness matrices and determines the effective elastic constants based on the laminate compliance matrix, **[a]**, as discussed by Yadama (2002b). These laminate elastic constants were further adjusted to account for the between strand void volume determined in an earlier study (Yadama 2002d). Elastic properties, E_x, E_y, G_{xy}, and ν_{xy}, were predicted for panel groups with experimentally determined undulation angle distributions given in Yadama (2002d). Predicted properties were compared with experimentally determined values on specimens from panels tested in tension and compression by Meyers (2001).

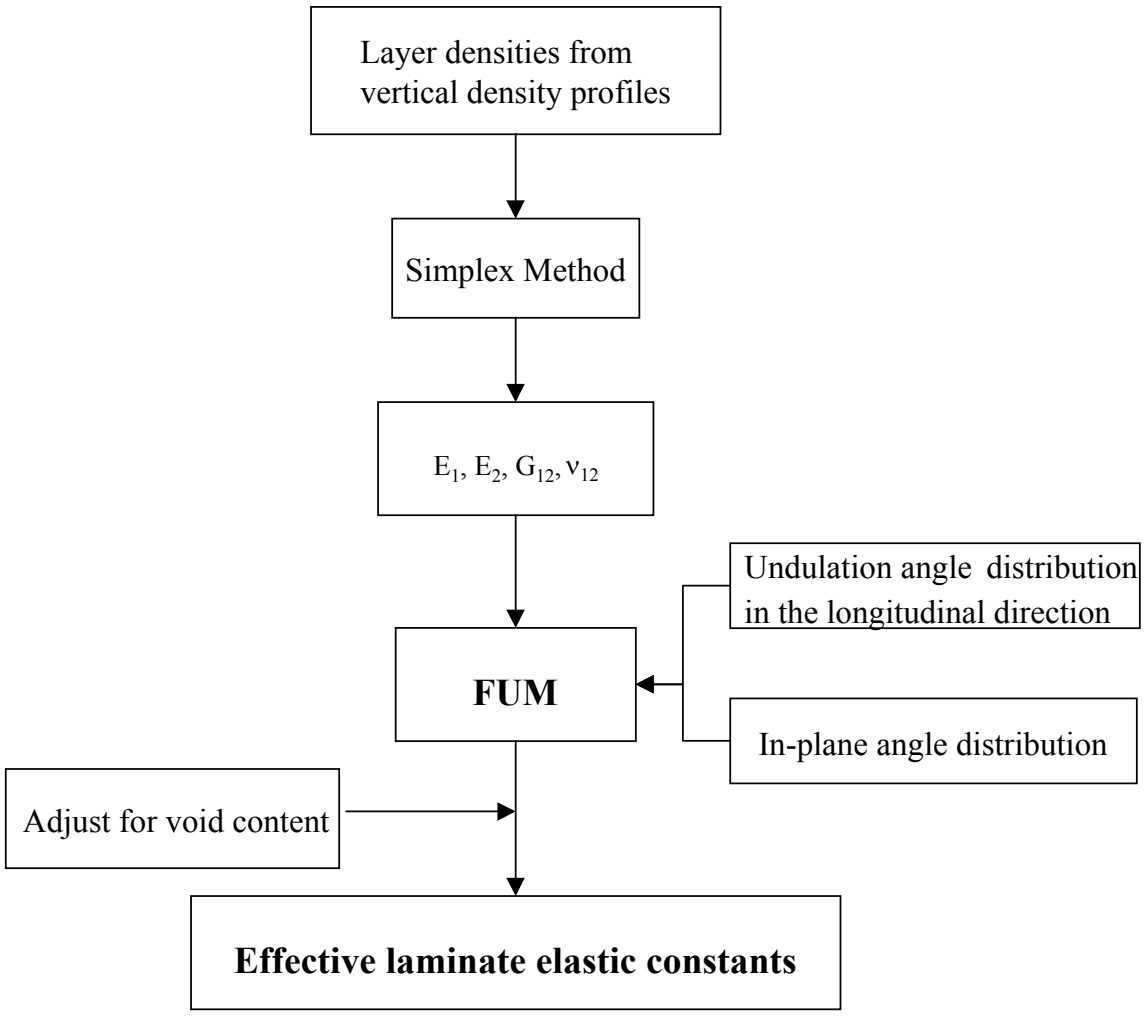

Figure 6. 3. Model flow chart.

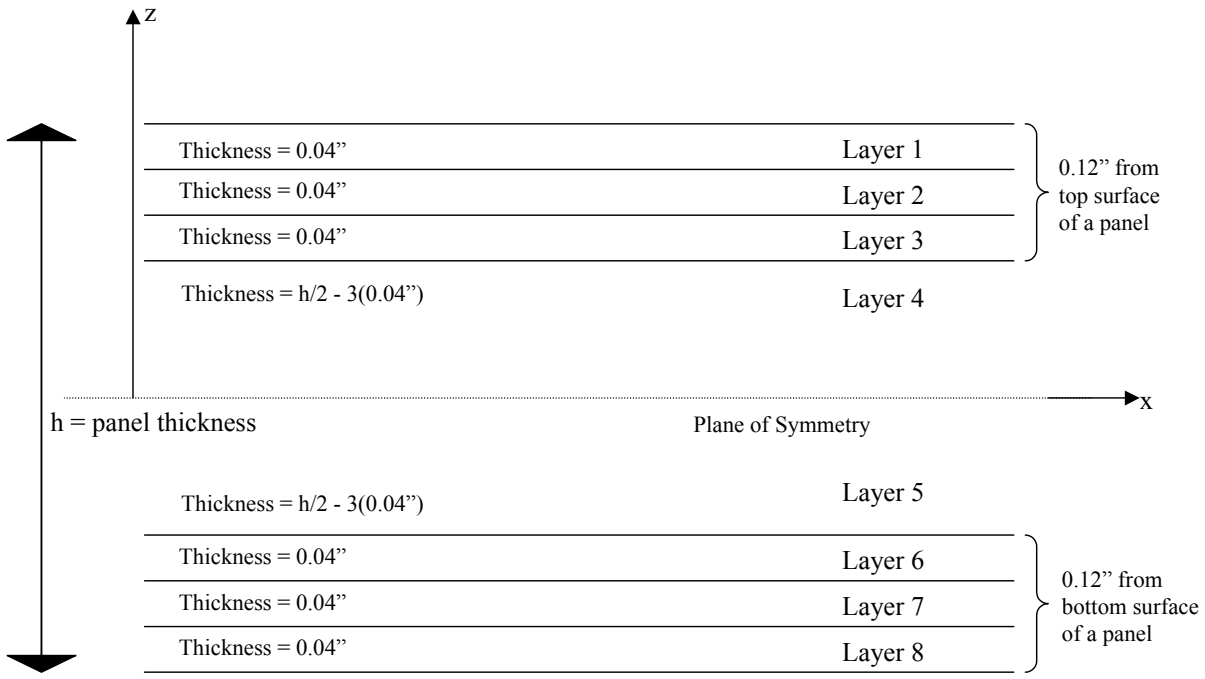

Figure 6. 4. Composite panel considered as a laminate with eight layers.

Panel Shear Modulus

Off-axis tensile tests were conducted to compute shear moduli, G_{xy}, of the panels. One off-axis tensile specimen (3 x 28 inches) was cut from each panel at 15 degrees to the machine direction. The specimen was tapered to 2 inches wide over a 6-inch gauge length. Prior to testing, all specimens were conditioned at 55% relative humidity and 77 degrees F to attain a moisture content between 8 and 9% at testing. With the exception of the specimen size, all testing was performed in accordance with ASTM D5456-98 (ASTM 1998) and D4761-96 (ASTM 1996) using a screw-driven, universal testing machine equipped with a ± 0.2 inch stroke LVDT fastened directly to the specimen.

The off-axis elastic modulus, E_{x15}, of each specimen was computed from experimentally determined stress-strain relationship using the procedure followed by

Meyers (2001). The value for G_{xy} was determined using E_{x15} from the off-axis tests and the average E_x and E_y of corresponding panel group determined by Meyers (2001) using the following transformation equation:

$$\frac{1}{E_{x15}} = \frac{1}{E_x}\cos^4\phi + \left(\frac{1}{G_{xy}} - \frac{2\upsilon_{xy}}{E_x}\right)\sin^2\phi\cos^2\phi + \frac{\sin^4\phi}{E_y} \qquad \textbf{Equation 6.4}$$

where $\phi = 15$ degrees. Mean values of E_{x15} obtained from three replicates were used in the equation to estimate one average value of G_{xy} for each panel group. Since ν_{xy} was not experimentally determined in this study, a value of 0.56 reported for aspen laminated strand lumber in a recent publication (Janowiak et al. 2001) was assumed.

Results and Discussion

Panel Shear Modulus

Mean shear moduli for each of the panel groups is presented in Table 6.2. Cells with missing data indicate values that were very large and could not logically be estimates of G_{xy}. Shear moduli values ranged from 110,000 to 286,000-psi with a coefficient of variation of 30%. In general, panels produced from short strands yielded higher values for shear modulus which could be attributed to lower degree of strand alignment with short strands. Janowiak et al. (2001) reported an average G_{xy} of 133,000-psi for laminated strand lumber manufactured with aspen strands. The results of this study indicate the limits of shear moduli for panels fabricated for this project.

Table 6. 2. Average shear moduli of panel groups determined from off-axis tensile tests.

Vane Spacing (in.)	Length (in.)	Width (in.)	G_{xy} (psi)
1.50	4.00	0.50	187248
		0.75	286133
		1.00	248663
	8.00	0.50	110008
		0.75	246596
		1.00	168008
3.00	4.00	0.50	-
		0.75	248609
		1.00	-
	8.00	0.50	199585
		0.75	126238
		1.00	-
	12.00	0.50	166678
		0.75	280397
		1.00	-
		Overall Average (psi)	**206197**
		COV (%)	**30**

Model Predictions

Elastic constants estimated, for all panel groups, by the fiber undulation model are compared with experimentally measured values for E_x and E_y by Meyers (2001) (Table 6.3). Ratios of the predicted to measured values for each of the elastic properties are

presented. The model results are compared graphically with the experimental results for E_x and E_y in Figures 6.5 and 6.6.

Table 6. 3. Comparison of FUM predictions of panel elastic properties with experimental results.

Vane Spacing (in.)	Length (in.)	Width (in.)	Ratios of Predicted/Measured Values					
			Tensile Properties		Compressive Properties			
			E_x (psi)	E_y (psi)	E_x (psi)	E_y (psi)	G_{xy} (psi)	v_{xy}
1.5	4	0.75	0.58	1.23	1.12	0.79	0.44	0.70
	8	0.75	0.86	2.32	1.39	1.66	0.50	0.59
3	4	0.5	0.91	0.87	1.28	0.75	0.72	0.77
		0.75	0.73	0.78	1.34	0.76	0.68	0.79
		1	0.79	1.03	1.53	0.91	0.73	0.77
	8	0.75	0.67	0.98	1.01	0.78	0.49	0.68
	12	0.5	0.82	1.11	1.30	1.21	0.49	0.61
		0.75	0.63	1.36	0.87	0.82	0.42	0.63
		1	0.74	1.52	1.07	1.31	0.44	0.59

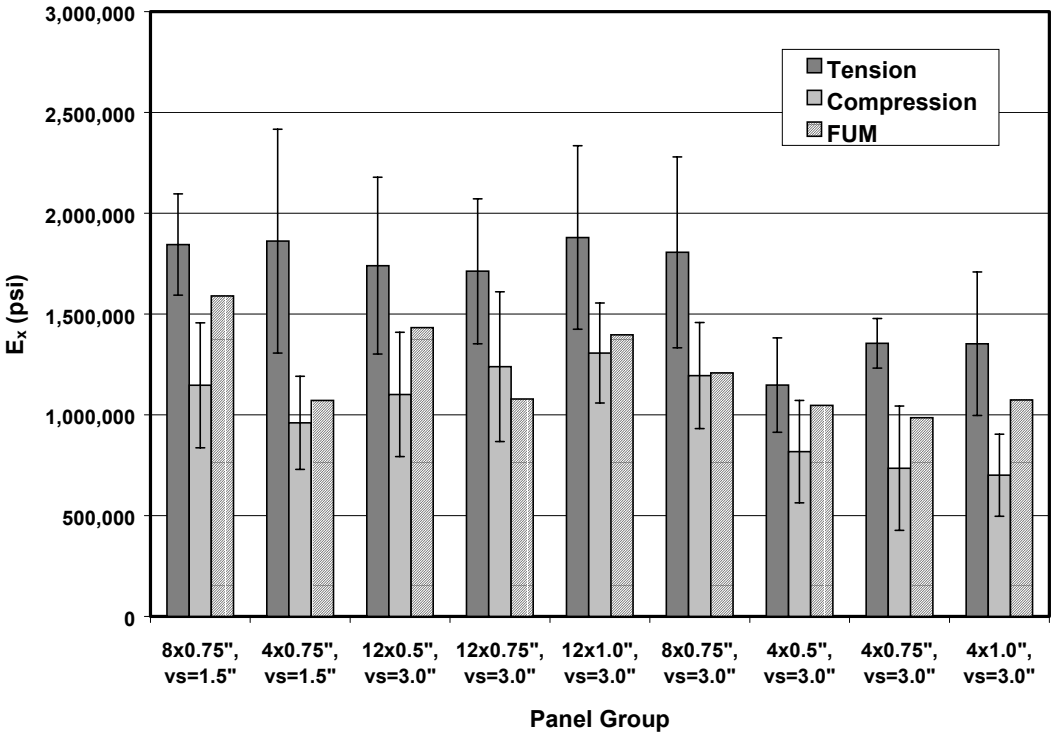

Figure 6. 5. Comparison of tensile and compression experimental E_x against predicted E_x (vs = vane spacing).

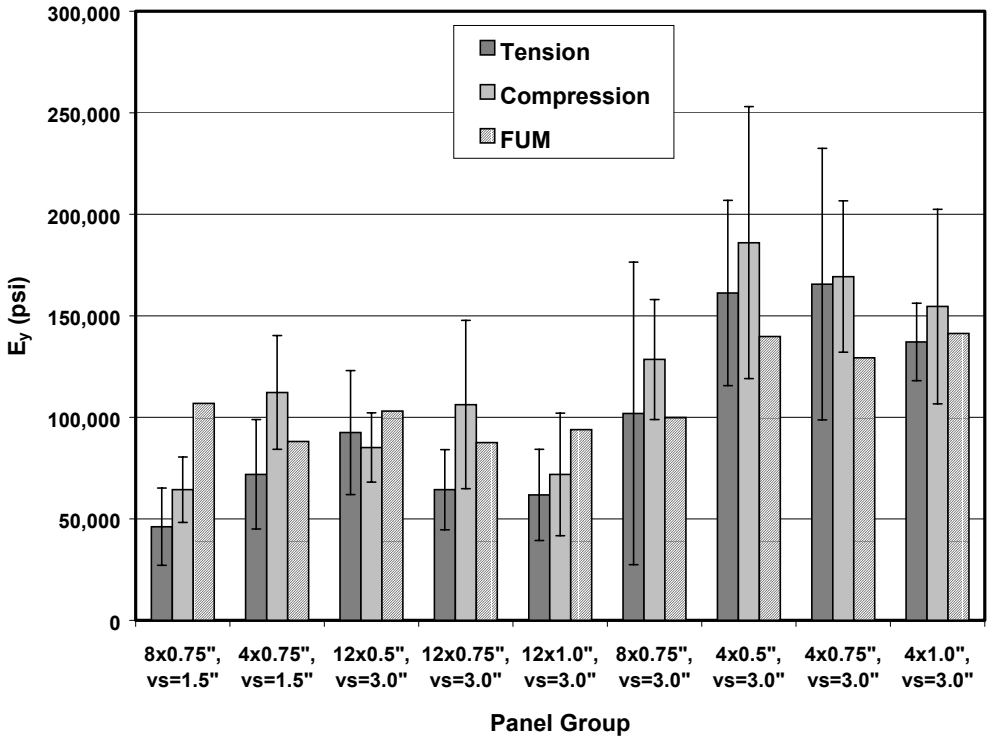

Figure 6. 6. Comparison of experimental tension and compression E_y against predicted E_y (vs = vane spacing).

For all panel groups, the FUM consistently under-predicted tensile E_x and over-predicted compressive E_x for all but one panel group. The percent error ranged from 9% to 42% for tensile E_x and 1% to 53% for compression E_x. Close examination of Figure 6.5 shows that the majority of the FUM results fell within one standard deviation of compression E_x and within two standard deviations of tensile E_x. For E_y, the percent error between the FUM predictions and experimental values ranged from 2% to 132% for tensile E_y and from 9% to 66% for compression E_y. The FUM predictions were lower than tensile E_y and higher than compression E_y for majority of the panel groups. The FUM consistently under-predicted both tension and compression E_y compared to the

experimental values for panels manufactured with shorter strands (4-inch strands). In general, however, FUM predictions of E_y fell within one standard deviation from mean experimental values. Reduction in E_x due to strand undulations ranged from 4.5% to 8.8% depending on the panel group, with an average reduction of 6.9%.

Compared to the overall mean measured G_{xy} for all panel groups and published ν_{xy} of 0.56 (Janowiak et al. 2001), the FUM predictions were under-predicted by 23 to 56 percent. Experimentally measuring longitudinal and transverse strain simultaneously for the specimens in this study to determine Poisson's ratio would have probably yielded more accurate values of G_{xy} and better agreement with the FUM predictions of both G_{xy} and ν_{xy}. Full potential of the fiber undulation model could probably be harnessed when predicting the behavior of a wood-strand composite in the inelastic region.

Summary and Conclusions

A statistical method to include the effects of out-of-plane strand undulations in a mechanics based approach to estimate elastic constants of wood-strand panels was discussed. A series rule of mixtures with probability density functions of angular distributions was utilized in the model to transform the elastic constants in the constitutive matrix of the material for in- and out-of-plane strand deviations. Even though only strand undulations in the longitudinal direction were accounted for in this study, similar approach could be used to adjust the lamina properties for transverse strand undulations. Shear moduli of panels were determined using off-axis tensile testing of oriented strand panels. The fiber undulation model was used to predict elastic properties, E_x, E_y, G_{xy}, and ν_{xy}, of panels manufactured for this project.

Model predictions consistently under-predict tensile E_x and over-predict compression E_x. Predictions of E_y in both tension and compression were reasonably good for certain panel groups (25 to 30% error). The model under-predicted G_{xy} and ν_{xy} for all panel groups. It is expected that experimental evaluation of ν_{xy} for the specimens in this study would yield closer agreement between predicted and measured values for G_{xy} and ν_{xy}. In general, however, the FUM predictions fell within one or two standard deviations from the mean experimental values. Reduction in E_x due to strand undulations ranged from 4.5% to 8.8% depending on the panel group, with an average reduction of 6.9%.

References

ASTM. 1996. Standard Methods for Mechanical Properties of Lumber and Wood-Base Structural Material. Standard D4761-96. American Society of Testing and Materials. Volume 4.10.

ASTM. 1998. Standard Specification for Evaluation of Structural Composite Lumber Products. Standard D5456-98a. American Society of Testing and Materials. Volume 4.10.

Barnes, D. 2000. An integrated model of the effect of processing parameters on the strength properties of oriented strand wood products. Forest Products Journal. 50(11/12):33-42.

_____. 2001. A model of the effect of strand length and strand thickness on the strength properties of oriented wood composites. Forest Products Journal. 51(2):36-46.

_____. 2002a. A model of the effect of strand angle and grain angle on the strength properties of oriented veneer and strand wood composites. Forest Products Journal. 52(4):39-47.

_____. 2002b. A model of the effect of orienter design and operating variables on the mean angular deviation of oriented wood strands. Forest Products Journal. 52(7/8):63-71.

Bodig, J. and B. A. Jayne. 1982. Mechanics of wood and wood composites. Van Nostrand Reinhold Company, New York, NY.

Dong, Chung-Ching. 1979. The mechanical properties of flakeboards related to flake orientation. Ph.D. Dissertation. College of Engineering, Washington State University. 157pp.

Geimer, R. L. 1976. Flake alinement in particleboard as affected by machine variables and particle geometry. USDA Forest Service Research Paper FPL 275. 16 pp.

_____. 1979. Data basic to the engineering design of reconstituted flakeboard. In Proceedings of the 13t^{h} Washington State University International Symposium on Particleboard. pp. 105-125.

Hoover, W. L., M. O. Hunt, R. C. Lattanzi, J. H. Bateman, J. A. Youngquist. 1992. Modeling Mechanical Properties of Single-Layer, Aligned, Mixed-Hardwood Strand Panels. Forest Products Journal. 42(5):12-18.

Janowiak, J. J., Daniel P. Hindman, and H. B. Manbeck. 2001. Orthotropic behavior of lumber composite materials. Wood and Fiber Science. 33(4):580-594.

Triche, M. H. and M. O. Hunt. 1993. Modeling of parallel-aligned wood strand composites. Forest Products Journal. 43(11/12):33-44.

Meyers, K. L. 2001. Impact of strand geometry and orientation on mechanical properties of strand composites. Master's Thesis. Dept. of Civil and Environmental Engineering, Washington State University. 115pp.

Shaler, M. S. and P. R. Blankenhorn. 1990. Composite model prediction of elastic moduli for flakeboard. Wood and Fiber Science. 22(3):246-261.

_____. 1991. Comparing two measures of flake alignment. Wood Sci. Technol. 26:53-61.

Xu, W. and O. Suchsland. 1998. Modulus of elasticity of wood composite panels with a uniform vertical density profile: A model. Wood and Fiber Science. 30(3):293-300.

Yadama, V. 2002a. Characterization and modeling of oriented strand composites: Chapter 2. Ph.D. Dissertation. Washington State University.

Yadama, V. 2002b. Characterization and modeling of oriented strand composites: Chapter 3. Ph.D. Dissertation. Washington State University.

Yadama, V. 2002c. Characterization and modeling of oriented strand composites: Chapter 4. Ph.D. Dissertation. Washington State University.

Yadama, V. 2002d. Characterization and modeling of oriented strand composites: Chapter 5. Ph.D. Dissertation. Washington State University.

Chapter 7

Project Summary and Conclusions

A mechanics based analytical approach to predict the elastic properties of oriented strand composites was developed, verified, and validated. A fiber undulation model (FUM), commonly used to model woven synthetic composite fabrics, was utilized in this study to estimate the elastic properties of laboratory manufactured oriented strand panels. This model incorporates the effects strand deviations in two different planes of a wood-strand composite along with density variation through the thickness. A response model was developed to include the hot pressing effects on strand elastic properties.

A systematic experimental study was performed to verify the fiber undulation model for wood-strand composites. Predetermined strand undulations were induced in wood-strand laminates to examine the effects of out-of-plane strand undulations on laminate elastic properties. A discrete Fourier series expansion was shown to accurately describe strand undulations in wood-strand laminates. Increasing strand undulation was shown to degrade Young's modulus in both tension and compression. Very good agreement was found between model results and experimental results from compression tests (a difference of two to four percent). However, predicted results varied from tension values by as much as 12%. On average, experimental tensile Young's moduli of laminates were 7 to 14 percent greater than compression moduli, with larger differences at higher undulation angles.

After verifying the FUM with carefully fabricated wood-strand laminates, the research concentrated on validating the model for aspen oriented strand panels. A

sequence of studies was conducted to obtain the necessary information regarding the properties of the constituents of the panels, arrangement of strands in the panels and the presence of voids between strands in a panel. Material properties, E_1 and ν_{12}, of aspen strands were experimentally evaluated. Then using tensor transformation relations, E_2 and G_{12} were estimated. Tensor transformation was shown to be an effective way to relate fiber angle to Young's modulus of aspen strands. A study on the effects of hot pressing on strand elastic properties indicated a direct relation between densification during hot pressing and E_1. Response models based on mixture design, considering the hot pressing effects, were developed to predict E_1 and ν_{12} of aspen strands. Even though the effect of resin content on strand elastic properties was statistically not significant, the results of the simplex method suggest an increase in E_1 and a decrease in ν_{12} as resin content is increased. Results of this study support findings by other researchers that hot pressing increases strand elastic properties due to increase in cellulose crystallinity in the wood in response to heat treatment, densification and plasticization.

Oriented strand composite panel structure was characterized with between strands void volume and strand undulations through panel thickness in the longitudinal direction of a panel. In general, between strands void volume ranged from 0.01 to 0.03 for different strand geometries. Very high coefficients of variation indicate that more data is needed to determine conclusive trends between strand geometry, vane spacing and between strands void volume. For a vane spacing of 1.5 inches, the void volume fraction showed a tendency to increase as strand width was increased. However, this trend was not so apparent for vane spacing of 3.0 inches.

In this study, out-of-plane strand undulations were investigated and quantified in both the transverse and longitudinal directions of a panel. Undulation angle distributions of surface strands were significantly different than those of core strands in both directions. Vane spacing did not significantly influence the undulation angle distribution when strand geometry was kept constant. Panels made with short strands resulted in higher percentages of larger undulation angles than long strands. The effect of strand width was not significant, however cumulative density plots indicate that it could influence the undulation angles for longer strands. In the longitudinal direction, strand undulation angles were found to range between 0 and 30 degrees for the core strands and between 0 an 20 degrees for the surface strands.

For the transverse direction, strand deviation angles ranged between 0 and 60 degrees for the core strands and between 0 and 50 degrees for the surface strands. More than the effect of strand length, it is the combination of strand length and width that seemed to influence the transverse undulation angles. Long strands with narrow widths tend to result in higher values of undulation angles. Two-parameter Weibull probability density functions adequately fit both longitudinal and transverse direction strand undulation data. The results of this study show that random and incidental strand undulations in the longitudinal and transverse directions, which are inherent attributes of oriented strand composites, are significant and could potentially influence their physical and mechanical behavior.

The shear moduli of panels were determined using off-axis tensile testing of specimens from oriented strand panels. A fiber undulation model that incorporated density variation through panel depth and the effects of hot pressing on strand elastic

properties was used to predict elastic properties, E_x, E_y, G_{xy}, and ν_{xy}, of panels manufactured for this project. A series rule of mixtures with probability density functions of angular distributions was utilized to account for the effects of out-of-plane strand waviness and in-plane strand deviations on wood-strand composite's elastic constants. In general, predicted values were reasonable and showed a good agreement with experimental results from compression tests. Model predictions consistently under-predict tensile E_x and over-predict compression E_x. Predictions of E_y in both tension and compression were also reasonably good for most panel groups. The model under-predicted G_{xy} and ν_{xy} for all panel groups. It is the opinion of the investigator that better experimental evaluation of G_{xy} and ν_{xy} would yield closer agreement between model and measured values. In general, however, the FUM predictions fell within one or two standard deviations from mean experimental values. Reduction in E_x due to strand undulations ranged from 4.5% to 8.8% depending on the panel group, with an average reduction of 6.9%. The use of the fiber undulation model would probably be more beneficial when estimating the nonlinear behavior of a wood-strand composite.

Appendices

Appendix A: Lay-up of verification specimen with induced undulating strands

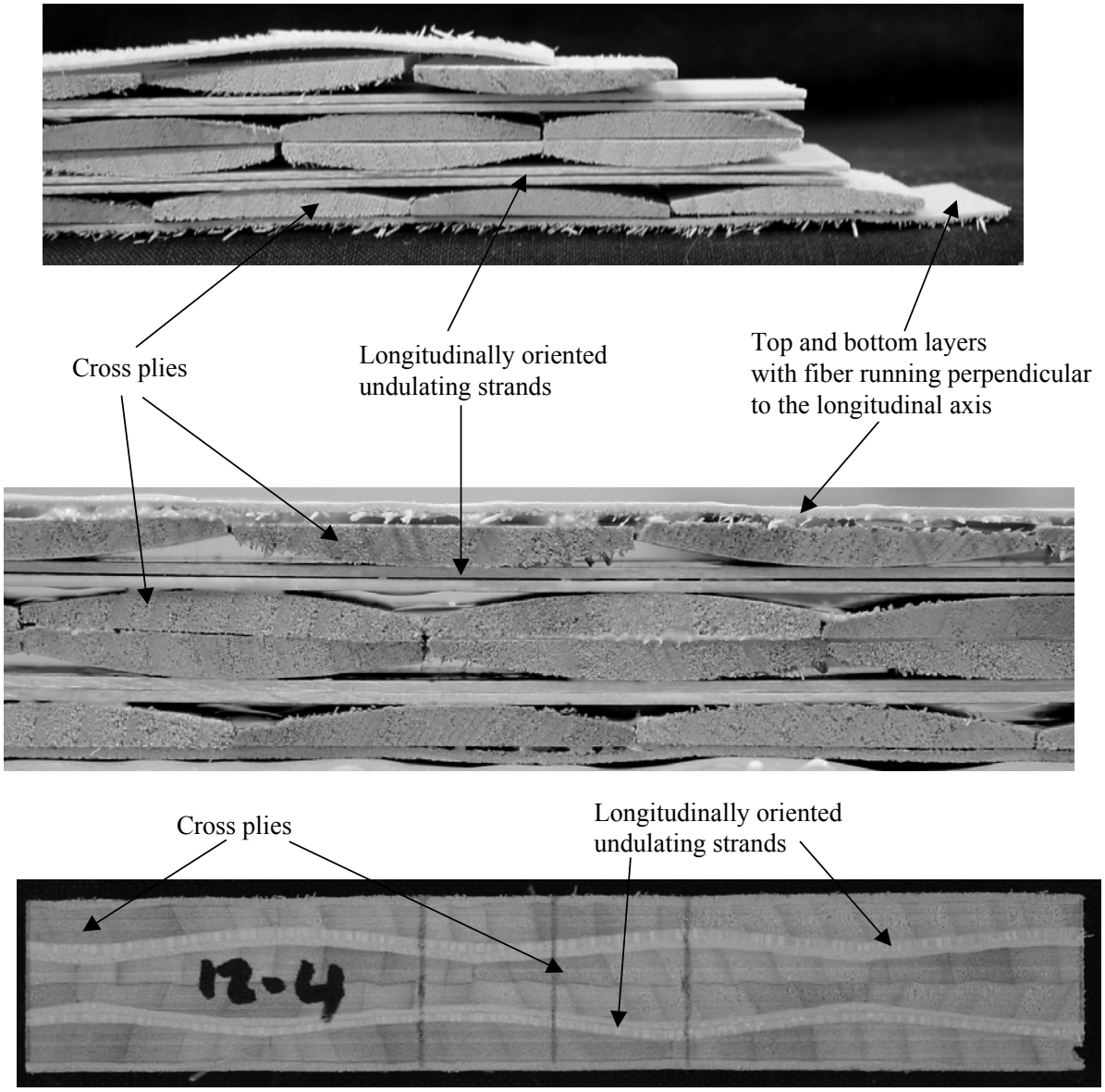

Appendix B: Discrete Fourier Series to Describe Strand Undulation

Discrete Fourier Series To Describe Flake Undulation -- even Delta_X of 50 Pixels

data1 := xy_coordinate_filename

$x := data1^{\langle 1 \rangle}$ $y := data1^{\langle 2 \rangle}$

$tot := length(x)$ $deltax := x_2 - x_1$

$T := x_{tot}$

$i := 14$ $nn := 0.02$ $T =$

$k := 1 .. i$

$$a0 := \frac{1}{T} \cdot \left[\sum_{n=1}^{tot} \left(y_n \cdot deltax \right) \right]$$

$$a_k := \frac{2}{T} \cdot \left[\sum_{n=1}^{tot} \left(\left(y_n \cdot \cos\left(\frac{2 \cdot \pi \cdot k \cdot x_n}{T} \right) \cdot deltax \right) \right) \right] \qquad b_k := \frac{2}{T} \cdot \left[\sum_{n=1}^{tot} \left(\left(y_n \cdot \sin\left(\frac{2 \cdot \pi \cdot k \cdot x_n}{T} \right) \cdot deltax \right) \right) \right]$$

$xx := 0, nn .. T$ $w := 2 \cdot \pi$

$wt := \frac{w}{T}$

$$h(xx) := \left[\sum_{j=1}^{i} \left(a_j \right) \cdot \cos\left(\left(j \cdot \frac{w \cdot xx}{T} \right) \right) + b_j \cdot \sin\left(j \cdot \frac{w \cdot xx}{T} \right) \right] + a0$$

$$\theta(xx) := \operatorname{atan}\left(\frac{d}{dxx} h(xx) \right)$$

$$deg(xx) := \theta(xx) \cdot \frac{180}{\pi}$$

```
col1 := | m ← 1
        | for xx ∈ 0.1, .1 + nn .. T
        |     | v_m ← xx
        |     | m ← m + 1
        | v
```

```
col2 := | m ← 1
        | for xx ∈ 0.1, .1 + nn .. T
        |     | v_m ← h(xx)
        |     | m ← m + 1
        | v
```

```
col3 := | m ← 1
        | for xx ∈ 0.1, .1 + nn .. T
        |     | v_m ← deg(xx)
        |     | m ← m + 1
        | v
```

```
col12 := augment(col1, col2)

allcol := augment(col12, col3)
```

WRITEPRN( ) := allc

Appendix C: Fiber Undulation Model – For Verification Specimens

Fiber Undulation Model -- In phase with repeating unit

For Compression Specimen

$L := 5.921$ $\quad thickness := 0.665$ $\quad w := 2\cdot\pi$

$$hb1(x) := 0.026 + 0.01\cdot\cos\left(\frac{w\cdot x}{L}\right) - 0.013\cdot\cos\left(\frac{4\cdot w\cdot x}{L}\right) - 0.017\cdot\sin\left(\frac{w\cdot x}{L}\right) + 0.024\cdot\sin\left(\frac{4\cdot w\cdot x}{L}\right)$$

$$ht1(x) := -0.01 + 0.017\cdot\cos\left(\frac{4\cdot w\cdot x}{L}\right) - 0.018\cdot\sin\left(\frac{w\cdot x}{L}\right) - 0.028\cdot\sin\left(\frac{4\cdot w\cdot x}{L}\right)$$

$ht2(x) := ht1(x)$ $\quad hb2(x) := hb1(x)$

$$\theta t(x) := \operatorname{atan}\left(\frac{d}{dx}ht1(x)\right) \qquad \theta b(x) := \operatorname{atan}\left(\frac{d}{dx}hb1(x)\right)$$

$$limit1 := \left(\frac{L}{2}\right) - 2$$

$tc\theta(x) := \cos(\theta t(x))$ $\quad ts\theta(x) := \sin(\theta t(x))$

$$limit2 := \left(\frac{L}{2}\right) + 2$$

$bc\theta(x) := \cos(\theta b(x))$ $\quad bs\theta(x) := \sin(\theta b(x))$

$x := limit1, limit1 + 0.1 .. limit2$ $\quad deg(x) := \theta t(x)\cdot\frac{180}{\pi}$

$t1E1 := 1476000$	$E2 := 79570$	$E3 := 79570$	$t2E1 := 1118000$	$b1E1 := 111300($
$G12 := 44130$	$G13 := 44130$	$G23 := 22450$	$cE1 := 1929000$	$b2E1 := 146800($
$\nu12 := 0.5$	$\nu13 := 0.50$	$\nu23 := 0.5$	$cE2 := 79570$	
$\nu32 := 0.5$	$\nu21 := 0.035$	$\nu31 := 0.035$	$cG12 := 44130$	
			$c\nu12 := .50$	

$$t1EOP1(x) := \frac{1}{\left[\frac{tc\theta(x)^4}{t1E1} + \left(\frac{1}{G13} - \frac{2\cdot\nu 13}{t1E1}\right)\cdot tc\theta(x)^2\cdot ts\theta(x)^2 + \frac{ts\theta(x)^4}{E3}\right]}$$

$$t2EOP1(x) := \frac{1}{\left[\frac{tc\theta(x)^4}{t2E1} + \left(\frac{1}{G13} - \frac{2\cdot\nu 13}{t2E1}\right)\cdot tc\theta(x)^2\cdot ts\theta(x)^2 + \frac{ts\theta(x)^4}{E3}\right]}$$

$$b1EOP1(x) := \frac{1}{\left[\frac{bc\theta(x)^4}{b1E1} + \left(\frac{1}{G13} - \frac{2\cdot\nu 13}{b1E1}\right)\cdot bc\theta(x)^2\cdot bs\theta(x)^2 + \frac{bs\theta(x)^4}{E3}\right]}$$

$$b2EOP1(x) := \frac{1}{\left[\frac{bc\theta(x)^4}{b2E1} + \left(\frac{1}{G13} - \frac{2\cdot\nu 13}{b2E1}\right)\cdot bc\theta(x)^2\cdot bs\theta(x)^2 + \frac{bs\theta(x)^4}{E3}\right]}$$

$$t\nu OP21(x) := \nu 31\cdot tc\theta(x)^2 + \nu 23\cdot ts\theta(x)^2$$

$$tGOP12(x) := G12\cdot tc\theta(x)^2 + G23\cdot ts\theta(x)^2$$

$$tEOP2(x) := E2$$

$$b\nu OP21(x) := \nu 31\cdot bc\theta(x)^2 + \nu 23\cdot bs\theta(x)^2$$

$$bGOP12(x) := G12\cdot bc\theta(x)^2 + G23\cdot bs\theta(x)^2$$

$$bEOP2(x) := E2$$

$$t1Dv(x) := 1 - \frac{t\nu OP21(x)^2\cdot tEOP2(x)}{t1EOP1(x)} \qquad t2Dv(x) := 1 - \frac{t\nu OP21(x)^2\cdot tEOP2(x)}{t2EOP1(x)}$$

$$b1Dv(x) := 1 - \frac{b\nu OP21(x)^2\cdot bEOP2(x)}{b1EOP1(x)} \qquad b2Dv(x) := 1 - \frac{b\nu OP21(x)^2\cdot bEOP2(x)}{b2EOP1(x)}$$

$$DvIP := 1 - \frac{\nu 21^2\cdot cE2}{cE1}$$

$$t1QF(x) := \begin{bmatrix} \frac{t1EOP1(x)}{t1Dv(x)} & \frac{tEOP2(x) \cdot tvOP21(x)}{t1Dv(x)} & 0 \\ \frac{tEOP2(x) \cdot tvOP21(x)}{t1Dv(x)} & \frac{tEOP2(x)}{t1Dv(x)} & 0 \\ 0 & 0 & tGOP12(x) \end{bmatrix}$$

$$t2QF(x) := \begin{bmatrix} \frac{t2EOP1(x)}{t2Dv(x)} & \frac{tEOP2(x) \cdot tvOP21(x)}{t2Dv(x)} & 0 \\ \frac{tEOP2(x) \cdot tvOP21(x)}{t2Dv(x)} & \frac{tEOP2(x)}{t2Dv(x)} & 0 \\ 0 & 0 & tGOP12(x) \end{bmatrix}$$

$$b1QF(x) := \begin{bmatrix} \frac{b1EOP1(x)}{b1Dv(x)} & \frac{bEOP2(x) \cdot bvOP21(x)}{b1Dv(x)} & 0 \\ \frac{bEOP2(x) \cdot bvOP21(x)}{b1Dv(x)} & \frac{bEOP2(x)}{b1Dv(x)} & 0 \\ 0 & 0 & bGOP12(x) \end{bmatrix}$$

$$b2QF(x) := \begin{bmatrix} \frac{b2EOP1(x)}{b2Dv(x)} & \frac{bEOP2(x) \cdot bvOP21(x)}{b2Dv(x)} & 0 \\ \frac{bEOP2(x) \cdot bvOP21(x)}{b2Dv(x)} & \frac{bEOP2(x)}{b2Dv(x)} & 0 \\ 0 & 0 & bGOP12(x) \end{bmatrix}$$

$$QIP := \begin{bmatrix} \frac{cE1}{DvIP} & \frac{cE2 \cdot v21}{DvIP} & 0 \\ \frac{cE2 \cdot v21}{DvIP} & \frac{cE2}{DvIP} & 0 \\ 0 & 0 & cG12 \end{bmatrix}$$

$$Tperp := \begin{bmatrix} \cos\left(\frac{\pi}{2}\right)^2 & \sin\left(\frac{\pi}{2}\right)^2 & 2\cdot\cos\left(\frac{\pi}{2}\right)\cdot\sin\left(\frac{\pi}{2}\right) \\ \sin\left(\frac{\pi}{2}\right)^2 & \cos\left(\frac{\pi}{2}\right)^2 & -2\cdot\cos\left(\frac{\pi}{2}\right)\cdot\sin\left(\frac{\pi}{2}\right) \\ -\cos\left(\frac{\pi}{2}\right)\cdot\sin\left(\frac{\pi}{2}\right) & \cos\left(\frac{\pi}{2}\right)\cdot\sin\left(\frac{\pi}{2}\right) & \cos\left(\frac{\pi}{2}\right)^2 - \sin\left(\frac{\pi}{2}\right)^2 \end{bmatrix}$$

$$QIP1 := Tperp^{-1}\cdot QIP$$

$$TperpT := Tperp^{T}$$

$$QbIP := QIP1\cdot TperpT^{-1}$$

$$A(x) := (thickness - (4\cdot 0.043))\cdot QbIP + 0.043\cdot t1QF(x) + 0.043\cdot t2QF(x) + 0.043\cdot b1QF(x) + 0.043\cdot b2QF(x)$$

$$a(x) := A(x)^{-1}$$

$$aavg11 := \frac{1}{(limit2 - limit1)}\cdot\int_{limit1}^{limit2} a(x)_{0,0}\,dx$$

$$EffEx := \frac{1}{aavg11\cdot thickness}$$

Appendix D: Specimen Cutting Scheme

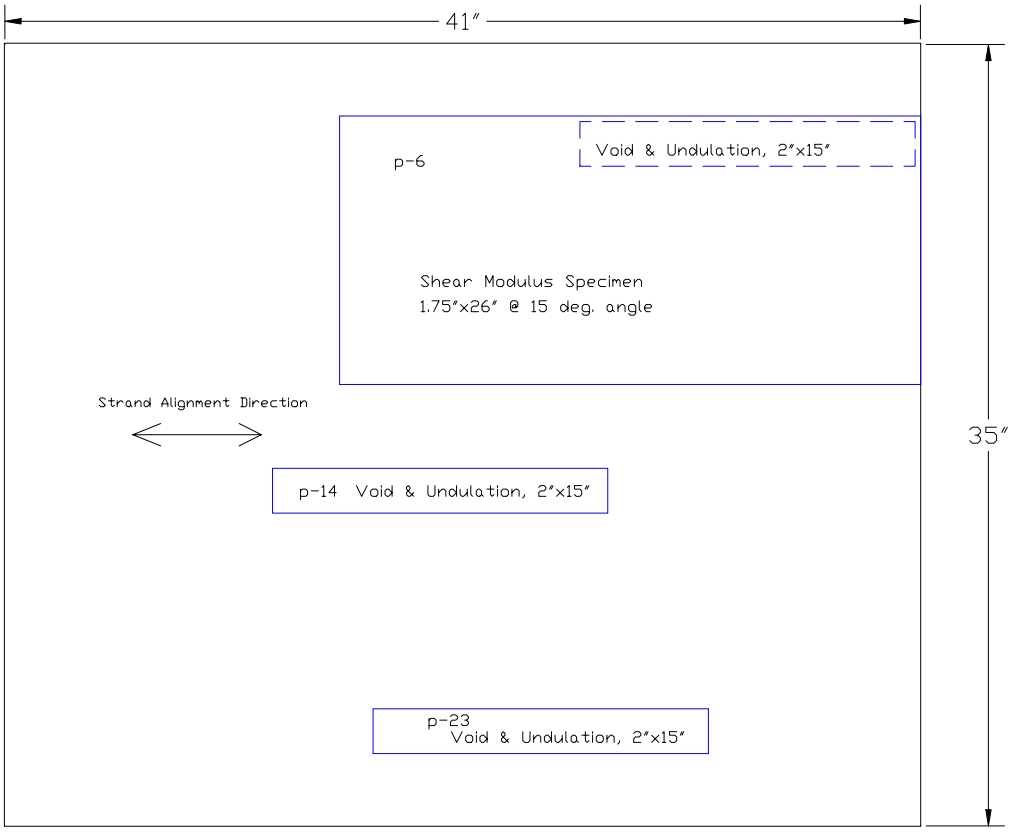

Appendix E: Cumulative distribution plots of undulation data

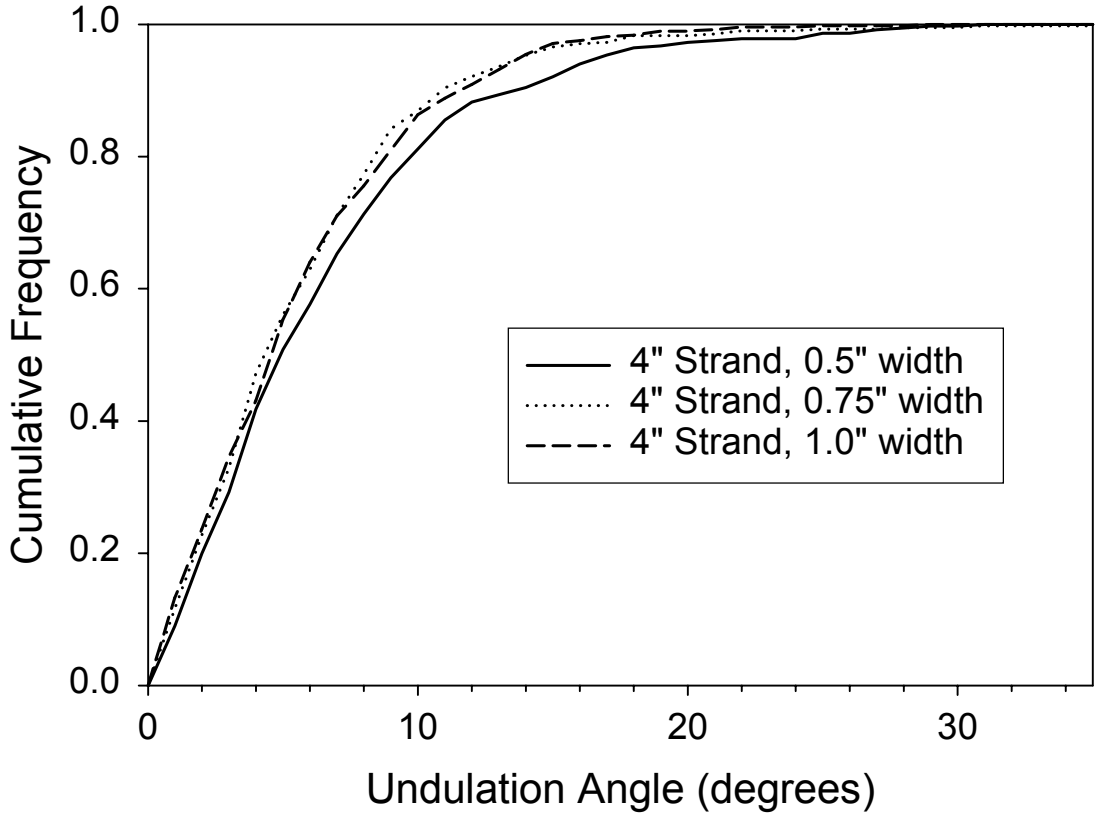

Figure E. 6. Strand width effect on cumulative density distributions of undulation angles for 4-inch long strands in the longitudinal direction (vane spacing = 3").

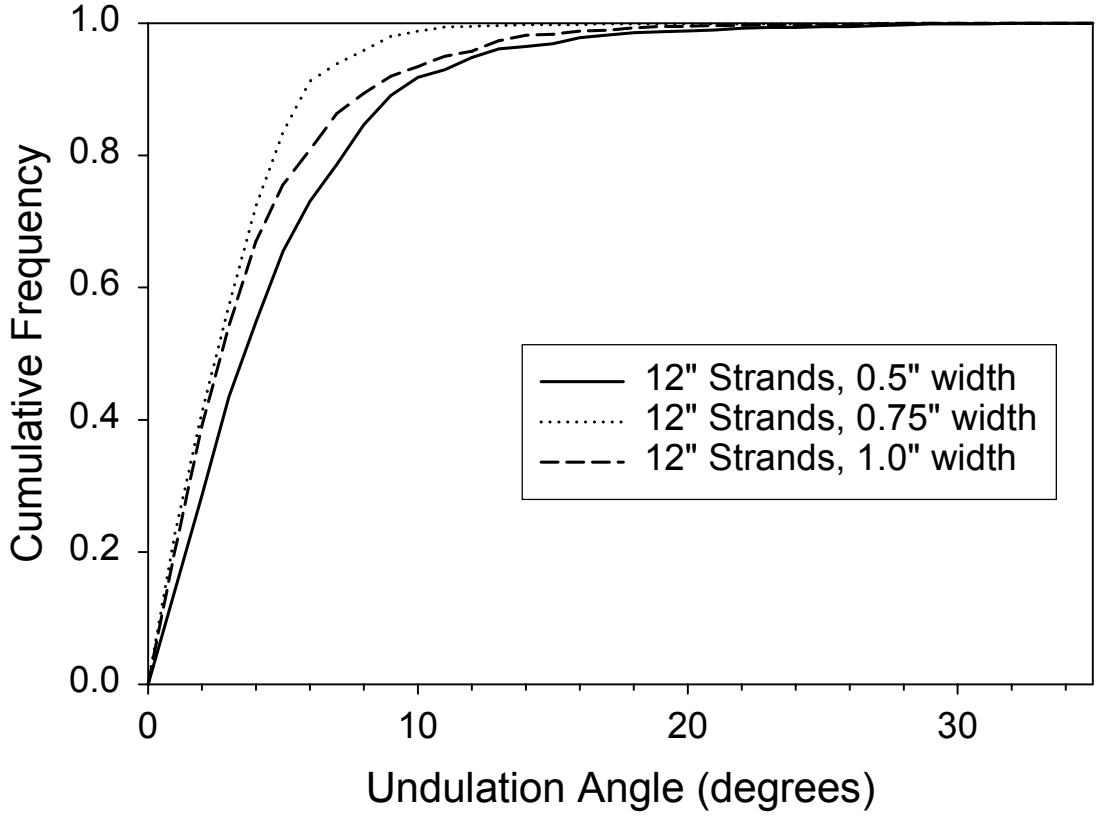

Figure E. 7. Strand width effect on cumulative density distributions of undulation angles for 12-inch strands in the longitudinal direction (vane spacing = 3”).

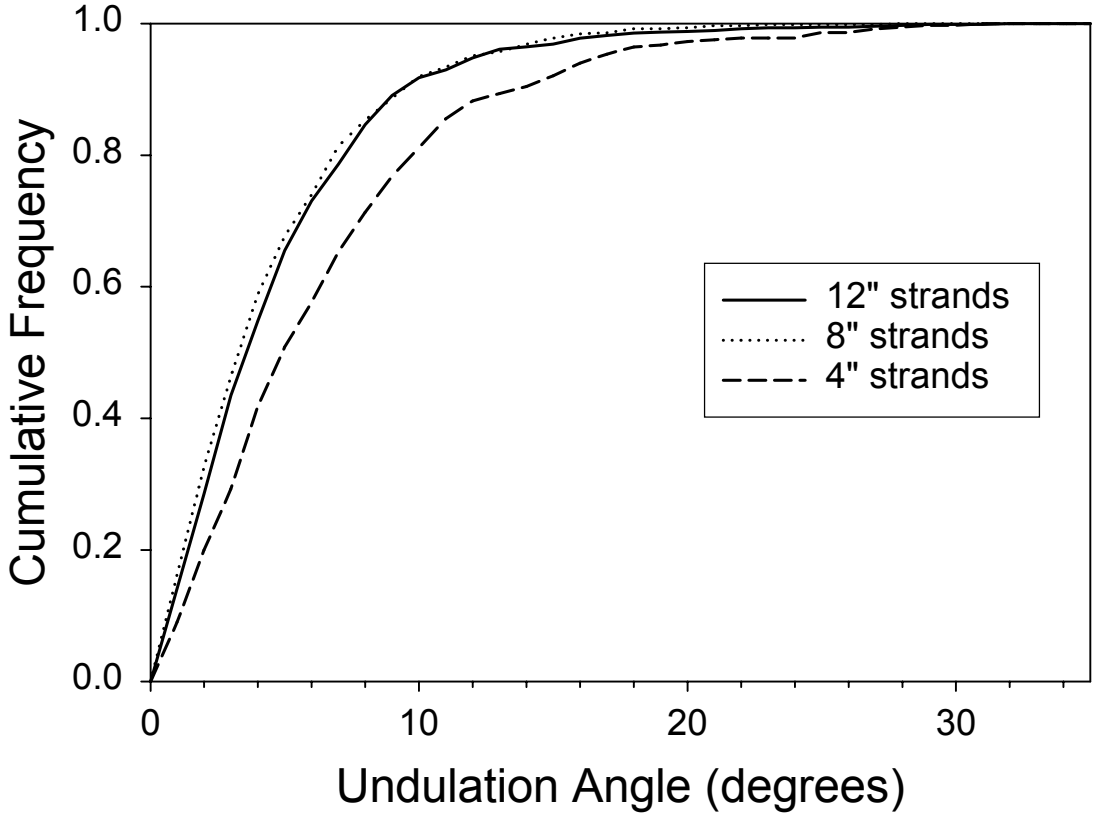

Figure E. 8. Strand length effect on cumulative density distributions of undulations angles in the longitudinal direction (strand width = 0.75”; vane spacing = 3”).

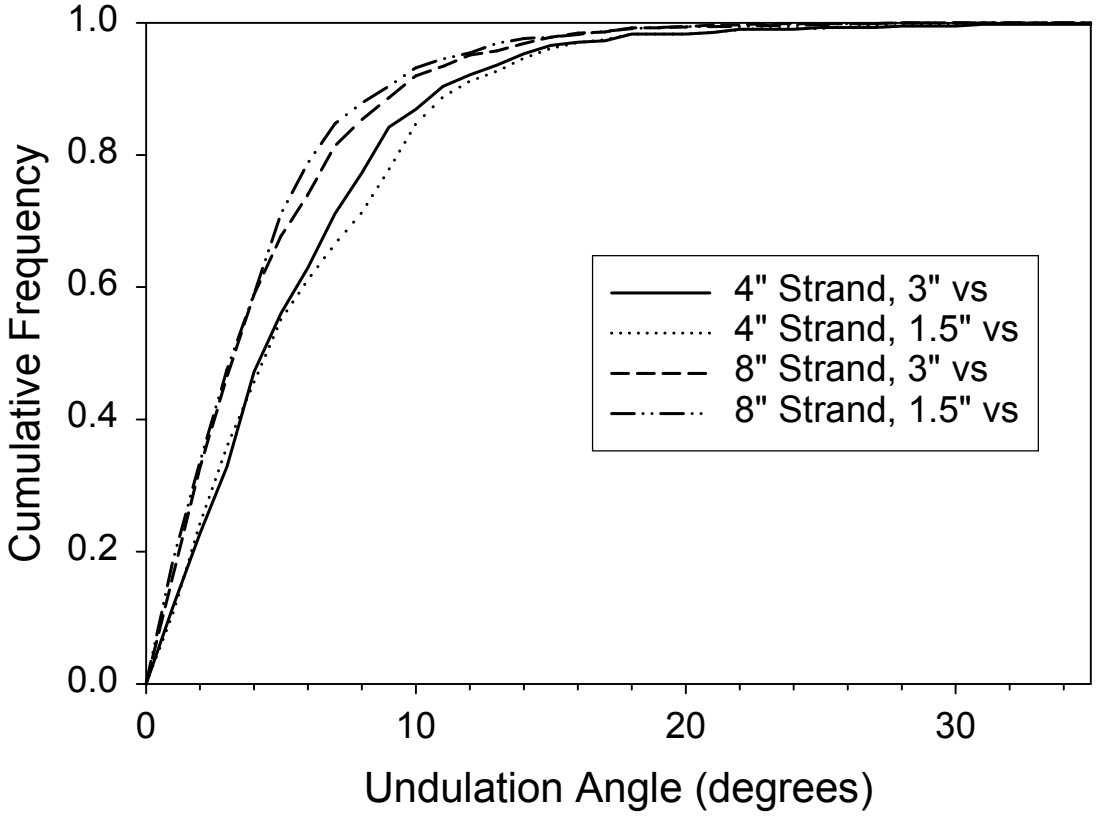

Figure E. 9. Effect of vane spacing on cumulative density distributions of undulation angles for 4-inch and 8-inch long strands in the longitudinal direction (strand width = 0.75").

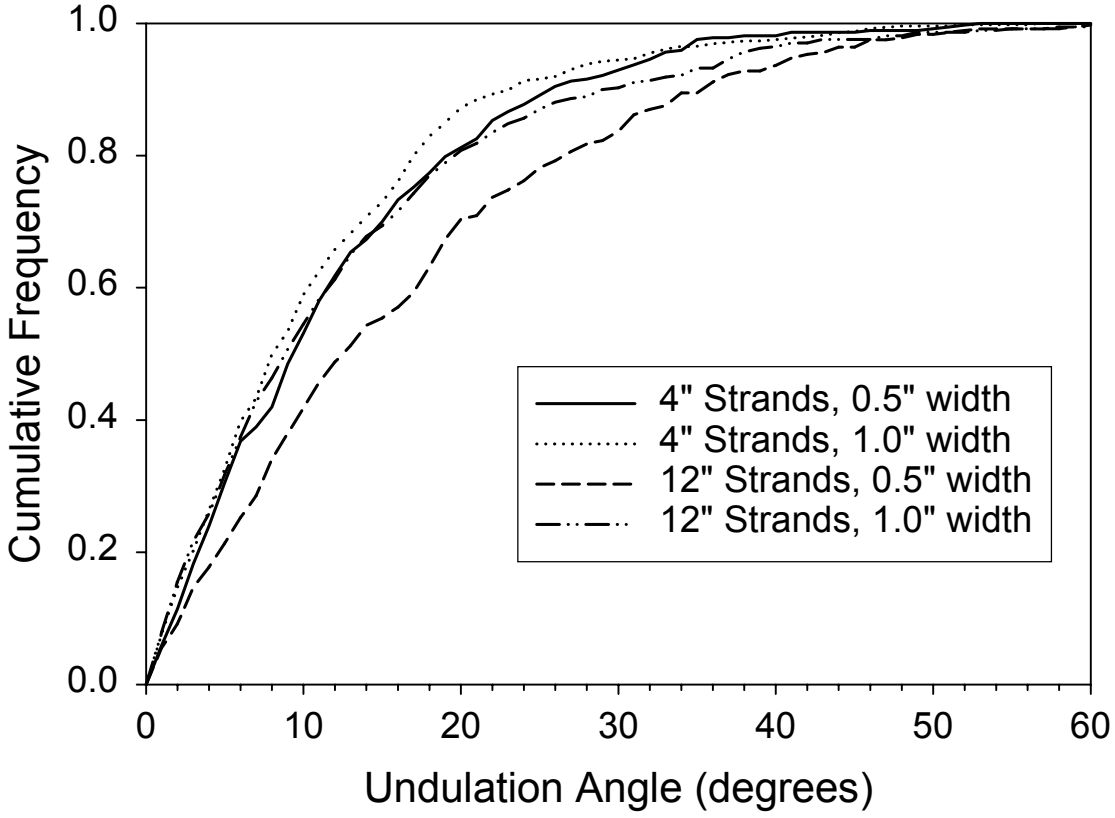

Figure E. 10. Effect of strand length and width on cumulative density distributions of undulation angles in the transverse direction (strand width = 0.75”; vane spacing = 3”).

Appendix F: Fiber Undulation Model – OSL Validation

Fiber Undulation Model -- OSL

Angle Distributions

$$\phi s := \begin{bmatrix} -2 \\ -6 \\ -12 \\ -18 \\ -24 \\ -30 \\ -36 \\ -42 \\ -48 \\ -54 \\ -60 \\ -66 \\ -72 \\ -78 \\ -84 \end{bmatrix} \cdot \text{deg} \qquad \phi := \begin{bmatrix} 2 \\ 6 \\ 12 \\ 18 \\ 24 \\ 30 \\ 36 \\ 42 \\ 48 \\ 54 \\ 60 \\ 66 \\ 72 \\ 78 \\ 84 \end{bmatrix} \cdot \text{deg} \qquad \theta := \begin{bmatrix} 1 \\ 3 \\ 5 \\ 7 \\ 9 \\ 11 \\ 13 \\ 15 \\ 17 \\ 19 \\ 21 \\ 23 \\ 25 \\ 27 \\ 29 \\ 31 \\ 33 \end{bmatrix} \cdot \text{deg}$$

Laminate Thickness and Between Strand Void Fraction

$$\text{thickness} := 0.734$$

$$\text{vbs} := 0.0176$$

Transformation Matrix for In-Plane Angle (1-2 Plane)

$$T12(k) := \begin{bmatrix} \cos(\phi_k)^2 & \sin(\phi_k)^2 & 0 & 0 & 0 & 2\cdot\cos(\phi_k)\cdot\sin(\phi_k) \\ \sin(\phi_k)^2 & \cos(\phi_k)^2 & 0 & 0 & 0 & -2\cdot\cos(\phi_k)\cdot\sin(\phi_k) \\ 0 & 0 & 1 & 0 & 0 & 0 \\ 0 & 0 & 0 & \cos(\phi_k) & -\sin(\phi_k) & 0 \\ 0 & 0 & 0 & \sin(\phi_k) & \cos(\phi_k) & 0 \\ -\cos(\phi_k)\cdot\sin(\phi_k) & \cos(\phi_k)\cdot\sin(\phi_k) & 0 & 0 & 0 & \cos(\phi_k)^2 - \sin(\phi_k)^2 \end{bmatrix}$$

For symmetric layers

$$T12s(k) := \begin{bmatrix} \cos(\phi s_k)^2 & \sin(\phi s_k)^2 & 0 & 0 & 0 & 2\cdot\cos(\phi s_k)\cdot\sin(\phi s_k) \\ \sin(\phi s_k)^2 & \cos(\phi s_k)^2 & 0 & 0 & 0 & -2\cdot\cos(\phi s_k)\cdot\sin(\phi s_k) \\ 0 & 0 & 1 & 0 & 0 & 0 \\ 0 & 0 & 0 & \cos(\phi s_k) & -\sin(\phi s_k) & 0 \\ 0 & 0 & 0 & \sin(\phi s_k) & \cos(\phi s_k) & 0 \\ -\cos(\phi s_k)\cdot\sin(\phi s_k) & \cos(\phi s_k)\cdot\sin(\phi s_k) & 0 & 0 & 0 & \cos(\phi s_k)^2 - \sin(\phi s_k)^2 \end{bmatrix}$$

Transformation Matrix for Longitudinal Undulation (1-3 Plane)

$$T13(k) := \begin{bmatrix} \cos(\theta_k)^2 & 0 & \sin(\theta_k)^2 & 0 & 2\cdot\cos(\theta_k)\cdot\sin(\theta_k) & 0 \\ 0 & 1 & 0 & 0 & 0 & 0 \\ \sin(\theta_k)^2 & 0 & \cos(\theta_k)^2 & 0 & -2\cdot\cos(\theta_k)\cdot\sin(\theta_k) & 0 \\ 0 & 0 & 0 & \cos(\theta_k) & 0 & -\sin(\theta_k) \\ -\cos(\theta_k)\cdot\sin(\theta_k) & 0 & \cos(\theta_k)\cdot\sin(\theta_k) & 0 & \cos(\theta_k)^2 - \sin(\theta_k)^2 & 0 \\ 0 & 0 & 0 & \sin(\theta_k) & 0 & \cos(\theta_k) \end{bmatrix}$$

In-Plane Angle Probabilities

$\alpha i := 1.18 \qquad \beta i := 13.9$

$$Fip(xi) := 1 - e^{-\left(\frac{xi}{\beta i}\right)^{\alpha i}}$$

$$Fi(k) := Fip(k \cdot 10) - Fip(k \cdot 10 - 10)$$

Longitudinal Undulation Angle Probabilities

Surface Strands

$s\alpha ul := 1.252 \qquad s\beta ul := 3.159$

$$sFul(sxul) := 1 - e^{-\left(\frac{sxul}{s\beta ul}\right)^{s\alpha ul}}$$

$$sFl(k) := sFul(2 \cdot k) - sFul(2 \cdot k - 2)$$

Core Strands

$m\alpha ul := 1.096 \qquad m\beta ul := 4.318$

$$mFul(mxul) := 1 - e^{-\left(\frac{mxul}{m\beta ul}\right)^{m\alpha ul}}$$

$$mFl(k) := mFul(2 \cdot k) - mFul(2 \cdot k - 2)$$

Layer 1

Material Properties

$resin := 0.06 \qquad D1 := 50.0 \qquad thk1 := 0.04$

$$sg1 := \frac{D1}{62.4}$$

$$void1 := \left(1 - \frac{sg1}{1.5}\right) - resin$$

$$cw1 := 1 - resin - void1$$

$$E1L1 := 4711775 cw1 + 4612091 resin + 678475 void1 - 89340000 void1 \cdot resin$$

$$v12L1 := 0.083487 cw1 + 0.497837 resin + 0.340432 void1$$

$$E2L1 := \frac{E1L1}{21} \qquad G12L1 := \frac{E1L1}{24}$$

$$G13L1 := G12L1 \qquad E3L1 := E2L1 \qquad v13L1 := v12L1$$

$$v23L1 := 0.5 \qquad v21L1 := 0.035 \qquad G23L1 := \frac{G12L1}{2}$$

$$v32L1 := v23L1 \qquad v31L1 := v21L1$$

$$S1 := \begin{bmatrix} \frac{1}{E1L1} & \frac{-v12L1}{E1L1} & \frac{-v13L1}{E1L1} & 0 & 0 & 0 \\ \frac{-v12L1}{E1L1} & \frac{1}{E2L1} & \frac{-v32L1}{E3L1} & 0 & 0 & 0 \\ \frac{-v13L1}{E1L1} & \frac{-v32L1}{E3L1} & \frac{1}{E3L1} & 0 & 0 & 0 \\ 0 & 0 & 0 & \frac{1}{G23L1} & 0 & 0 \\ 0 & 0 & 0 & 0 & \frac{1}{G13L1} & 0 \\ 0 & 0 & 0 & 0 & 0 & \frac{1}{G12L1} \end{bmatrix}$$

Transform for Longitudinal Undulations

$$Sbar1(k) := T13(k)^{T} \cdot S1 \cdot T13(k)$$

$$Sbaravg1 := \sum_{n=1}^{17} sFl(n) \cdot Sbar1(n)$$

Transform for In-plane Angles

$$Sbar11(k) := T12(k)^{T} \cdot Sbaravg1 \cdot T12(k)$$

$$Sbaravg11 := \sum_{n=1}^{15} Fi(n) \cdot Sbar11(n)$$

$$CL1b := Sbaravg11^{-1}$$

Layer 2

Material Properties

$resin := 0.06 \qquad D2 := 46.3 \qquad thk2 := 0.04$

$$sg2 := \frac{D2}{62.4}$$

$$void2 := \left(1 - \frac{sg2}{1.5}\right) - resin$$

$$cw2 := 1 - resin - void2$$

$$E1L2 := 4711775 cw2 + 4612509 resin + 678475 void2 - 89340000 void2 \cdot resin$$

$$v12L2 := 0.083487 cw2 + 0.497837 resin + 0.340432 void2$$

$$E2L2 := \frac{E1L2}{21} \qquad G12L2 := \frac{E1L2}{24}$$

$G13L2 := G12L2 \qquad E3L2 := E2L2 \qquad v13L2 := v12L2$

$v23L2 := 0.5 \qquad v21L2 := 0.035$

$$G23L2 := \frac{G12L2}{2}$$

$v32L2 := v23L2 \qquad v31L2 := v21L2$

$$S2 := \begin{bmatrix} \frac{1}{E1L2} & \frac{-v12L2}{E1L2} & \frac{-v13L2}{E1L2} & 0 & 0 & 0 \\ \frac{-v12L2}{E1L2} & \frac{1}{E2L2} & \frac{-v32L2}{E3L2} & 0 & 0 & 0 \\ \frac{-v13L2}{E1L2} & \frac{-v32L2}{E3L2} & \frac{1}{E3L2} & 0 & 0 & 0 \\ 0 & 0 & 0 & \frac{1}{G23L2} & 0 & 0 \\ 0 & 0 & 0 & 0 & \frac{1}{G13L2} & 0 \\ 0 & 0 & 0 & 0 & 0 & \frac{1}{G12L2} \end{bmatrix}$$

Transform for Longitudinal Undulations

$$Sbar2(k) := T13(k)^{T} \cdot S2 \cdot T13(k)$$

$$Sbaravg2 := \sum_{n=1}^{17} sFl(n) \cdot Sbar2(n)$$

Transform for In-plane Angles

$$Sbar22(k) := T12s(k)^{T} \cdot Sbaravg2 \cdot T12s(k)$$

$$Sbaravg22 := \sum_{n=1}^{15} Fi(n) \cdot Sbar22(n)$$

$$CL2b := Sbaravg22^{-1}$$

Layer 3

Material Properties

$resin := 0.06$ $D3 := 40.7$ $thk3 := 0.04$

$$sg3 := \frac{D3}{62.4}$$

$$void3 := \left(1 - \frac{sg3}{1.5}\right) - resin$$

$$cw3 := 1 - resin - void3$$

$$E1L3 := 4711775 cw3 + 4612509 resin + 678475 void3 - 89340000 void3 \cdot resin$$

$$v12L3 := 0.083487 cw3 + 0.497837 resin + 0.340432 void3$$

$$E2L3 := \frac{E1L3}{21} \qquad G12L3 := \frac{E1L3}{24}$$

$G13L3 := G12L3$ $E3L3 := E2L3$ $v13L3 := v12L3$

$v23L3 := 0.5 \qquad v21L3 := 0.035 \qquad G23L3 := \frac{G12L3}{2}$

$v32L3 := v23L3 \qquad v31L3 := v21L3$

$$S3 := \begin{bmatrix} \frac{1}{E1L3} & \frac{-v12L3}{E1L3} & \frac{-v13L3}{E1L3} & 0 & 0 & 0 \\ \frac{-v12L3}{E1L3} & \frac{1}{E2L3} & \frac{-v32L3}{E3L3} & 0 & 0 & 0 \\ \frac{-v13L3}{E1L3} & \frac{-v32L3}{E3L3} & \frac{1}{E3L3} & 0 & 0 & 0 \\ 0 & 0 & 0 & \frac{1}{G23L3} & 0 & 0 \\ 0 & 0 & 0 & 0 & \frac{1}{G13L3} & 0 \\ 0 & 0 & 0 & 0 & 0 & \frac{1}{G12L3} \end{bmatrix}$$

Transform for Longitudinal Undulations

$$Sbar3(k) := T13(k)^{T} \cdot S3 \cdot T13(k)$$

$$Sbaravg3 := \sum_{n=1}^{17} sFl(n) \cdot Sbar3(n)$$

Transform for In-plane Angles

$$Sbar33(k) := T12(k)^{T} \cdot Sbaravg3 \cdot T12(k)$$

$$Sbaravg33 := \sum_{n=1}^{15} Fi(n) \cdot Sbar33(n)$$

$$CL3b := Sbaravg33^{-1}$$

Layer 4

Material Properties

$resin := 0.06 \qquad D4 := 35.0 \qquad thk4 := 0.5 \cdot thickness - (thk1 + thk2 + thk3)$

$$sg4 := \frac{D4}{62.4}$$

$$void4 := \left(1 - \frac{sg4}{1.5}\right) - resin$$

$$cw4 := 1 - resin - void4$$

$$E1L4 := 4711775 cw4 + 4612509 resin + 678475 void4 - 89340000 void4 \cdot resin$$

$$v12L4 := 0.083487 cw4 + 0.497837 resin + 0.340432 void4$$

$$E2L4 := \frac{E1L4}{21} \qquad G12L4 := \frac{E1L4}{24}$$

$$G13L4 := G12L4 \qquad E3L4 := E2L4 \qquad v13L4 := v12L4$$

$$v23L4 := 0.5 \qquad v21L4 := 0.035 \qquad G23L4 := \frac{G12L4}{2}$$

$$v32L4 := v23L4 \qquad v31L4 := v21L4$$

$$S4 := \begin{bmatrix} \frac{1}{E1L4} & \frac{-v12L4}{E1L4} & \frac{-v13L4}{E1L4} & 0 & 0 & 0 \\ \frac{-v12L4}{E1L4} & \frac{1}{E2L4} & \frac{-v32L4}{E3L4} & 0 & 0 & 0 \\ \frac{-v13L4}{E1L4} & \frac{-v32L4}{E3L4} & \frac{1}{E3L4} & 0 & 0 & 0 \\ 0 & 0 & 0 & \frac{1}{G23L4} & 0 & 0 \\ 0 & 0 & 0 & 0 & \frac{1}{G13L4} & 0 \\ 0 & 0 & 0 & 0 & 0 & \frac{1}{G12L4} \end{bmatrix}$$

Transform for Longitudinal Undulations

$$Sbar4(k) := T13(k)^{T} \cdot S4 \cdot T13(k)$$

$$Sbaravg4 := \sum_{n=1}^{17} sFl(n) \cdot Sbar4(n)$$

Transform for In-plane Angles

$$Sbar44(k) := T12s(k)^{T} \cdot Sbaravg4 \cdot T12s(k)$$

$$Sbaravg44 := \sum_{n=1}^{15} Fi(n) \cdot Sbar44(n)$$

$$CL4b := Sbaravg44^{-1}$$

Layer 5

$$CL5b := CL4b \qquad thk5 := thk4$$

Layer 6

$$CL6b := CL3b \qquad thk6 := thk3$$

Layer 7

$$CL7b := CL2b \qquad thk7 := thk2$$

Layer 8

$$CL8b := CL1b \qquad thk8 := thk1$$

Calculate Laminate Extensional Stiffness Matrix, A, and Extensional Compliance Matrix, a

$$A := thk1 \cdot CL1b + thk2 \cdot CL2b + thk3 \cdot CL3b + thk4 \cdot CL4b + thk5 \cdot CL5b + thk6 \cdot CL6b + thk7 \cdot CL7b + thk8 \cdot CL8b$$

$$a := A^{-1}$$

Calculate Effective Engineering Properties of Laminate

$$EffEx := \frac{1}{a_{1,1} \cdot thickness} \cdot (1 - vbs)$$

$$EffEy := \frac{1}{a_{2,2} \cdot thickness} \cdot (1 - vbs)$$

$$EffGx := \frac{1}{a_{6,6} \cdot thickness} \cdot (1 - vbs)$$

$$Effvxy := \frac{-a_{1,2}}{a_{1,1}}$$